NBSIR 86-3044

ELECTROMECHANICAL PROPERTIES OF SUPERCONDUCTORS FOR DOE FUSION APPLICATIONS

J. W. Ekin
J. Moreland
J. C. Brauch

National Bureau of Standards
U.S. Department of Commerce
Boulder, Colorado 80303

March 1986

NBSIR 86-3044

ELECTROMECHANICAL PROPERTIES OF SUPERCONDUCTORS FOR DOE FUSION APPLICATIONS

J. W. Ekin
J. Moreland
J. C. Brauch

Electromagnetic Technology Division
Center for Electronics and Electrical Engineering
National Engineering Laboratory
National Bureau of Standards
Boulder, Colorado 80303

March 1986

Prepared for
Department of Energy
Office of Fusion Energy
Washington, DC 20545
(Interagency Agreement #DE-AI01-84ER52113)

U.S. DEPARTMENT OF COMMERCE, Malcolm Baldrige, Secretary

NATIONAL BUREAU OF STANDARDS, Ernest Ambler, Director

PREFACE

This is an interim report covering the work performed in the first year and a half of a three-year contract (3/4 staff year per year). The objective of the research is to obtain data on superconductor performance under mechanical load; these data are needed for the mechanical design of superconducting magnets for DOE fusion energy systems. A further aim is to measure and understand the electromechanical properties of promising new superconductor materials with strong application potential.

Testing is proceeding along two lines. First, a new measurement system has been built to measure critical current as a function of transverse compressive strain. Preliminary tests of the apparatus have been completed, and a new adaptation for measuring single superconductor strands has been constructed. Engineering data on the effect of this transverse component of strain have not been measured previously, although it has a significant role in present magnet designs.

Second, new superconducting material testing has been performed at very high magnetic fields using an apparatus for measuring axial strain effects in fields up to 24 T. Results have been obtained on several experimental superconductors, including the first strain-effect data on a Chevrel phase superconductor, $PbMo_6S_8$, which has strong application potential above 20 T, and several new Nb_3Sn conductors specially fabricated for economical operation at higher fields (14 to 18 T).

In addition to these two main thrusts, two ancillary projects have been started. A new diagonostic tool for probing the microstructure of practical superconductors has been developed using electron tunneling, and thermal contraction data have been obtained on several new candidate materials for superconductor sheathing and strengthening. The latter should eventually result in significantly less electrical degradation of the critical current in reinforced superconductors.

The first year's efforts have resulted in three publications:

1. "Electromechanical and Metallurgical Properties of Liquid-infiltration Nb-Ta/Sn Multifilamentary Superconductor," by J. W. Ekin and M. Hong, Appl. Phys. Letters 45, 297 (1984).

2. "Effect of Uniaxial Strain on the Critical Current and Critical Field of Chevrel Phase $PbMo_6S_8$ Superconductors," by J. W. Ekin, T. Yamashita, and K. Hamasaki, IEEE Trans. Magn. MAG-21, 474 (1985).

3. "Electron Tunneling Into Superconducting Filaments Using Mechanically Adjustable Barriers," by John Moreland and J. W. Ekin, Appl. Phys. Letters 47, 175 (1985).

Next year's objectives include the first direct measurements of the effect of transverse compression on the critical current of Nb_3Sn and design of an apparatus to measure uniaxial tension and transverse-compression effects simultaneously. The electromechanical properties of several new superconducting materials and processes will also be evaluated; these include modified $PbMo_6S_8$ superconductors, Nb_3Sn with new additions, V_3Ga, hot-isostatic-pressure treatment, powder metallurgy and in-situ processes, and modifications to the internal-tin and jelly-roll Nb_3Sn conductors. A fundamental study of the origin of the strain effect will also be made.

This report is divided into five sections. Electromechanical-property data are presented in the first section for several experimental (short-length) superconductors, and in the second section for several commercial Nb_3Sn conductors that are present candidates for fusion applications. The transverse-pressure test apparatus, thermal-contraction data, and tunneling diagnostic probe are treated in Secs. 3, 4, and 5, respectively. References are given at the end of each section. The appendix contains a trip report covering superconductor-technology developments in Japan and two publications on relevant work performed under an earlier contract. The latter two treat electromechanical degradation in structurally reinforced Nb_3Sn conductors and details of liquid-tin-infiltrated Nb_3Sn superconductors described in Sec. 2C.

SUMMARY OF MAIN RESULTS:

* The first studies of strain vs. critical-current were made on a Chevrel-phase superconductor, $PbMo_6S_8$; Chevrel phase superconductors were found to have a large strain effect, comparable in magnitude to A-15 superconductors like Nb_3Sn.

* Electromechanical properties measurements of an experimental liquid-tin-infiltrated Nb_3Sn conductor showed it to have an irreversible-strain limit twice as large as bronze-process superconductors and a significantly higher overall critical-current density; the liquid-infiltration process thus has the potential for development of a practical Nb_3Sn conductor with both superior critical-current density and extremely good mechanical properties.

* Experimental internal-tin Nb_3Sn superconductors have a high irreversible-strain limit ($\sim$0.9%), but a low strain-free upper critical field and consequently low critical-current density at fields above 12 T.

* Experimental jelly-roll Nb_3Sn superconductors have a very low irreversible-strain limit (0.14%) but high overall critical-current density over a wide range of magnetic field compared with other long-length Nb_3Sn superconductors.

* Thermal contraction data were obtained on several new candidate materials for superconductor sheathing. With respect to degradation of the critical current from differential thermal contraction, it was found that high Mn stainless steel offers no significant advantage over JBK-75 and 300 series austenitic stainless steels as a Nb_3Sn reinforcing material.

* A new diagnostic tool for probing the energy gap of practical superconductors has been developed using electron tunneling.

The participation of a number of people in this project is gratefully acknowledged: M. Austin for performing some of the thermal expansion measurements; J. Sherman and M. Allen for their help in machining the apparatus; and D. Rule and V. Cima for their help in reducing much of the data. Many helpful discussions were held with the other members of the Superconductor and Magnetic Measurements group. Special thanks to A. F. Clark, R. B. Goldfarb, and L. F. Goodrich for a critical reading of this report.

CONTENTS

ELECTROMECHANICAL PROPERTIES OF SUPERCONDUCTORS FOR DOE FUSION APPLICATIONS

J. W. Ekin, J. Moreland, and J. C. Brauch

Electromagnetic Technology Division
National Bureau of Standards
Boulder, Colorado 80303

This is an interim report presenting data on superconductor performance under mechanical load, which are needed for the selection of superconductors and the mechanical design of superconducting magnets for DOE fusion energy systems. A further aim of the reported research is to measure and understand the electromechanical properties of promising new superconductor materials with strong application potential at high magnetic fields. Results include the following. The first strain vs. critical-current studies were made on a Chevrel-phase superconductor, $PbMo_6S_8$. Chevrel-phase superconductors were found to have a large strain effect, comparable in magnitude to A-15 superconductors like Nb_3Sn. Electromechanical-property measurements of an experimental liquid-tin-infiltrated Nb_3Sn conductor showed it to have an irreversible strain limit twice as large as bronze-process superconductors and a significantly higher overall critical-current density; the liquid-infiltration process thus has the potential for development of practical Nb_3Sn conductor with both superior critical-current density and extremely good mechanical properties. Electromechanical parameters were obtained on several Nb_3Sn conductors that are candidate materials for superconducting fusion magnets, including conductors fabricated by the bronze, internal-tin, and jelly-roll processes. Thermal contraction data are reported on several new structural materials for superconductor sheathing and reinforcement, and a new diagnostic tool for probing the energy gap of practical superconductors has been developed using electron tunneling.

Key words: electromechanical; electron tunneling; energy gap; fusion; ICCS superconductor; liquid-infiltration superconductor; Nb_3Sn; $PbMo_6S_8$; stress effect; transverse stress effect; uniaxial stress effect

UNIAXIAL STRAIN-EFFECT CHARACTERIZATION OF NEW HIGH-FIELD EXPERIMENTAL SUPERCONDUCTORS

1. "ELECTROMECHANICAL AND METALLURGICAL PROPERTIES OF LIQUID-INFILTRATION Nb-Ta/Sn MULTIFILAMENTARY SUPERCONDUCTORS" J. W. Ekin and M. Hong, Appl. Phys. Letters 45, 297 (1984).

2. "EFFECT OF UNIAXIAL STRAIN ON THE CRITICAL CURRENT AND CRITICAL FIELD OF CHEVREL PHASE $PbMo_6S_8$ SUPERCONDUCTORS" J. W. Ekin, T. Yamashita, and K. Hamasaki, IEEE Trans. Magn. MAG-21, 474 (1985).

3. "EFFECT OF UNIAXIAL STRAIN ON Nb_3Sn WITH Mg ADDITIONS" J. W. Ekin.

Appl. Phys. Letters 45, 297 (1984)

ELECTROMECHANICAL AND METALLURGICAL PROPERTIES OF LIQUID-INFILTRATION Nb-Ta/Sn MULTIFILAMENTARY SUPERCONDUCTORS

J. W. Ekin
National Bureau of Standards
Boulder, Colorado 80303

and

M. Hong
AT&T Bell Laboratories
Murray Hill, New Jersey 07974

Abstract

Data are presented on the strain dependence of the critical current and critical field of Nb-Ta/Sn superconductors fabricated by the liquid Sn infiltration process. The results show that liquid infiltrated Nb-Ta/Sn superconductors have several significant advantages over bronze-process Nb/Sn superconductors: an overall J_c that is 3 to 10 times higher for magnetic fields in the range 13 to 20 T, an irreversible (damage) strain limit twice as large, and a J_c elastic-strain sensitivity less than half as large at fields above $\sim$16 T. These improved properties are attributed to several unique characteristics of the liquid infiltration process: a tough Nb-Ta matrix, fine equiaxial A15 grains and a uniform stoichiometric Sn concentration.

This letter reports results showing that liquid-infiltrated Nb/Sn composites have a damage strain tolerance nearly double that of commercial bronze-process Nb_3Sn conductors and the highest overall critical-current density measured thus far for a Nb/Sn-based superconductor at fields above 13 T.

Unlike conventional bronze-process Nb_3Sn conductors, liquid-infiltrated Nb_3Sn conductors offer the possibility of simultaneously obtaining both a desirable metallurgical microstructure of small, equiaxial A15 grains and a uniform, stoichiometric Sn concentration across the reacted A15 region.[1-3] As a result, high critical temperatures of 17.9 K, determined inductively, with sharp transition width ($\leq$ 0.3 K) can be obtained along with extremely high critical current densities J_c (10^5 A/cm^2 at 12 T and 10^4 A/cm^2 at 19 T, both at 4.2 K).[3] The addition of 2 wt.% Ta to the niobium has been found to increase further the overall critical current to 1.6×10^4 A/cm^2 at 4.2 K and 20 T because of an enhancement of the bulk upper critical field, B^*_{c2} ($=\mu_o H^*_{c2}$).[4]

The question remained however of how the mechanical properties of liquid-infiltrated conductors compared with those of conventional bronze-process conductors. From the practical standpoint of conductor development, it is important to optimize not only J_c, but also the strain limit ε_{irrev} where the conductor is permanently damaged. Also, the strain sensitivity of the J_c of the conductor is significant in setting strain limits for the mechanical design of high field magnets.[5] It is the purpose of this letter to report measurements of the prestrain ε_m, ε_{irrev} and the strain sensitivity of J_c and H_{c2} for a liquid-infiltrated Nb-2wt.%Ta/Sn composite and compare the parameters for this type of conductor with those of conventional bronze-process Nb_3Sn conductors.

Liquid infiltrated Nb-2wt.%Ta/Sn composite wires were fabricated using laboratory-scale powder-metallurgy processing techniques. First, a Nb-2wt.%Ta alloyed ingot was made by arc-melting pure components under an argon atmosphere.

The starting materials were Nb and Ta with 99.9% purity and very low oxygen content. The arc furnace employed a water-cooled nonconsumable tungsten electrode and a copper hearth. High-purity argon was passed over heated zirconium to remove residual oxygen and nitrogen and through a cold trap to condense moisture before being introduced into the furnace. The samples were inverted on the copper hearth and remelted four times to completely alloy the Nb and Ta. No noticeable weight loss of Nb or Ta was observed after melting. The arc-cast ingot was heat treated in a vacuum furnace at 1250°C for 24 hours to achieve further homogenization. The Nb-2wt.%Ta alloyed powder was then obtained from the homogenized ingot using a hydride-dehydride technique. NbTa powder (∿37-50 μm) was put in a cylindrical rubber mold and isostatically compacted at 220 MPa to form a porous rod. The sintering process was conducted at 2250°C for one hour under a vacuum of 1.3×10^{-4} Pa. After sintering, the porous Nb-Ta rod was immersed in a liquid Sn bath for infiltration.

The infiltrated composite, consisting of a Nb-Ta matrix and a continuous three-dimensional network of Sn, was clad with monel 400 tubing for wire fabrication. The composite, 5 mm in diameter, was first swaged and then drawn down to 0.23 mm in diameter or smaller. No difficulty was encountered and no intermediate annealing was required during the wire drawing. Laboratory-scale Nb-Ta/Sn wires more than 20 meters long were obtained. A short sample for testing J_c vs. strain was prepared by chemically removing the monel and heat treating over a range of temperature from 750 C to 950 C to form the superconducting A15 phase. Copper stabilizer was later electroplated on the test sample. Note that all the processing steps are adaptable to industrial applications, except that the monel cladding would be replaced by a Ta diffusion barrier and copper stabilizer tube. In other tests, starting billets 13 mm in diameter have been drawn down to 0.13 mm in diameter, again with no

intermediate annealing required. Therefore, the scale-up of the liquid-infiltration Nb-Ta/Sn or Nb/Sn process is feasible. The overall chemical composition of the wires was (Nb-2wt.%Ta)-8wt.%Sn.

Critical temperatures (T_c) were measured inductively at a frequency of 100 Hz in an applied field of 4×10^{-5} T. Critical currents were obtained using an apparatus designed to simultaneously apply tensile strain, current, and a perpendicular magnetic field to short wire samples at 4.2 K. A detailed description is given in Reference 6. A critical-current criterion of 2 μV/cm was used. The overall noncopper critical current density described below was determined using the combined area of tin, superconductor and unreacted Nb, excluding only the copper-stabilizer area.

The data were also corrected for the current carried by the stabilizer, which can become significant at very high fields as B^*_{c2} is approached. This is accomplished by measuring the resistance of the conductor in the normal state, R_n, either at fields above the critical field or above the critical strain.[7] The normal current carried by the conductor is then calculated as $I_n = E_c/R_n$, where E_c is the electric field criterion used to determine the critical current. I_n is then subtracted from the measured critical current to obtain the true critical current of the superconductor. For this sample I_n was determined to be 21 mA, which amounts to about 4% of I_c at 23 T, and becomes rapidly less significant at lower fields.

Figure 1 shows the strain dependence of the critical current at fields ($B = \mu_o H$) from 10 to 23 T. Data were obtained by measuring the critical current density J_c as a function of magnetic field under constant applied strain. The strain was then increased, and J_c again obtained as a function of B. The process was repeated for higher and higher strains until eventually the superconductor was permanently damaged at the irreversible strain point

ε_{irrev}.[8] From these data the J_c vs. ε curves of Fig. 1 were obtained. It is seen that J_c passes through a maximum at a strain ε_m of 0.13%. This is quite low compared to conventional bronze-process Nb_3Sn conductors where ε_m is typically between 0.2 and 0.4%.[8] The low value of ε_m is the result of the absence of a bronze matrix in liquid-infiltrated conductors; thermal contraction of the bronze matrix material is primarily responsible for the compressive prestrain introduced into the Nb_3Sn reaction layer of conventional bronze-process conductors.

The irreversible strain limit ε_{irrev} was determined by measuring the unloaded J_c at 10 T only. The + symbols in Fig. 1 indicate the critical current measured after unloading from the correspondingly labeled strain point. These data indicate the irreversible strain limit for this conductor is more than 1.1%. This corresponds to an intrinsic irreversible strain limit $\varepsilon_{o,irrev} = \varepsilon_{irrev} - \varepsilon_m$ of about 0.9%, which is nearly double that of bronze-process conductors. There $\varepsilon_{o,irrev}$ is consistently about 0.5% regardless of the value of ε_m. Consequently, the bending strain limits on the mechanical design of high-field magnets are also about double those of bronze process conductors.

The high irreversible strain limit ε_{irrev} can be explained by the unique metallurgical microstructures created in the reacted Nb-Ta/Sn composite wire. Prior to the reaction to form the superconducting A15 phase, an extremely high density of dislocation was observed in the Nb-Ta matrix, which is due to heavy deformation during the wire drawing process. Reaction at 750-900°C promptly formed the A15 phase. However, the existing dislocations in the matrix would not be annealed out since the reaction temperature was very low compared to the melting point of the Nb-Ta alloy. This was confirmed with high-resolution transmission electron microscopy as shown in Fig. 2. It is observed that a

very high density of dislocations still remains in the Nb-Ta matrix and the dislocation-free region is the A15 phase with small, equiaxial grains. In contrast to this, the dislocations in the Cu-Sn matrix of the bronze-process Nb-Sn wires were completely annealed out during the heat treatment because of the low melting point of the Cu-Sn. Therefore, after reaction the liquid infiltrated Nb-Ta/Sn wires still maintain a strong matrix while the conventional bronze-process Nb/Sn wires possess a soft Cu-Sn matrix.

During the reaction, the Nb-Ta dominantly and swiftly diffused into the liquid Sn because more defects were created in the liquid Sn than in the solid Nb-Ta. However, a small amount of Sn also quickly spread over the Nb-Ta matrix via pipe diffusion (because of the high density of dislocations) and by grain boundary diffusion. These were observed with a scanning transmission electron microscope coupled with an energy dispersive x-ray spectrometer.

The rapid solid (Nb-Ta)/liquid (Sn) interaction produces fine, equiaxial A15 grains across the reacted filament. This microstructure results from the random A15 nucleation sites in the liquid Sn region, which cannot be obtained from solid-state diffusion that occurs in bronze-process Nb/Sn wire. The A15 filaments, between 0.2 and 1.0 μm, lie parallel to each other about 5 μm apart. The fine A15 filaments are also in strong contrast to those in the bronze-process wires which are typically more than 4.0 μm in diameter.

As has been discussed, a tough Nb-Ta matrix was strengthened by the high density of dislocations along with some Sn alloying. This, coupled with small A15 grains, fine A15 filaments and interfilament spacing contribute to the high irreversible strain limit ε_{irrev}.

Figure 3 shows a comparison of the peak (nearly strain-free) critical current density at ε_m for the liquid infiltrated conductor of this study, a typical conventional bronze-process conductor, and a $NbSn_2$ powder conductor.

Note that a comparison of peak J_c values eliminates the effect of varying compressive prestress among different conductors, which can result in misleading comparison of initial (as-received) J_c values.[7] Figure 3 shows the critical current density of the liquid infiltrated conductor to be more than three times greater than bronze-process conductors at low fields and more than an order of magnitude greater at high fields. This is the largest overall J_c measured for a Nb/Sn conductor over the field range from 13 T to 20 T. The overall critical current density is about 1.8×10^4 A/cm^2 at 20 T, which is high enough for consideration of Nb/Sn superconducting magnets designed to be used at or above 20 T. The extremely high overall J_c at high fields is the result of the combination of a unique A15 microstructure, as was discussed earlier in this paper, and a uniform stoichiometric Sn concentration across the A15 region. The latter phenomenon can be explained by a new Nb-Sn phase diagram[2,3,9] in which the phase spread of the A15 structure is considerably narrower than that of the previously accepted phase diagram.[10]

Figure 4 shows the bulk average upper-critical field B^*_{c2} as a function of strain. B^*_{c2} is the field at which the pinning force extrapolates to zero. It was determined by fitting the measured pinning force curve, $F(\equiv J_c B)$ vs. B, at a given strain level to a general function suggested by pinning theories: $J_c B = A\,(B/B^*_{c2})^p\,(1 - B/B^*_{c2})^q$. The fit is made in terms of the four parameters B^*_{c2}, A, p, and q. Here p and q are independent of strain and had the values of 0.5 and 1.4, respectively.[6] The strain dependence of B^*_{c2} for the liquid-infiltrated conductor is shown in Fig. 4 by open circles. The solid line represents the nearly universal strain dependence of B^*_{c2} for bronze-process binary Nb_3Sn. As seen in Fig. 4, the elastic strain dependence of B^*_{c2} for liquid-tin infiltrated Nb_3Sn with 2 wt.% Ta added is nearly identical to that of bronze-process Nb_3Sn conductors.

Although the elastic strain dependence of B^*_{c2} is nearly the same for the two types of conductors, the dependence of J_c on elastic strain is very different. This arises from two factors.[11] First, the peak (nearly strain free) bulk upper critical field B^*_{c2} for the liquid infiltrated Nb-2wt.%Ta/Sn conductor was approximately 23.5 T compared with a B^*_{c2m} of about 21 T for bronze-process Nb_3Sn. Thus, for a given field, J_c of the liquid-infiltrated Nb-2wt.%Ta/Sn conductor is less affected by strain because the reduced field ($b = B/B^*_{c2}$) of this conductor is smaller. The further B is from B^*_{c2}, the less J_c is affected by the strain-degradation of B^*_{c2}. Secondly, the pinning force F of the Nb-Ta/Sn conductor approaches zero as $(1-b)^{1.4}$ rather than $(1-b)^2$, as in the case of binary Nb_3Sn. The steeper the slope of the F vs. B characteristic of a conductor, the more sensitive is J_c to changes in B^*_{c2}.[11] Thus, for both these reasons, the elastic strain sensitivity of J_c in the Nb-2wt.%Ta/Sn conductor is less than that of binary Nb_3Sn. Further enhancement of B^*_{c2m} by additions of Ta slightly greater than 2 wt.% should produce higher values of J_c and further reductions in the J_c strain sensitivity.[12]

In summary, Nb-Ta/Sn conductors fabricated by the liquid Sn-infiltration process offer a unique combination: an overall J_c which is 3 to 10 times higher than conventional bronze-process multifilamentary Nb/Sn conductors, an irreversible (damage) strain limit twice as large, and a J_c elastic strain sensitivity comparable to other Nb_3Sn conductors with ternary additions.

Valuable discussions and experimental assistance from J. T. Holthuis of Lawrence Berkeley Laboratory are gratefully acknowledged. The authors thank J. C. Brauch for his assistance in reducing the data. The support of part of this work by the Naval Ship Research and Development Center and the Center for Electronics and Electrical Engineering, National Bureau of Standards is gratefully acknowledged.

References

1. M. Hong, G. W. Hull, Jr., J. T. Holthuis, W. V. Hassenzahl, and J. M. Hong, Appl. Phys. Lett. 42:621 (1983).
2. M. Hong, G. W. Hull, Jr., J. T. Holthuis, W. V. Hassenzahl, and J. W. Ekin, IEEE Trans. Magn. MAG-19:912 (1983).
3. M. Hong, F. Hellman, D. M. Maher, G. W. Hull, Jr., and T. H. Geballe (unpublished).
4. M. Hong, G. W. Hull, Jr., E. O. Fuchs, and J. T. Holthuis, Materials Lett. 2(2) (1983).
5. J. W. Ekin, Ch. 7 in: Superconductor Materials Science, S. Foner and B. Schwartz, eds., Plenum Press, New York (1981) pp. 455-509.
6. J. W. Ekin, Cryogenics 20:611 (1980).
7. J. W. Ekin, "Strain Effects in Superconducting Compounds - An Overview and Synthesis," Adv. Cryog. Eng. 30:823 (1984).
8. J. W. Ekin, IEEE Trans. Magn. MAG-15:197 (1979).
9. R. A. Shiffman and D. M. Bailey, High Temperature Science 15:165 (1982).
10. J. P. Charlesworth, I. Macphail, and P. E. Madsen, J. Mat. Sci. 5:580 (1970).
11. J. W. Ekin, H. Sekine, and K. Tachikawa, J. Appl. Phys. 52:6252 (1981).
12. See Figure 6 in D. O. Welch, Adv. Cryog. Eng. 30:671 (1984).

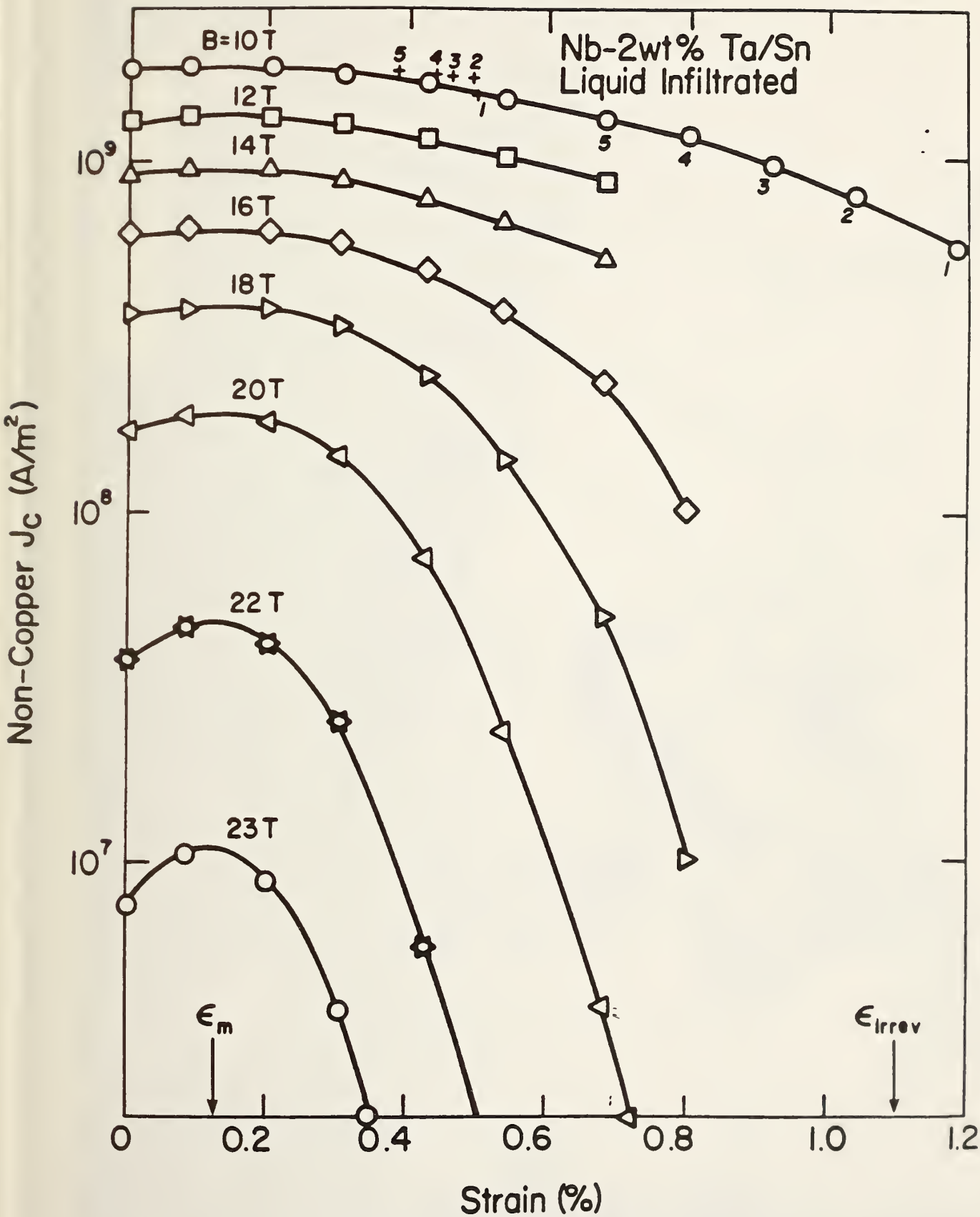

Fig. 1. Effect of uniaxial tensile strain on the critical current of a liquid-infiltrated Nb-2wt.%Ta/Sn superconductor at magnetic fields from 10 to 23 T. The parameter ϵ_m indicates the strain at which the critical current is a maximum; ϵ_{irrev} indicates the irreversible strain limit where the superconductor is permanently damaged.

Fig. 2. Typical transmission electron micrograph showing fine equiaxed A15 grains embedded in the Nb-Ta matrix filled with a high density of dislocations. The mark in the figure is 0.1 μm long.

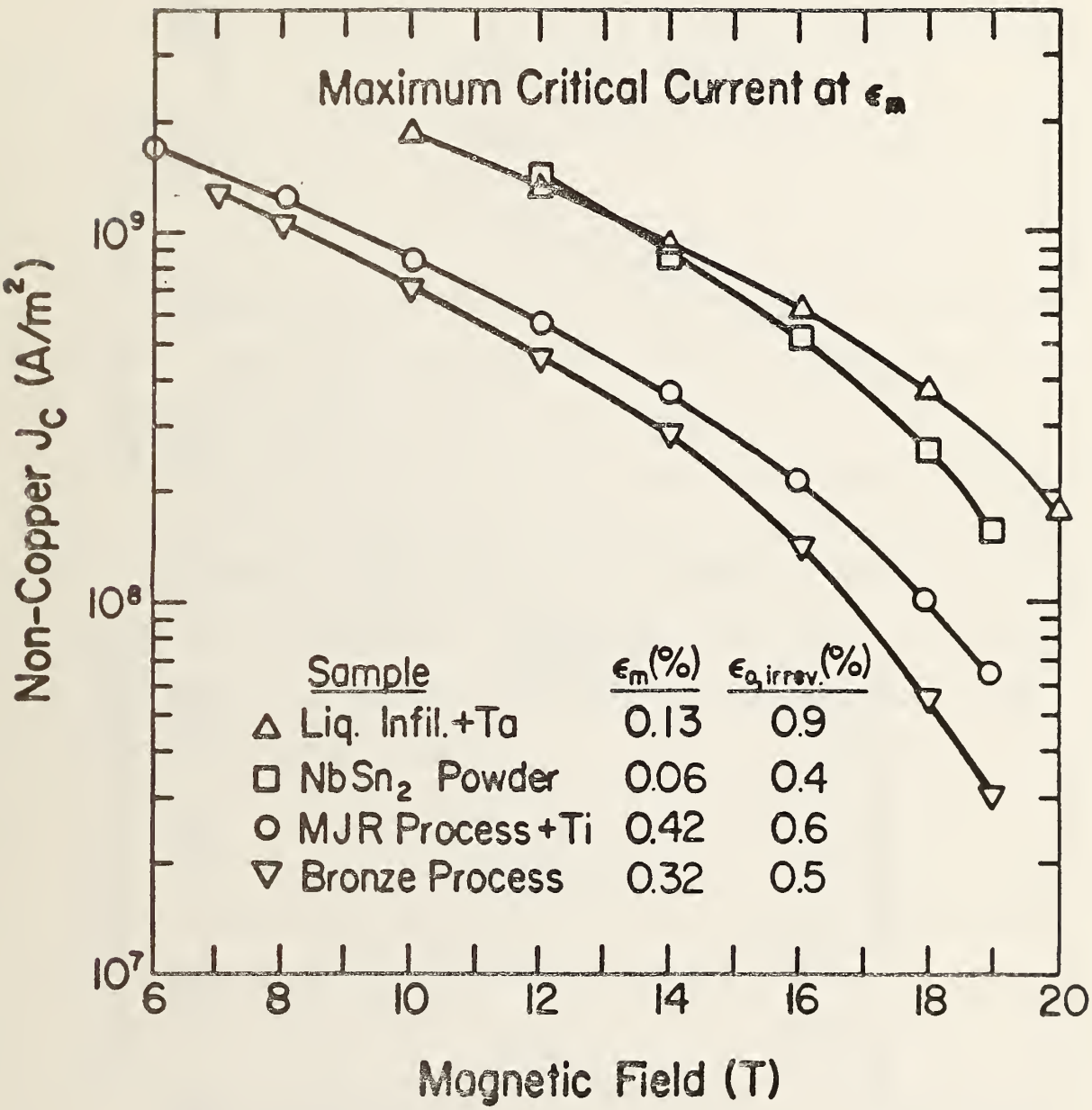

Fig. 3. Comparison of peak critical-current densities measured at ε_m for several Nb/Sn based superconductors: triangle - liquid Sn infiltrated, 2 wt.%Ta added to Nb; square - $NbSn_2$ powder process; circle - modified jelly roll process, 1.5 at.%Ti added to Nb; inverted triangle - 13wt%Sn bronze process.

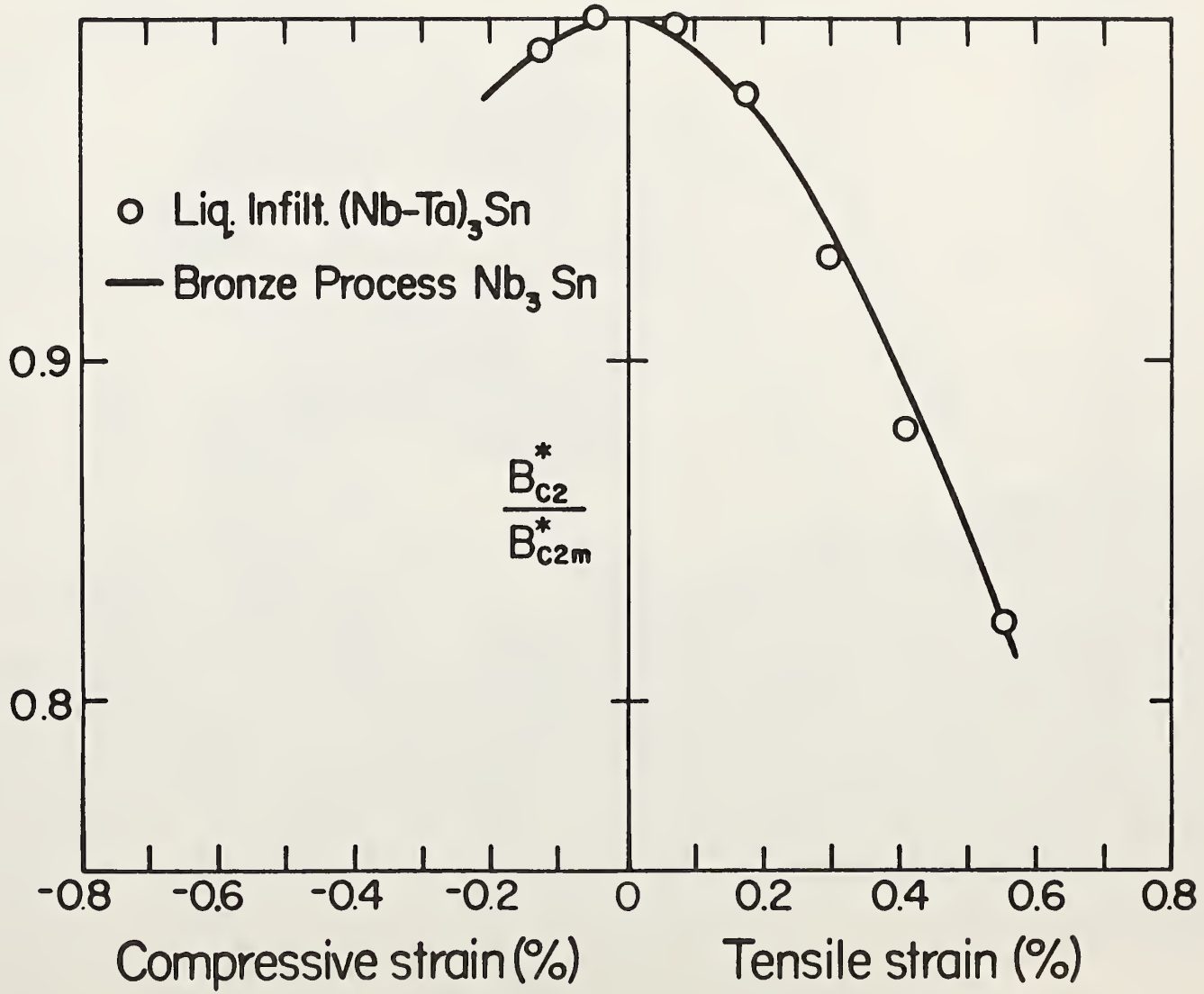

Fig. 4. Comparison of the relative effect of uniaxial strain on the upper critical field of liquid-infiltrated Nb-Ta/Sn and commercial bronze-process Nb_3Sn superconductors. The maximum value of the upper critical field, B^*_{c2m}, is 23.5 T for the Nb-Ta/Sn conductor compared with approximately 21 T for commercial Nb_3Sn superconductors.

IEEE Trans. Magn. MAG-21, 474 (1985)

EFFECT OF UNIAXIAL STRAIN ON THE CRITICAL CURRENT AND CRITICAL FIELD OF CHEVREL PHASE $PbMo_6S_8$ SUPERCONDUCTORS*

J. W. Ekin
National Bureau of Standards
Boulder, Colorado 80303

and

T. Yamashita and K. Hamasaki
Technical University of Nagaoka
Nagaoka, Japan

Abstract

The first measurements of the effect of uniaxial strain on the critical current of a Chevrel phase superconductor, $PbMo_6S_8$, have been obtained at 4.2 K in magnetic fields from 2 T to 24 T. The data show there is a very significant reversible effect of elastic strain on the critical current of $PbMo_6S_8$, comparable in magnitude to that observed in Nb_3Sn. This is because both the peak pinning force and upper critical field are very sensitive to elastic strain. A correlation is made between the elastic strain effect, radiation sensitivity, and phonon anharmonicity in the A15, B1, C15, and Chevrel phase superconductors.

Introduction

All A15 superconductors tested thus far show a significant reversible effect of uniaxial strain on their critical current,[1 10] critical field,[4,11] and critical temperature.[12,13] All B1 and C15 superconductors tested thus far show no measurable strain effect.[14 16] What about Chevrel phase superconductors? No electromechanical measurements on the critical parameters of these superconductors have been reported. The objective of this study was to have a first look at the effect of uniaxial strain on the critical current and critical field of a Chevrel phase superconductor, $PbMo_6S_8$. Critical current

versus strain measurements were made over a wide range of magnetic field from 2 T to 24 T. This was done in order to study the effect of strain on both the peak pinning force (which dominates the character of the critical current at low fields) and the upper critical field (which dominates at high fields).

Sample Preparation

Tests were conducted on both wire and tape samples, each made by an electroplating technique.[17,18] For the wire sample, a Mo wire of 0.3 mm diameter was electroplated with lead. The plating time was adjusted to produce a layer of lead approximately 0.5 mm thick on the surface of the Mo wire. The wire was then sealed in an evacuated quartz tube with crushed MoS_2 powder. The quartz tube was heated to about 1000°C, and held there for 6 to 14 hours. After heat treatment, it was slowly cooled to room temperature in about 5 hours. The final sample was a wire with a Mo core of about 220 μm diameter and a Pb-Mo-S layer about 110 μm thick. The sample was then coated with additional lead to stabilize the superconductor for critical-current testing.

*Contribution of NBS, not subject to copyright.

Manuscript received September 10, 1984

The $PbMo_6S_8$ tape sample was made by electroplating a Mo tape, 1.5 mm wide and 50 μm thick, with lead. The tape was then heat treated in MoS_2 vapor for 14 hours at about 1000°C. The final sample was a tape with a Mo core less than 10 μm thick, surrounded by a $PbMo_6S_8$ layer about 125 μm thick. The tape was then coated with additional lead for stabilization.

Data were obtained using a high-field uniaxial-strain apparatus described previously.[6] A 2 μV/cm electric-field criterion was used in determining the critical-current values presented below. Accuracy of the critical current measurements is about ±1%. The strain was measured to within ±0.02%.

Results

Effect of Uniaxial Strain on Critical Current

Figure 1 shows the effect of uniaxial strain ε on the critical current I_c of the $PbMo_6S_8$ wire sample at magnetic fields from 2 T to 19.5 T. The strain effect was reversible for strains less than 0.2%; that is, below 0.2% the critical current recovered to its former value upon removing the uniaxial force on the superconductor. Beyond 0.2% strain, however, the critical current did not completely recover when the force was removed, indicating the onset of permanent damage.

Up to this irreversible strain limit the critical current of $PbMo_6S_8$ showed a dramatic dependence on elastic strain (note that the ordinate is a logarithmic scale). This reversible strain effect is comparable in size to that seen in Nb_3Sn. Figure 2 shows the elastic strain effect in a typical multifilamentary Nb_3Sn conductor strand[6] for comparison. The large percentage change in the critical current of both types of superconductors is noted. The reversible degradation of the critical current of $PbMo_6S_8$ at strains less than 0.2% (the irreversible strain limit) amounts to about a 20% change in I_c at low fields (2 T), 40% at high fields (18 T).

A major difference between the two types of superconductors is the scaling of the strain effect with magnetic field. In Nb_3Sn the sensitivity of the critical current to uniaxial strain at low fields is relatively small, but increases significantly as the field is increased. In $PbMo_6S_8$, on the other hand, the strain sensitivity of the critical current is relatively great at both low and high fields. This is due to a combination of the very high upper critical field in $PbMo_6S_8$ and the relatively high strain sensitivity of the pinning force in $PbMo_6S_8$, as described in more detail in the Discussion and Summary section.

Another difference between Figs. 1 and 2 is the absence of any peak in the J_c versus ε curves for $PbMo_6S_8$. This results from the inverse differential thermal contraction between the superconducting material and matrix in $PbMo_6S_8$ compared with Nb_3Sn. In bronze-process Nb_3Sn conductors, the bronze matrix contacts more than the Nb_3Sn, placing the superconductor in compression when cooled from the reaction temperature of 700°C. Mo, however, contracts about three times less than the $PbMo_6S_8$ on cooling from the reaction temperature of about 1000°C.[19] In the $PbMo_6S_8$ conductors studied here, this places the $PbMo_6S_8$ portion of the conductor under axial tension (and radially into compression, probably enhancing the shear strain effect). In the wire $PbMo_6S_8$ sample, the effect of the Mo is relatively large because the volume ratio of $PbMo_6S_8$-to-Mo in this sample is only 1.8.

Consequently a tape $PbMo_6S_8$ sample was tested, because with the tape geometry a ∿50% higher volume ratio of $PbMo_6S_8$-to-Mo could be obtained and the amount of axial pretension reduced. Figure 3 shows the I_c versus ε data obtained in a $PbMo_6S_8$ tape sample with a $PbMo_6S_8$-to-Mo ratio of 2.9. The effect of uniaxial strain on the critical current of the tape sample was reversible up to the fracture strain of ∿0.4%. The tensile prestrain in this

sample is smaller, near zero (<0.05%), as evidenced by the nearly zero slope of the I_c versus ε curves at zero applied strain. Figure 3 can be compared directly with the data for Nb_3Sn in Fig. 2 by considering only the tensile side of the Nb_3Sn data (that is, the unshaded region in Fig. 2).

The tensile prestrain initially present in the wire $PbMo_6S_8$ sample was determined to be about +0.2% from a correlation of the I_c versus ε data in Fig. 3 with those in Fig. 1. This prestrain value is also consistent with an approximate analysis of the differential thermal contraction rates and volume fractions of $PbMo_6S_8$ and Mo in each conductor. Thus the data on the wire $PbMo_6S_8$ sample in Fig. 1 should be compared with the Nb_3Sn data at strains above 0.5% in Fig. 2. Also note that the initial I_c values for the $PbMo_6S_8$ wire sample are not optimum strain-free values, but are degraded by the tensile prestrain about 10% at low fields, 15% at high fields.

Effect of Uniaxial Strain on B_{c2}

The strain dependence of the upper critical field B_{c2} ($B = \mu_o H$) of $PbMo_6S_8$ was determined by fitting the I_c versus B curve at constant strain to a general function suggested by pinning theory: $J_c B = K(B/B^*_{c2m})^p(1-B/B^*_{c2})^q$. The fit is made in terms of the four parameters B^*_{c2}, K, p, and q. Here K is a strain-dependent parameter proportional to the peak pinning force, and p and q are parameters independent of strain that were measured to have the values 0.14 and 1.8 respectively. The asterisk on B^*_{c2} indicates a bulk average upper-critical field.

Figure 4 shows the results obtained for B^*_{c2} as a function of strain. The results for the wire and tape $PbMo_6S_8$ samples have been combined assuming $\varepsilon_m = 0\%$ for the tape conductor and $\varepsilon_m = 0.2\%$ tension for the wire conductor. The maximum strain-free value of B^*_{c2} at 4.2 K was $B^*_{c2m} \cong 36$ T. The results

shown in Fig. 4 indicate that the relative degradation of B^*_{c2} for $PbMo_6S_8$ is comparable or slightly greater than in Nb_3Sn. For Nb_3Sn under tension, $d(\ln B^*_{c2})/d(@e@^{1.7}) = 1250,6$ whereas for $PbMo_6S_8$, the preliminary value obtained from Fig. 4 is $d(\ln B^*_{c2})/d(@e@^{1.7}) = 1600$. Thus the effect of strain on the upper critical field of $PbMo_6S_8$ is relatively large, comparable to, or even slightly greater than for Nb_3Sn.

Effect of Strain on Peak Pinning Force

The relative strain dependence of the peak pinning force of $PbMo_6S_8$ is contained in the parameter "K" described in the preceding section. For the A15 superconductors, the relative strain sensitivity of the peak pinning force is nearly identical with that of the strain sensitivity of B^*_{c2}. That is, K(e) a $B^*_{c2}(e)$. However, for $PbMo_6S_8$, K(e) a $[B^*_{c2}(e)]^n$, where n was measured to be in the range from 2 to 3.

Discussion and Summary

At low magnetic fields (less than about half B^*_{c2}) the character of the critical current is dominated by the peak pinning force.6 Thus, in comparing Figs. 1-3, the strain sensitivity of $PbMo_6S_8$ is greater than that of Nb_3Sn mainly because of the very large effect of strain on the peak pinning force of $PbMo_6S_8$ relative to Nb_3Sn.

At high fields, in contrast, the behavior of the critical current is dominated by B^*_{c2}.6 Since B^*_{c2} is much larger in $PbMo_6S_8$ than in Nb_3Sn, its effect on the critical current of $PbMo_6S_8$ is smaller, even though the strain sensitivity of B^*_{c2} in $PbMo_6S_8$ is comparable to that of Nb_3Sn. For example, the effect of strain on the critical current of Nb_3Sn at 19 T in Fig. 2 is greater than in $PbMo_6S_8$ because these data were obtained very close to the

B^*_{c2m} of Nb_3Sn (21 T). In $PbMo_6S_8$, however, the maximum field where data was obtained (24 T) is still only about 66% of B^*_{c2m} (36 T). Thus, because of the high value of B^*_{c2m} in $PbMo_6S_8$, the relative effect of strain on the critical current of $PbMo_6S_8$ is smaller than in Nb_3Sn at fields above $^{3}14$ T.

The large reversible effect of strain on the critical current of $PbMo_6S_8$ probably accounts partially for the unexpectedly low critical-current densities reported in several earlier studies. For example, in their comprehensive grain-size study of $PbMo_6S_8$ Seeber et al.[19] noted that the observed critical-current density was lower than they had expected based on a grain-boundary pinning model. They speculated this was due to cracks and deformation. This is probably the main reason, but our results show that the low critical-current density may be due also, at least in part, to reversible degradation of the critical current caused by differential thermal contraction between $PbMo_6S_8$ and the Mo matrix material in their samples. The volume ratio of $PbMo_6S_8$ to Mo in their wire samples was about 0.3, considerably less than the ratios of 3 and 28 for the samples measured in this study. This would have resulted in more tensile prestrain in the $PbMo_6S_8$ layer of their samples and an accompanying large I_c degradation.

In summary, these data show that uniaxial strain has a significant effect on I_c and B^*_{c2} of $PbMo_6S_8$. The effect is reversible, up to an intrinsic irreversible strain limit of $^{3}0.4\%$ for these samples. At low magnetic fields the strain effect on the critical current is greater than in Nb_3Sn and results from a peak pinning force which is more sensitive to strain than in Nb_3Sn. At high fields the strain effect on the critical current results from an upper critical field which has a strain sensitivity comparable to that of Nb_3Sn. However, the effect on the critical current of $PbMo_6S_8$ is less than in Nb_3Sn at fields above $^{3}14$ T because the value of B^*_{c2m} for $PbMo_6S_8$ is much greater than for Nb_3Sn.

Generalizing from the fact that every A15 superconductor tested so far exhibits a significant strain effect,10 it is anticipated that the elastic strain sensitivity of the critical parameters of $PbMo_6S_8$ will extend to the entire class of Chevrel phase superconductors. Unlike the B1 and C15 superconductors, both A15 and Chevrel phase superconductors have significant phonon anharmonicity at liquid helium temperatures, which could account for the extreme elastic strain sensitivity of their superconducting properties.10

The same correlation with crystal phase also occurs for radiation damage. The critical current of both A15 and Chevrel phase superconductors is much more susceptible to radiation damage than the B1 and C15 superconductors.

Acknowledgments

This work was sponsored by the Department of Energy, Office of Fusion Energy under interagency agreement #DE-AI01-84ER52113. The high magnetic fields needed for this study were obtained using the National Magnet Laboratory magnet facilities. The assistance of J. C. Brauch in reducing the data is gratefully acknowledged.

References

1. J. W. Ekin, Appl. Phys. Lett. 29, 216 (1976).
2. D. S. Easton, R. E. Schwall, Appl. Phys. Lett. 29, 319 (1976).
3. J. L. McDougall, Proc. of the Int'l. Cryogenic Eng. Conf., IPC Science and Technology Press, 6, 396 (1976).
4. J. W. Ekin, IEEE Trans. Magn. MAG-15, 197 (1979).
5. R. Roberge, S. Foner, E. J. McNiff, Jr., B. B. Schwartz, and J. L. Fihey, IEEE Trans. Magn. MAG-13, 687 (1977).
6. J. W. Ekin, Cryogenics 20, 611 (1980).
7. D. U. Gubser, T. L. Francavilla, D. G. Howe, and L. D. Jones, Appl. Phys. Lett. 31, 230 (1977).
8. J. W. Ekin, IEEE Trans. Magn. MAG-17, 658 (1981).
9. J. W. Ekin and A. I. Braginski, IEEE Trans. Magn. MAG-15, 509 (1980).
10. J. W. Ekin, Adv. Cryog. Eng. 30, 823 (1984).
11. G. Rupp, IEEE Trans. Magn. MAG-15, 189 (1979).
12. T. Luhman and M. Suenaga, IEEE Trans. Magn. MAG-13, 800 (1977).

13. H. Hillman, H. Kuckuck, H. Pfister, G. Rupp, E. Springer, M. Wilhelm, K. Wohlleben, and G. Ziegler, IEEE Trans. Magn. MAG-13, 792 (1977). G. Rupp, IEEE Trans. Magn. MAG-13, 1565 (1977).
14. J. W. Ekin, J. R. Gavaler, and J. Greggi, Appl. Phys. Lett. 41, 996 (1982).
15. K. Inoue, H. Wada, T. Kuroda, and K. Tachikawa, Appl. Phys. Lett. 38, 939 (1981).
16. H. Wada, K. Inoue, K. Tachikawa, and J. W. Ekin, Appl. Phys. Lett. 40, 844 (1982).
17. K. Hamasaki, T. Yamashita, T.Komata, K. Noto, and K. Watanabe, Adv. Cryog. Eng. 30, 715 (1984).
18. K. Hamasaki, K. Hirata, T. Yamashita, T. Komata, K. Noto, and K. Watanabe, to be published.
19. B. Seeber, C. Rossel, O. Fischer, and W. Glaetyle, IEEE Trans. Magn. MAG-19, 402 (1983).

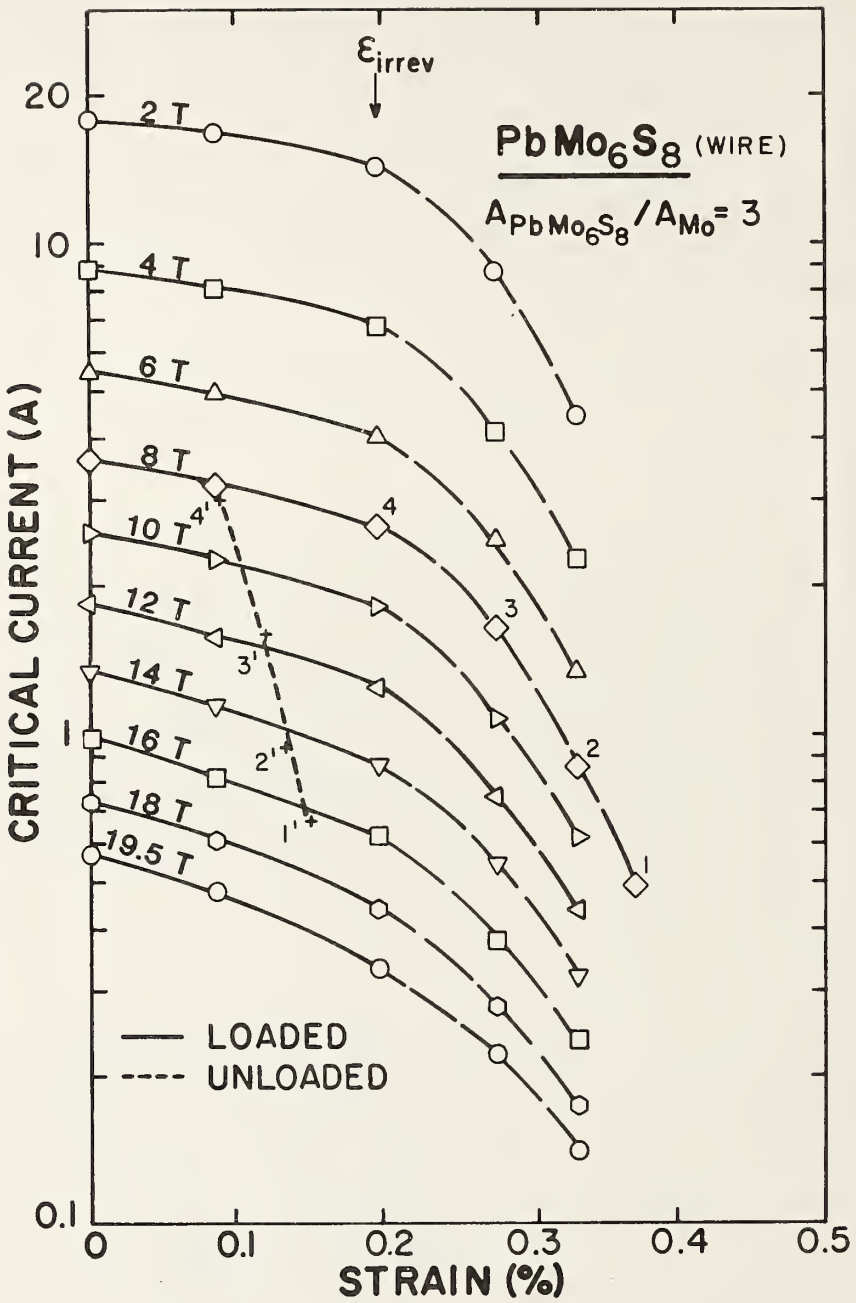

Fig. 1. Uniaxial-strain dependence of the critical current of a $PbMo_6S_8$ wire superconductor. The prestrain introduced by the Mo matrix is tensile, resulting in no maximum in the I_c-versus-e curve. e_{irrev} is the uniaxial strain where the the superconductor is permanently damaged, indicated by the I_c-versus-e curve being irreversible upon unloading. (Short-dashed curve and crosses + show the critical current after unloading.)

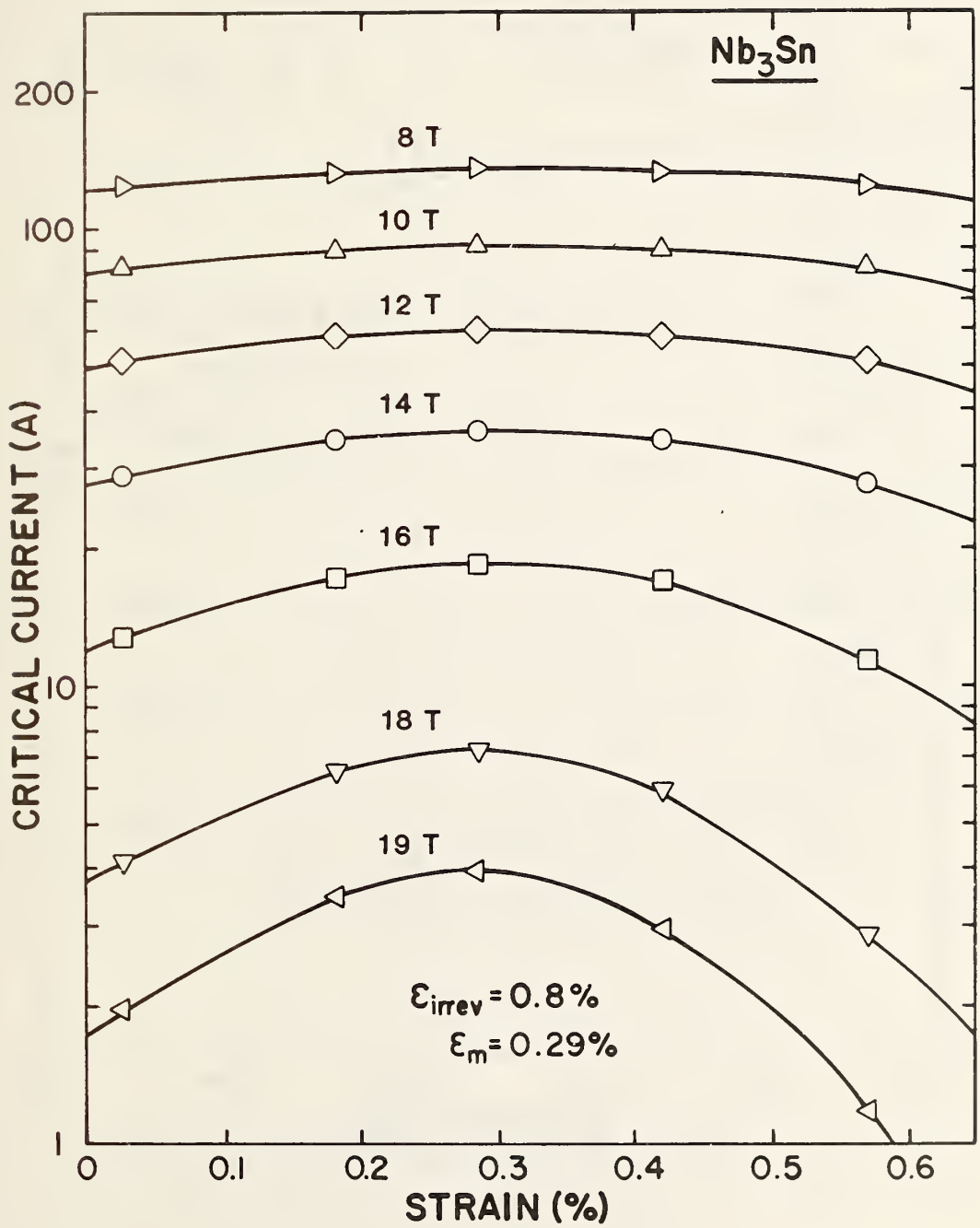

Fig. 2. Uniaxial-strain dependence of the critical current of a typical bronze-process Nb_3Sn superconductor. Data of Fig. 1 should be compared with these data at strains above $^{3}0.5\%$. Data of Fig. 3 should be compared with these data at strains beyond the maximum at 0.29% strain.

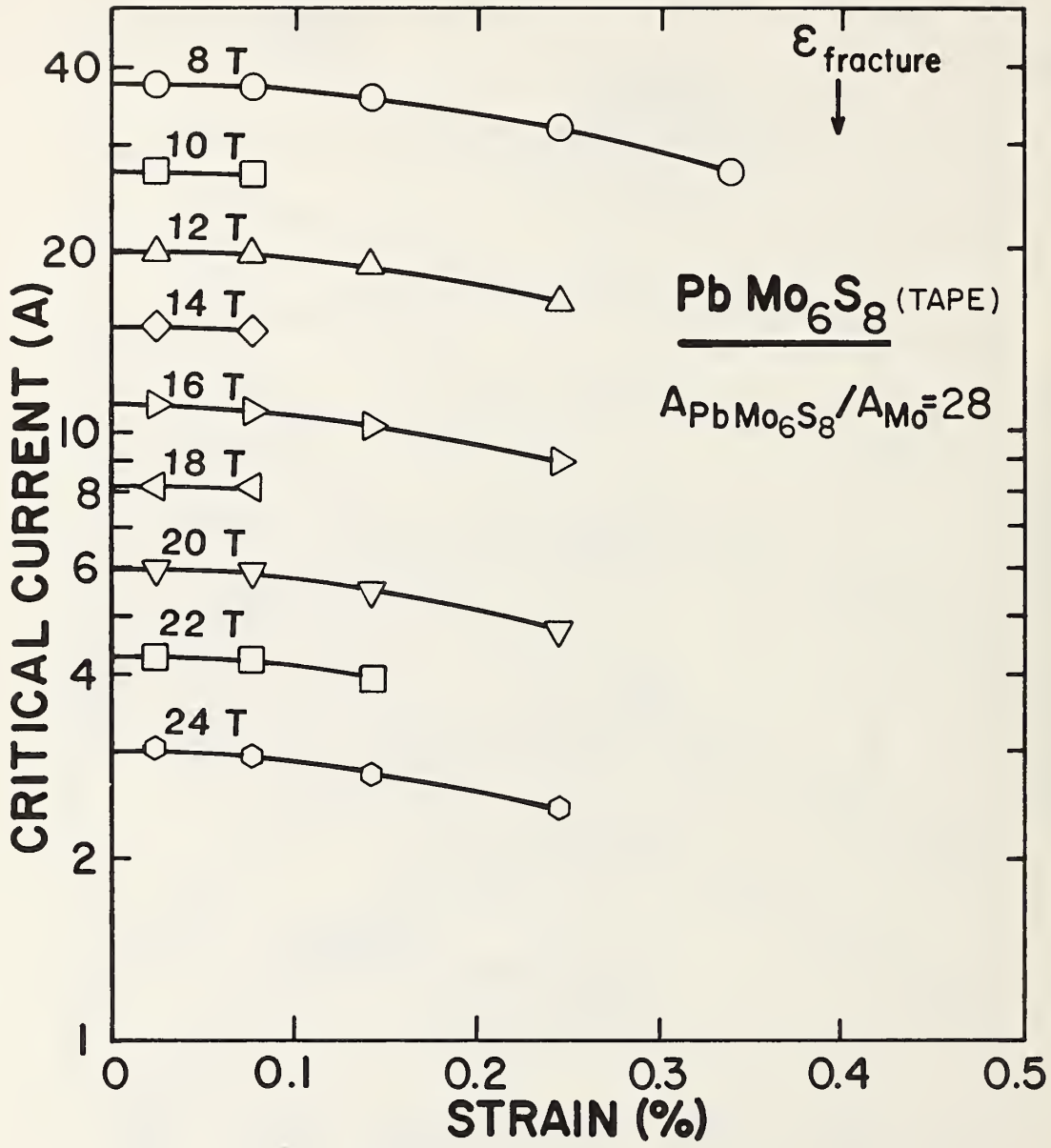

Fig. 3. Uniaxial-strain dependence of the critical current of a $PbMo_6S_8$ tape superconductor. The tensile prestrain introduced by the Mo matrix is small because of the greater $PbMo_6S_8$-to-Mo ratio in the sample compared with the $PbMo_6S_8$ wire sample of Fig. 1. The critical current versus strain curve was reversible up to the fracture strain.

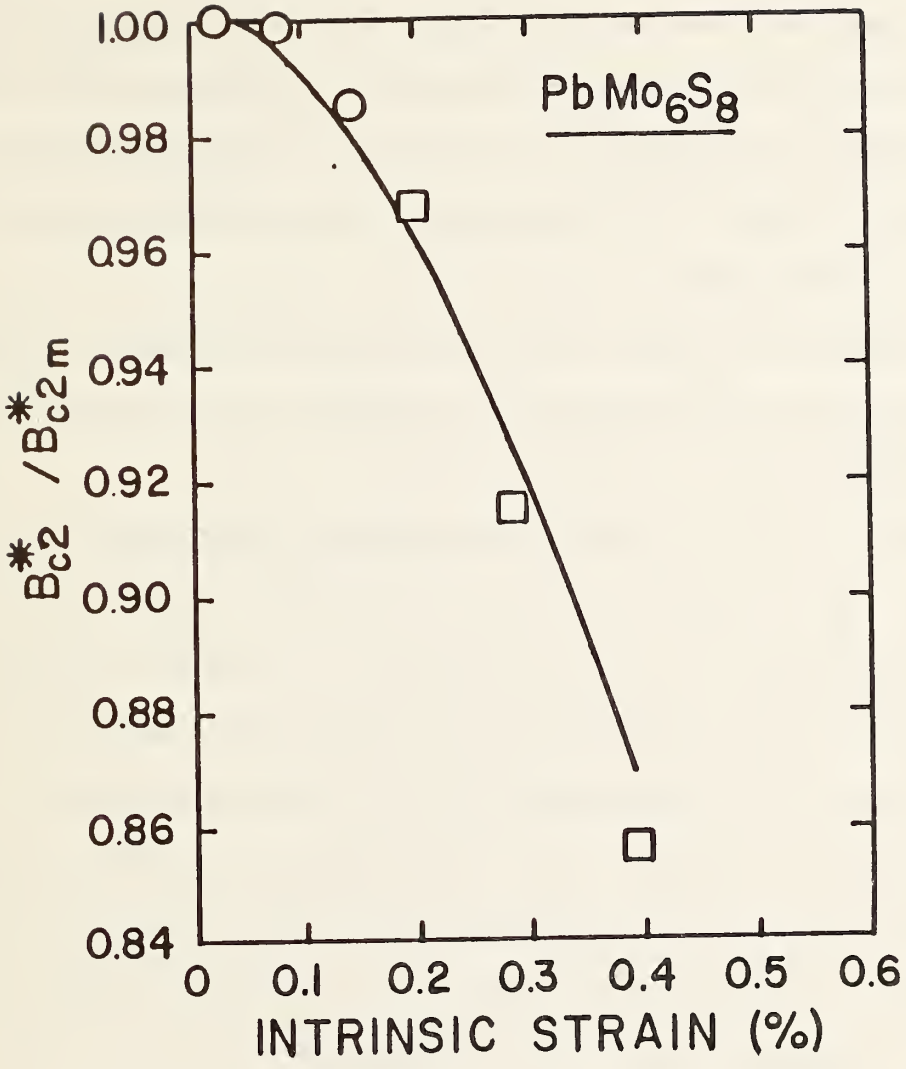

Fig. 4. Uniaxial strain dependence of the upper critical field B^*_{c2} for $PbMo_6S_8$. The maximum (nearly-strain-free) value of the critical field, B^*_{c2m}, at 4.2 K was approximately 36 T. Values of B^*_{c2}/B^*_{c2m} for both the wire and tape samples have been combined in this plot assuming no prestrain for the tape sample and a tensile prestrain of about 0.2% for the wire sample. (Circles indicate the tape data, squares the wire data.)

EFFECT OF UNIAXIAL STRAIN ON Nb_3Sn WITH Mg ADDITIONS

J. W. Ekin

This experimental conductor was made at Lawrence Berkeley Laboratory and is described in a paper by J. W. Wi et al, Appl. Phys. Lett. 45, 792 (1984). It contained 0.35 at % Mg in the bronze matrix prior to reaction. The test apparatus for obtaining these data and the procedure have already been described in Cryogenics 20, 614 (1980). A 2 μV/cm electric field criterion was used in determining the critical current.

The results are shown in Figs. 1 and 2 and listed in the Table. The main conclusions regarding the electromechanical properties of this conductor include the following:

1. The conductor had a very high strain ε_m where J_c is maximum, almost 0.8% (see Fig. 1). This resulted in a very low initial J_c value at high fields compared with the peak J_{cm} of the conductor. For example, the initial J_c was depressed by a factor of 50 compared with the measured peak J_{cm} at 18 T. This will be important in making comparisons with other conductors.

2. The intrinsic irreversible strain limit $\varepsilon_{o,irrev}$ for this conductor (strain beyond the maximum where permanent damage occurs) was about 0.3%. This was relatively low compared with commercial multifilamentary Nb_3Sn which has an intrinsic irreversible strain that is consistently about 0.5%. This is probably a result of the conductor geometry and very large compressive prestrain. A micrographic study of Kirkendall void formation in the conductor would probably be helpful in clarifying this.

3. The reaction-layer J_{cm} at 10 T (not the overall J_{cm}) was measured to be 2.8 GA/m^2.

4. The decrease in J_c with field is more rapid than for Nb_3Sn wires having other additives such as Ti or Ta. The peak J_{cm} vs. B characteristic

for this conductor (see Fig. 2) indicates that the fall-off in J_{cm} with field is very similar to binary Nb_3Sn.

The results suggest that not much Mg was incorporated into the Nb_3Sn after reaction, which would account for the electromechanical properties being essentially the same as for binary Nb_3Sn (except that the prestrain is greater). An x-ray spectrographic analysis of the Mg content in the Nb_3Sn reaction layer was consequently performed. The analysis was done by R. Sabotini at Brookhaven National Laboratory and showed the Mg actually incorporated into the Nb_3Sn compound was less than 0.1 at %. Thus, the amount was probably too small to significantly alter the properties of binary Nb_3Sn. It is suggested that a further test of Mg additions to Nb_3Sn be made on a sample with a higher Mg content in the Nb_3Sn compound.

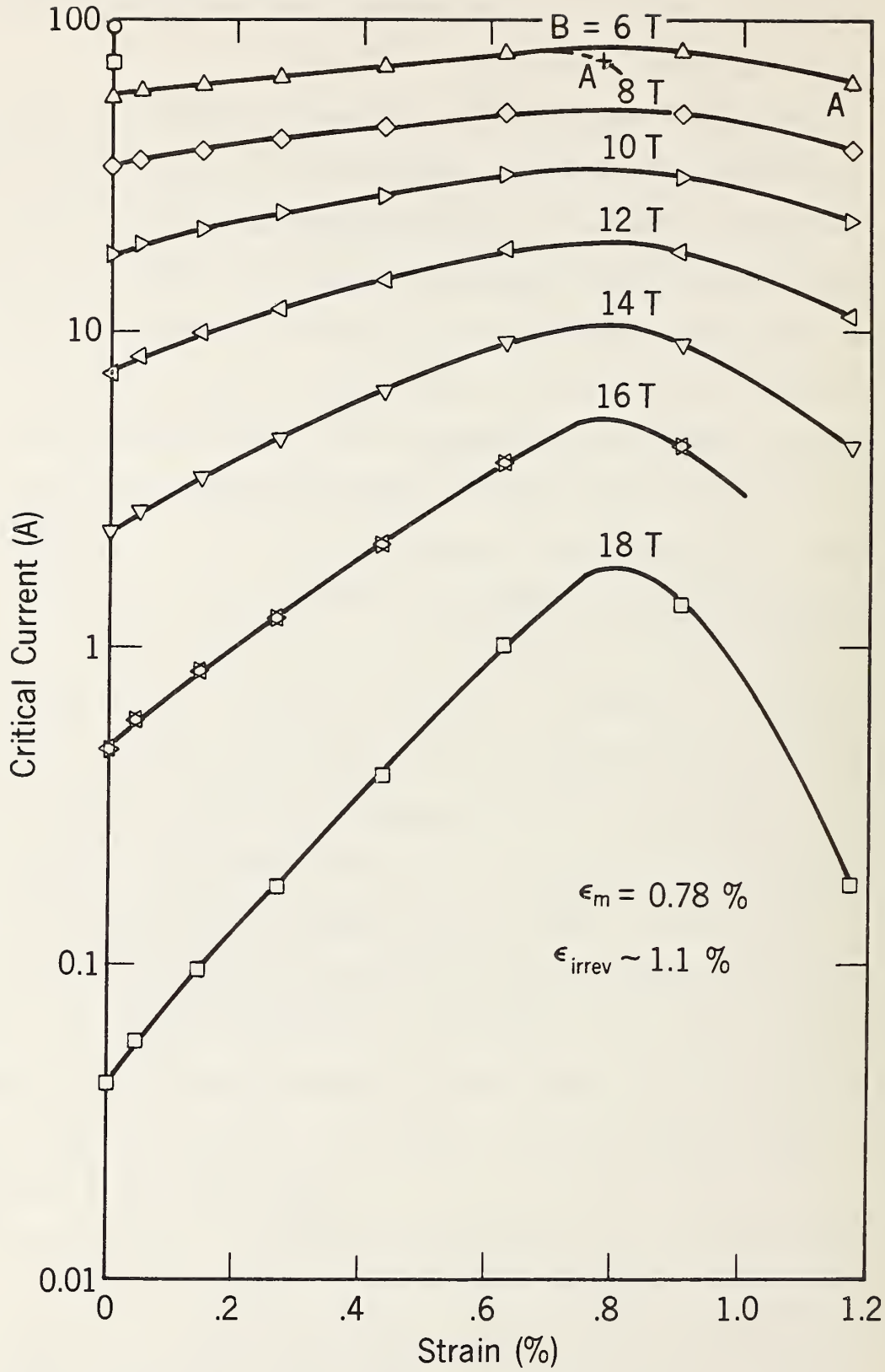

Fig. 1 Uniaxial strain dependence of the critical current. The cross indicates the critical current measured after unloading from the correspondingly-labeled loaded (open-symbol) data point.

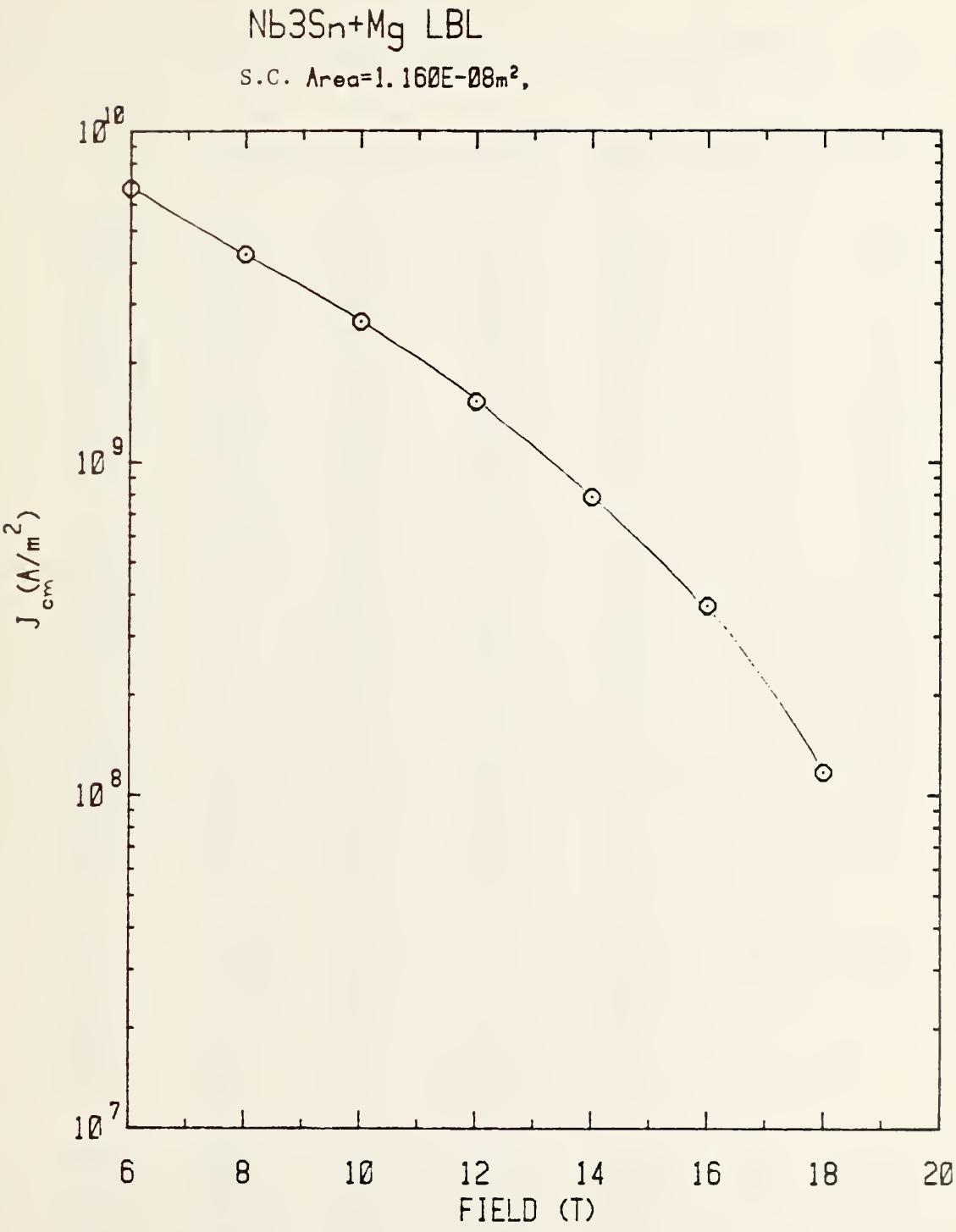

Fig. 2 Peak critical current density versus magnetic field measured at ε_m.

Table 1

Critical current of Nb_3Sn with Mg additive as a function of strain at magnetic fields from 6 T to 18 T. Jc is the critical current density referred to the area of superconductor only, E_{max} is the strain (in percent) where the critical current is maximum, and E_c is the electric field criterion used to determine the critical current.

Superconductor area = 1.160E-008 Emax = 0.78 Ec = 2.00uV/cm

E (%)	Eo (%)	Ic (Amperes)	Field (Tesla)	Jc (GA/m^2)	JcB (GN/m^3)	Ic/Icm
0.00	-.78	93.583	4.000	8.068	32.270	0.0000
		72.802	5.000	6.276	31.380	0.0000
		56.593	6.000	4.879	29.272	0.7267
		33.602	8.000	2.897	23.174	0.6832
		17.685	10.000	1.525	15.246	0.5727
		7.461	12.000	0.643	7.718	0.4221
		2.293	14.000	0.198	2.769	0.2513
		0.474	16.000	0.041	0.654	0.1105
		0.149	17.000	0.013	0.218	0.0000
		0.042	18.000	0.004	0.065	0.0309
0.05	-.73	58.707	6.000	5.061	30.365	0.7539
		35.035	8.000	3.020	24.162	0.7123
		19.107	10.000	1.647	16.472	0.6188
		8.351	12.000	0.720	8.639	0.4725
		2.664	14.000	0.230	3.215	0.2919
		0.590	16.000	0.051	0.814	0.1374
		0.057	18.000	0.005	0.088	0.0419
0.15	-.64	61.545	6.000	5.306	31.834	0.7903
		37.565	8.000	3.238	25.907	0.7637
		21.423	10.000	1.847	18.468	0.6938
		9.911	12.000	0.854	10.253	0.5607
		3.439	14.000	0.296	4.151	0.3769
		0.848	16.000	0.073	1.169	0.1973
		0.096	18.000	0.008	0.149	0.0706
0.27	-.51	64.783	6.000	5.585	33.508	0.8319
		40.930	8.000	3.528	28.227	0.8322
		23.876	10.000	2.058	20.583	0.7732
		11.806	12.000	1.018	12.214	0.6679
		4.569	14.000	0.394	5.514	0.5007
		1.247	16.000	0.108	1.720	0.2903
		0.175	18.000	0.015	0.272	0.1288
0.43	-.35	69.820	6.000	6.019	36.114	0.8966
		44.705	8.000	3.854	30.831	0.9089
		27.014	10.000	2.329	23.288	0.8749
		14.623	12.000	1.261	15.127	0.8273
		6.480	14.000	0.559	7.820	0.7100
		2.135	16.000	0.184	2.944	0.4959
		0.395	18.000	0.034	0.613	0.2907
0.62	-.16	76.994	6.000	6.637	39.824	0.9887
		49.669	8.000	4.282	34.254	1.0098
		31.576	10.000	2.722	27.221	1.0226

Table 1 continued

Superconductor area = 1.160E-008 Emax = 0.78 Ec = 2.00uV/cm

E (%)	Ec (%)	Ic (Amperes)	Field (Tesla)	Jc (GA/m^2)	JcB (GN/m^3)	Ic/Icm
0.62	-.16	18.221	12.000	1.571	18.850	1.0308
		9.216	14.000	0.794	11.123	1.0099
		3.896	16.000	0.336	5.373	0.9069
		1.020	18.000	0.088	1.583	0.7506
0.90	0.12	77.874	6.000	6.713	40.280	1.0000
		49.186	8.000	4.240	33.922	1.0000
		30.878	10.000	2.662	26.619	1.0000
		17.676	12.000	1.524	18.286	1.0000
		9.126	14.000	0.787	11.014	1.0000
		4.296	16.000	0.370	5.925	1.0000
		1.359	18.000	0.117	2.109	1.0000
1.17	0.39	61.237	6.000	5.279	31.675	0.7864
		37.881	8.000	3.266	26.125	0.7702
		22.529	10.000	1.942	19.422	0.7298
		11.123	12.000	0.959	11.507	0.6293
		4.296	14.000	0.370	5.185	0.4707
		0.178	18.000	0.015	0.276	0.1309
0.77	-.01	72.285	6.000	6.232	37.389	0.9282

HIGH-FIELD UNIAXIAL STRAIN-EFFECT CHARACTERIZATION OF CANDIDATE Nb_3Sn SUPERCONDUCTORS FOR FUSION APPLICATIONS

J. W. EKIN

The electromechanical properties of several candidate Nb_3Sn superconductors for fusion application are presented in this section. Two are under development: the internal-tin and jelly roll processes. The third is the bronze process conductor used in the Nb_3Sn magnet for the Large Coil Project.

A. Internal-Tin Nb_3Sn Conductor

High-field critical-current versus strain results were obtained for two internal-tin conductors manufactured by Intermagnetics General Corp.* One contained 19 subelements and had 2 μm diameter Nb filaments, the other had 61 subelements and 1 μm Nb filaments.

Characteristics of these two samples are as follows. The overall diameter of each conductor was 0.68 mm. The volume fraction of each component before reaction was 14% Nb, 8% Sn, 23% Cu, 7% Nb diffusion barrier, and 48% Cu stabilizer. The reaction heat treatment was made by M. Suenaga at Brookhaven National Lab and consisted of:

375° C for 48 h
580° C for 200 h
700° C for 48 h

The apparatus used to measure the strain effect has been described in Cryogenics 20, 614 (1980). The critical current was defined by a 2 μV/cm criterion.

*Certain commercial materials are identified to specify the experimental study adequately. In no case does such identification imply recommendation or endorsement by the National Bureau of Standards, nor does it imply that the material is necessarily the best available for the purpose.

The critical currents were corrected for the small current carried by the stabilizing matrix, which can become relatively significant at high fields where the critical current I_c approaches zero. For these data the correction was not particularly large, however. For the 61 subelement conductor it ranged from 72 mA at a field of 18 T to 96 mA at 16 T. (The variation with magnetic field occurs because of the magnetoresistance of the Cu stabilizing matrix.) For the 19 subelement conductor, the matrix-current correction ranged from 54 mA at 20 T to 64 mA at 18 T.

There was also a very large current-transfer voltage correction that had to be applied in determining I_c for these data. The correction becomes especially important at low fields where the critical currents are high. The current-transfer voltages in this sample were much larger than those of other samples we have tested, probably because of the relatively high matrix resistivity. The magnitude of the effect in the tests on the 19 subelement conductor was not realized at first in conducting these tests and consequently the V-I curves were not measured to a high enough voltage to allow the correction to be made. The correction is nonlinear and impossible to make without measuring I_c over a very wide voltage range. Consequently, accurate data for the 19 subelement sample were obtained only at high fields where the correction is negligible. For the 61 subelement sample, however, extended voltage data were obtained and current-transfer corrections were made accurately over the whole field range.

Critical-current versus strain data are shown for the 61 subelement conductor in Figs. 1, 2, and Table I. Fig. 3 shows the very-high-field data for the 19 subelement conductor. The principal results are summarized below:

1. The compressive prestrain ε_m was measured to be 0.39% for the 61 subelement conductor. It did not change significantly for the 19 subelement

conductor where it was measured to be 0.41%. This is a relatively large prestrain and will result in significant degradation of the J_c of the conductor at high fields if compared with other conductors without first correcting J_c to the peak value. The difference between the initial and peak values of J_c at 16 T, for example, amounts to a 63% decrease from the peak value. At 18 T the decrease is 94%.

2. The irreversible strain ε_{irrev} was measured to be 1.25% in the 19 subelement conductor. For the 61 subelement conductor ε_{irrev} was at least 1.2%. (Only a lower limit could be determined for this particular run because there was not time in the magnet shift to obtain data at higher strains.) It is expected that ε_{irrev} was at least 1.25% for this conductor as well. This is a very high irreversible strain, corresponding to an intrinsic irreversible strain $\varepsilon_{o,irrev}$ of about 0.9%. For comparison, typical values of $\varepsilon_{o,irrev}$ are invariably about 0.5% in bronze-process Nb_3Sn conductors (see Sec. C below).

3. The elongation at fracture was measured to be 1.3% in the 19 subelement conductor.

4. J_c was nearly identical for the two conductors at high fields (where the data overlapped).

5. The peak overall J_c was measured to be about 680 A/mm^2 at 12 T, using a 2 μV/cm criterion. This is significantly higher than for bronze-process Nb_3Sn conductors. The improvement is even greater at 10 T. However, at fields above 12 T, J_c is degraded from that of bronze-process Nb_3Sn conductors.

6. H^*_{c2} was measured to be about 2 T lower than for bronze-process Nb_3Sn (without additions). This probably accounts for the lower J_c at fields above 12 T noted in item 5.

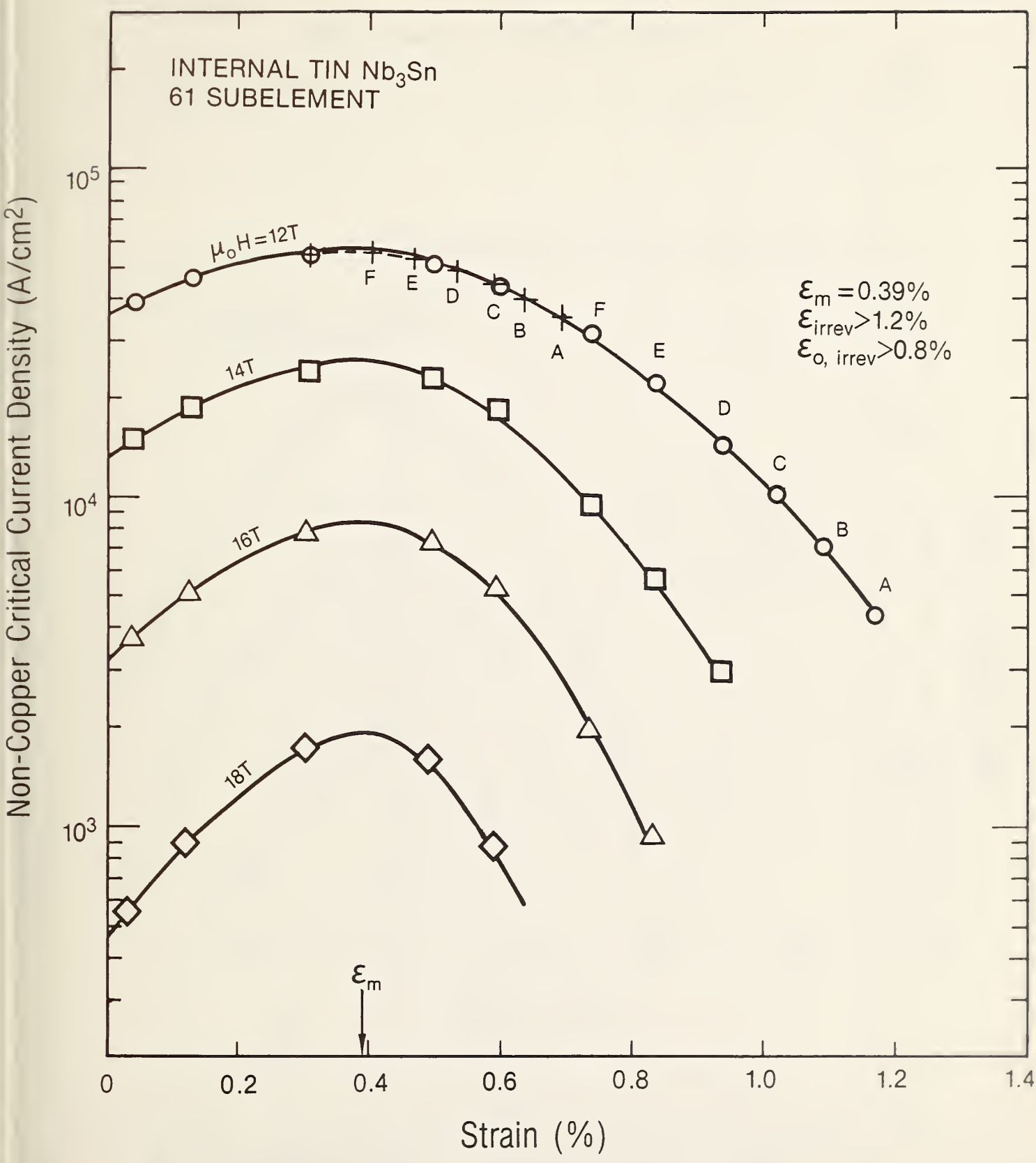

Fig. 1 Uniaxial strain dependence of the critical current. Crosses indicate the critical current measured after unloading from the correspondingly-labeled loaded (open-symbol) data point.

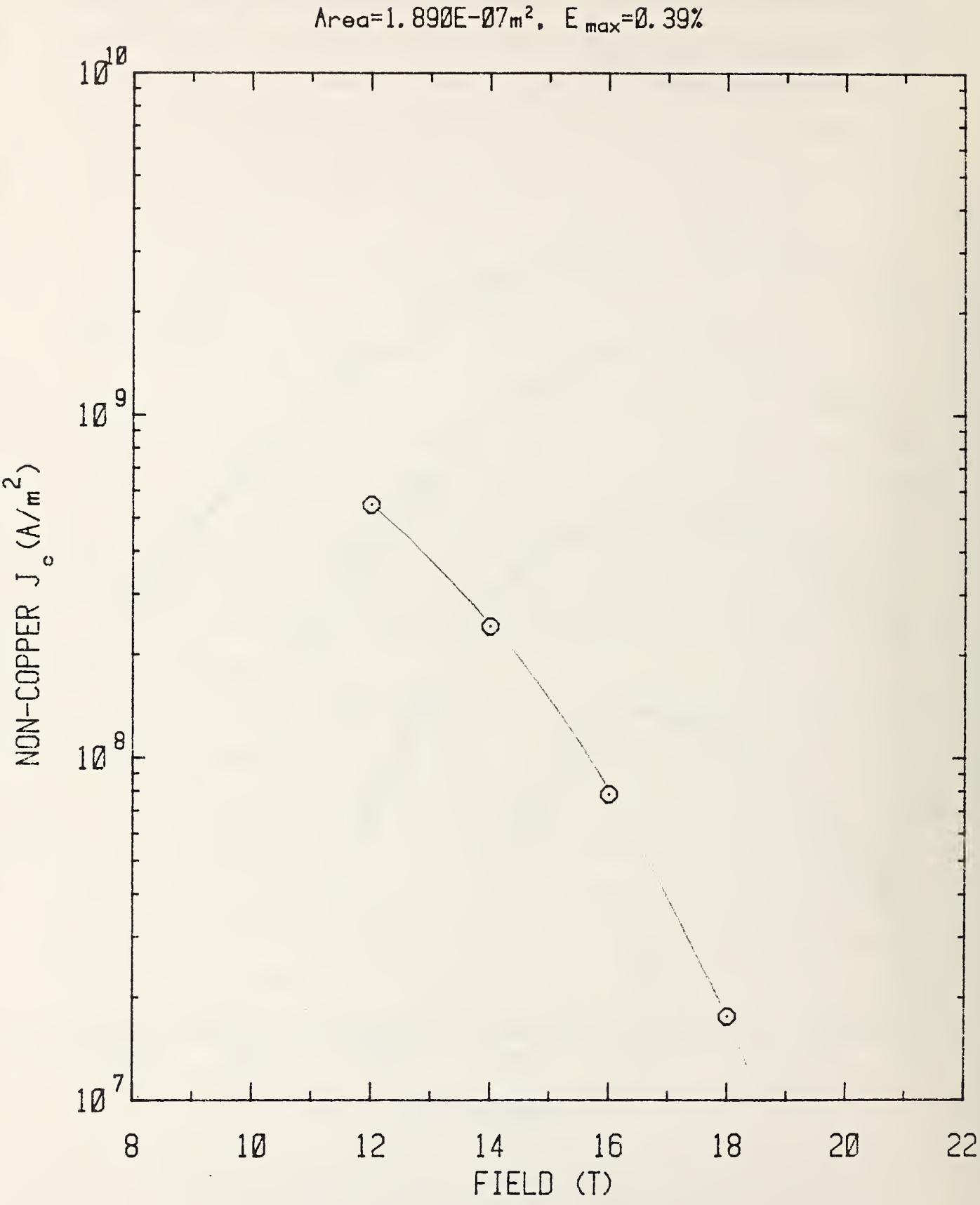

Fig. 2. Peak critical-current density measured at ε_m as a function of magnetic field.

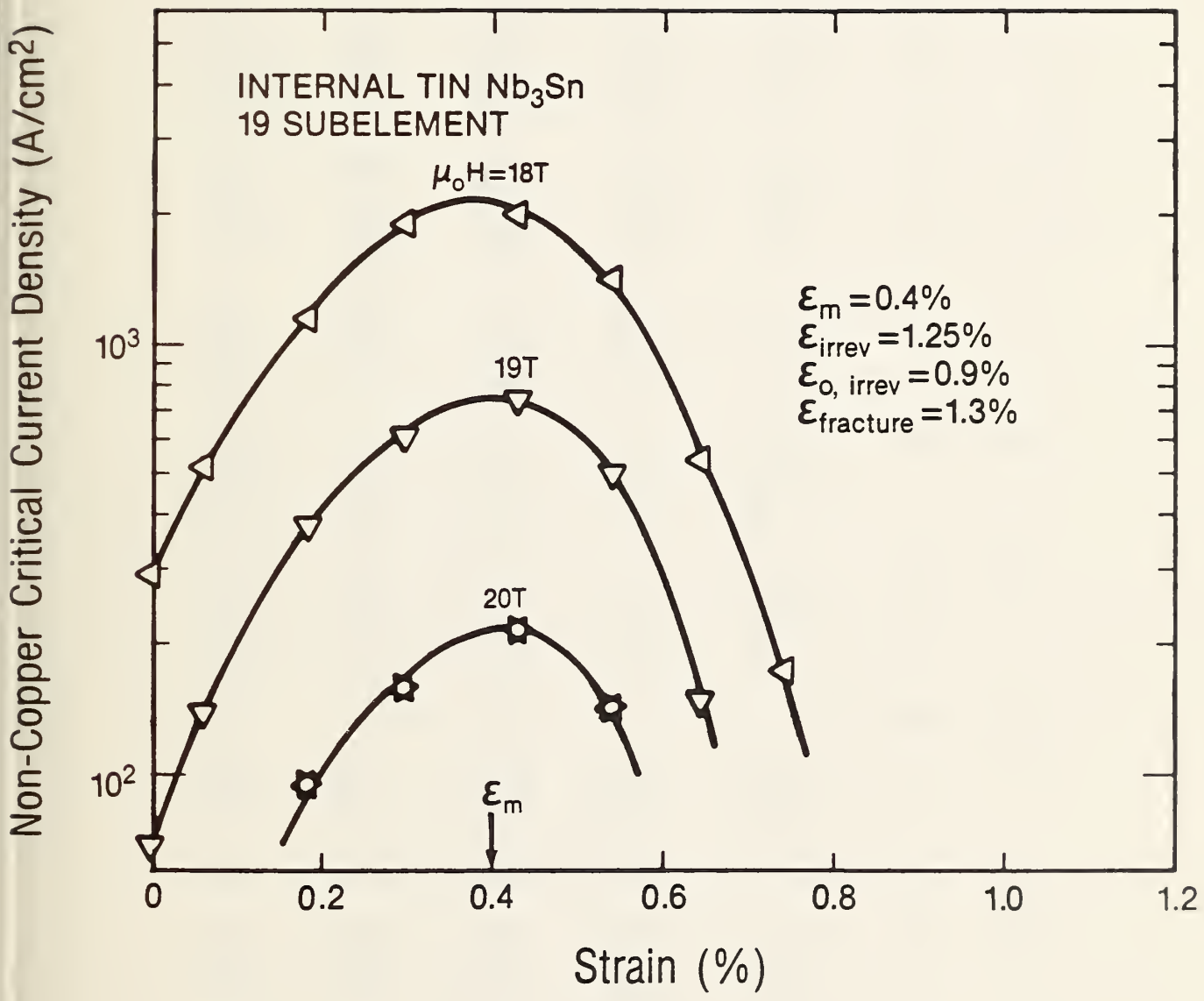

Fig. 3 Uniaxial strain dependence of the critical current at constant magnetic fields.

Table I. Critical current an internal-tin Nb_3Sn superconductor with 61 subelements as a function of strain at magnetic fields from 12 T to 18 T. J_c is the critical current density referred to the non-copper area of the conductor, E_{max} is the strain (in percent) where the critical current is maximum, and E_c is the critical-current electric-field criterion.

Non Cu area = 1.890E-007 Emax = 0.39 Ec = 2.00uV/cm Efract = 1.220

E (%)	Eo (%)	Ic (Amperes)	Field (Tesla)	Jc (GA/m^2)	JcB (GN/m^3)	Ic/Icm
0.04	-.35	73.704	12.000	0.390	4.686	0.7137
		28.114	14.000	0.149	2.090	0.6168
		7.011	16.000	0.038	0.602	0.4799
		1.020	18.000	0.006	0.104	0.3286
0.13	-.26	87.536	12.000	0.464	5.564	0.8474
		35.059	14.000	0.186	2.604	0.7687
		9.614	16.000	0.051	0.822	0.6557
		1.664	18.000	0.009	0.165	0.5229
0.31	-.09	103.310	12.000	0.547	6.566	1.0000
		45.639	14.000	0.242	3.388	1.0000
		14.713	16.000	0.078	1.254	1.0000
		3.248	18.000	0.018	0.316	1.0000
0.49	0.10	97.669	12.000	0.517	6.207	0.9454
		43.540	14.000	0.231	3.232	0.9541
		13.906	16.000	0.074	1.185	0.9455
		3.028	18.000	0.016	0.295	0.9337
0.60	0.21	83.547	12.000	0.443	5.311	0.8089
		35.309	14.000	0.187	2.623	0.7741
		10.101	16.000	0.054	0.863	0.6886
		1.662	18.000	0.009	0.165	0.5221
0.31	-.08	102.180	12.000	0.541	6.494	0.9891
0.74	0.35	60.565	12.000	0.321	3.852	0.5866
		18.157	14.000	0.097	1.352	0.3991
		3.769	16.000	0.020	0.327	0.2610
0.40	0.01	104.250	12.000	0.552	6.625	1.0091
0.83	0.44	43.023	12.000	0.228	2.738	0.4170
		10.914	14.000	0.058	0.816	0.2407
		1.803	16.000	0.010	0.161	0.1282
0.47	0.08	100.380	12.000	0.532	6.380	0.9717
0.94	0.55	28.058	12.000	0.149	1.788	0.2723
		5.747	14.000	0.031	0.433	0.1278
0.53	0.14	92.536	12.000	0.490	5.881	0.8958
1.02	0.63	20.060	12.000	0.107	1.280	0.1949
0.59	0.20	85.102	12.000	0.451	5.409	0.8239

Table I continued.

Nb3Sn Internal Sn;61 subel. BNL 11-28-84 In=var
Non Cu area = 1.890E-007 Emax = 0.39 Ec = 2.00uV/cm Efract = 1.220

E (%)	Eo (%)	Ic (Amperes)	Field (Tesla)	Jc (GA/m^2)	JcB (GN/m^3)	Ic/Icm
1.09	0.70	13.867	12.000	0.073	0.880	0.1342
0.63	0.24	76.261	12.000	0.404	4.842	0.7382
1.17	0.78	8.590	12.000	0.045	0.545	0.0831
0.69	0.30	67.564	12.000	0.357	4.290	0.6540

B. Jelly-Roll Nb_3Sn with 1.1 at% Ti additions

High-field I_c-strain results were also obtained for a jelly-roll, internal-tin conductor #CRE1031 containing about 1.1 at% Ti in the Nb_3Sn compound. The wire was manufactured by Teledyne Wah Chang Corp.* and was heat treated for 100 h at 680° C using the "cold tails" technique to contain the tin. The wire diameter was 0.71 mm, and in figuring the noncopper critical current densities, an area of 2.217×10^{-7} m^2 was used. The noncopper area of the sample was nominally 56%. The noncopper area consisted of 10% volume fraction vanadium diffusion barrier, 38.4% Nb, and 51.6% Sn-Cu matrix. The Sn-Cu matrix was 38.9 wt% tin with respect to Cu.

The apparatus used to measure the strain effect was the one described earlier in Cryogenics 20, 614 (1980). The critical current was defined by a 2 μV/cm criterion. The critical currents were also corrected for the small current carried by the stabilizing matrix, which can become significant at high fields. For these conductors the correction was small, however, amounting to 75 mA. The current-transfer voltage correction was negligible even though the separation between current and voltage taps was only 5 mm.

I_c versus strain data are shown at magnetic fields ranging from 15 T to 19.6 T in Figs. 4 and 5 and Table II. The principal results are summarized below:

1. The compressive prestrain ε_m was measured to be 0.22%. This is a relatively small prestrain. Values of ε_m typically range from 0.2% to 0.4% for commercial bronze-process Nb_3Sn conductors (see Sec. C).

2. The irreversible strain ε_{irrev} was measured to be 0.36%. This is a very low irreversible strain, corresponding to an intrinsic irreversible strain $\varepsilon_{o,irrev}$ of about 0.14%. For comparison, typical values of $\varepsilon_{o,irrev}$ are invariably about 0.5% in bronze-process Nb_3Sn conductors (see Sec. C).

Thus the handling limits of this conductor in its present form will be restrictive compared to other Nb_3Sn conductors.

3. The peak overall J_c was measured to be about 718 A/mm^2 at 15 T, using a 2 μV/cm criterion. This is a relatively high overall J_c for Nb_3Sn conductors.

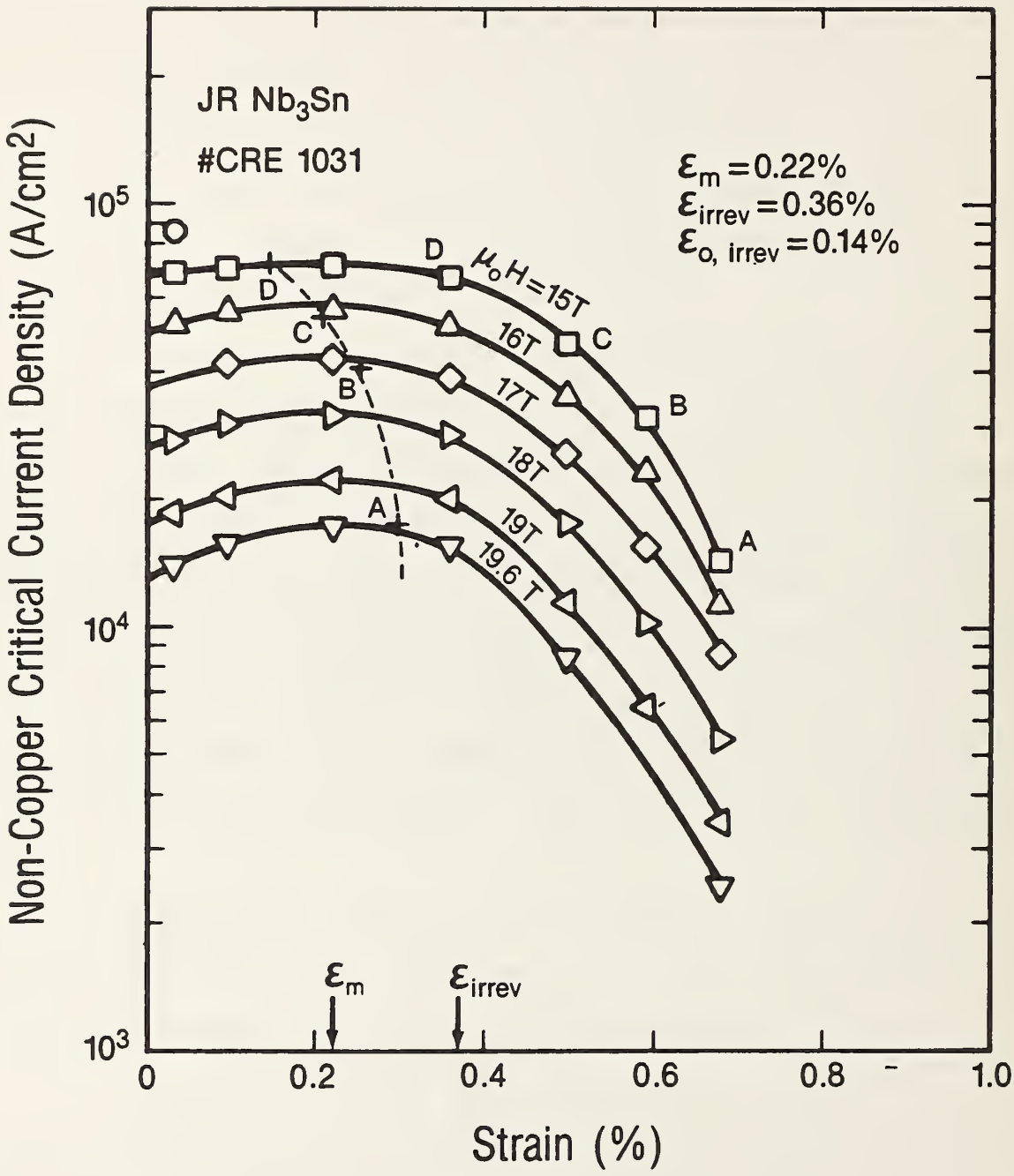

Fig. 4 Uniaxial strain dependence of the critical current. Crosses indicate the critical current measured after unloading from the correspondingly labeled loaded (open-symbol) data point.

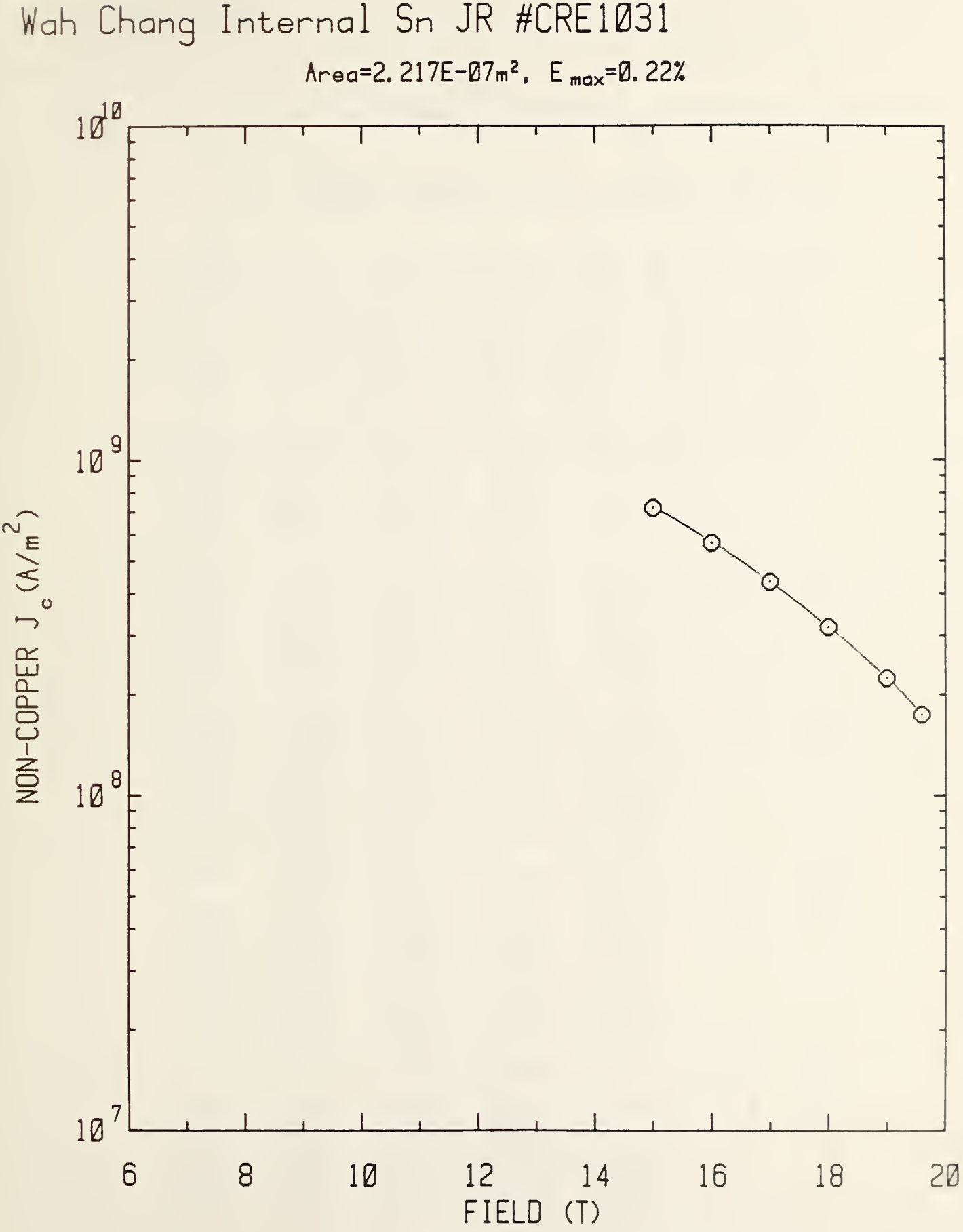

Fig. 5. Peak critical-current density measured at ε_m as a function of magnetic field.

Table II. Critical current of an internal tin jelly-roll Nb3Sn conductor (#CRE1031) as a function of strain at magnetic fields from 15 T to 19.6 T. J_c is the critical current density referred to the non-copper area of the conductor, E_{max} is the peak strain, and E_c is the critical-current electric-field criterion.

Non Cu area = 2.217E-007 Emax = 0.22 Ec = 4.00uV/cm

E (%)	Eo (%)	Ic (Amperes)	Field (Tesla)	Jc (GA/m^2)	JcB (GN/m^3)	Ic/Icm
0.03	-.20	192.780	14.000	0.870	12.174	0.0000
		153.160	15.000	0.691	10.363	0.9620
		115.830	16.000	0.522	8.359	0.9246
		61.405	18.000	0.277	4.985	0.8743
		41.295	19.000	0.186	3.539	0.8339
		31.180	19.600	0.141	2.757	0.8084
0.10	-.14	157.230	15.000	0.709	10.638	0.9876
		123.770	16.000	0.558	8.932	0.9880
		93.305	17.000	0.421	7.155	0.9728
		67.215	18.000	0.303	5.457	0.9570
		45.430	19.000	0.205	3.893	0.9174
		35.045	19.600	0.158	3.098	0.9086
0.22	-.01	159.210	15.000	0.718	10.772	1.0000
		125.270	16.000	0.565	9.041	1.0000
		95.915	17.000	0.433	7.355	1.0000
		70.235	18.000	0.317	5.702	1.0000
		49.520	19.000	0.223	4.244	1.0000
		38.570	19.600	0.174	3.410	1.0000
0.36	0.13	149.060	15.000	0.672	10.085	0.9363
		114.350	16.000	0.516	8.253	0.9128
		86.285	17.000	0.389	6.616	0.8996
		63.005	18.000	0.284	5.115	0.8971
		44.630	19.000	0.201	3.825	0.9013
		34.645	19.600	0.156	3.063	0.8982
0.15	-.09	159.730	15.000	0.720	10.807	1.0033
0.50	0.27	103.760	15.000	0.468	7.020	0.6517
		77.925	16.000	0.351	5.624	0.6221
		57.085	17.000	0.257	4.377	0.5952
		39.125	18.000	0.176	3.177	0.5571
		25.365	19.000	0.114	2.174	0.5122
		18.865	19.600	0.085	1.668	0.4891
0.21	-.02	120.110	15.000	0.542	8.127	0.7544
0.59	0.36	69.415	15.000	0.313	4.697	0.4360
		51.235	16.000	0.231	3.698	0.4090
		34.430	17.000	0.155	2.640	0.3590
		22.800	18.000	0.103	1.851	0.3246
		14.405	19.000	0.065	1.235	0.2909
		10.428	19.500	0.047	0.917	0.0000

Table II continued.

Wah Chang Internal Sn JR #CRE1031

Non Cu area = 2.217E-007 Emax = 0.22 Ec = 4.00uV/cm

E (%)	Eo (%)	Ic (Amperes)	Field (Tesla)	Jc (GA/m^2)	JcB (GN/m^3)	Ic/Icm
0.25	0.02	91.125	15.000	0.411	6.165	0.5724
0.68	0.45	32.045	15.000	0.145	2.168	0.2013
		25.145	16.000	0.113	1.815	0.2007
		19.135	17.000	0.086	1.467	0.1995
		12.078	18.000	0.054	0.981	0.1720
		7.710	19.000	0.035	0.661	0.1557
		5.445	19.500	0.025	0.479	0.0000
0.30	0.07	38.750	15.000	0.175	2.622	0.2434

C. Bronze Process Nb_3Sn

As a reference, we also present here data on the effect of axial tensile strain measured in a bronze-process Nb_3Sn conductor obtained earlier. This conductor was manufactured by Oxford Superconductors* (#336-1-X) and used as the strand material in the Westinghouse* LCP conductor. It was reacted for 240 hours at 750°C.

The data were obtained using the high-field magnet facilities at the Francis Bitter National Magnet Laboratory and an apparatus designed and built at NBS (used in the above two studies). The J_c-ε results for the Oxford Superconductor strand are shown in Figs. 6 and 7, and tabulated in Table III.

The main results are as follows:

1. The compressive prestrain ε_m was measured to be 0.3%. This is typical for bronze-process Nb_3Sn conductors, where the prestrain is usually in the range 0.2% to 0.4%.

2. The irreversible strain limit ε_{irrev} was measured to be about 0.8%, corresponding to an intrinsic irreversible strain limit $\varepsilon_{o,irrev}$ of 0.5%. The value of $\varepsilon_{o,irrev}$ is invariably about 0.5% in commercial bronze-process Nb_3Sn conductors.

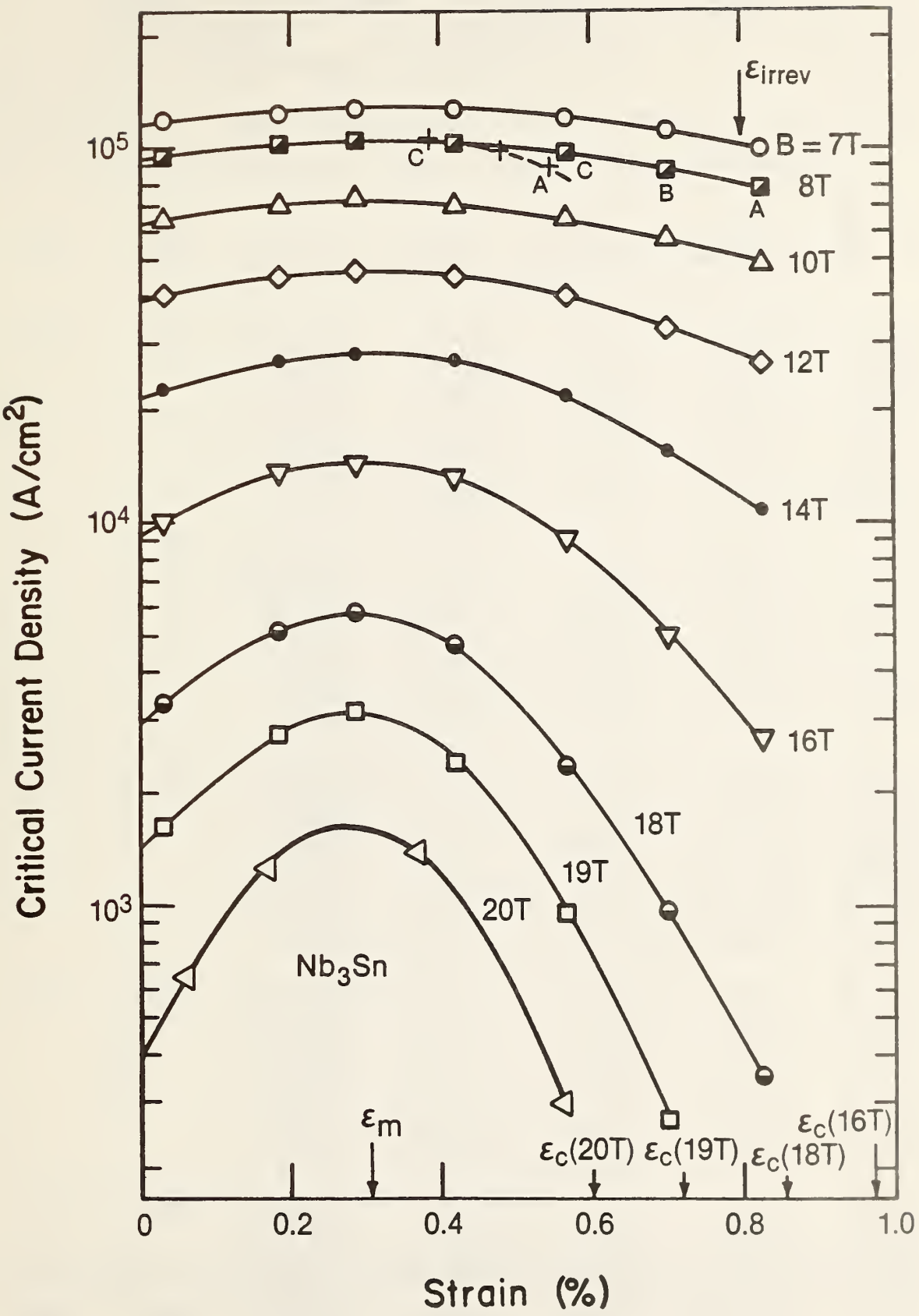

Fig. 6 Critical-current density versus axial-tensile strain for the LCP ICCS conductor strand at constant magnetic fields from 7 T to 20 T.

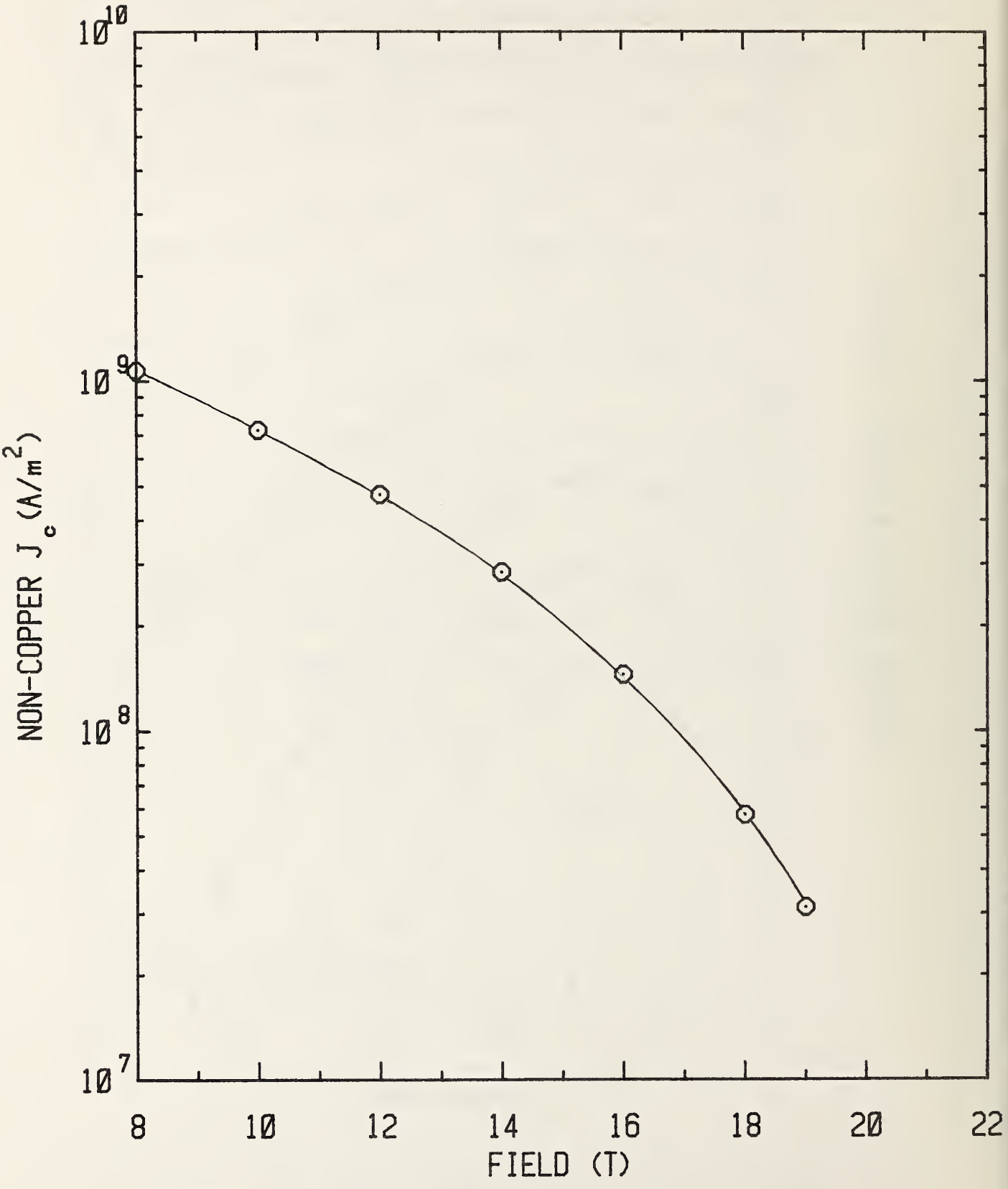

Fig. 7. Peak critical-current density measured at ε_m as a function of magnetic field.

Table III Critical current of an individual strand from the LCT ICCS conductor as a function of strain at magnetic fields from 7 T to 19 T. J_c is the critical current density referred to the non-copper area of the conductor, E_{max} is the strain (in percent) where the critical current is maximum, and E_c is the electric field criterion used to determine the critical current.

AIRCO 336-1-X

Non Cu area = 1.350E-007 Emax = 0.287 Ec = 2.00uV/cm

E (%)	Eo (%)	Ic (Amperes)	Field (Tesla)	Jc (GA/m^2)	JcB (GN/m^3)	Ic/Icm
0.03	-.26	151.100	7.000	1.119	7.835	0.922
		123.300	8.000	0.913	7.307	0.915
		82.000	10.000	0.607	6.074	0.898
		51.300	12.000	0.380	4.560	0.859
		28.800	14.000	0.213	2.987	0.802
		12.800	16.000	0.095	1.517	0.699
		4.150	18.000	0.031	0.553	0.572
		1.970	19.000	0.015	0.277	0.500
0.18	-.10	159.500	7.000	1.182	8.271	0.973
		131.800	8.000	0.976	7.810	0.978
		88.800	10.000	0.658	6.578	0.973
		57.900	12.000	0.429	5.147	0.970
		34.400	14.000	0.255	3.567	0.958
		17.150	16.000	0.127	2.033	0.937
		6.560	18.000	0.049	0.875	0.905
		3.470	19.000	0.026	0.488	0.881
0.29	0.00	163.900	7.000	1.214	8.499	1.000
		134.800	8.000	0.999	7.988	1.000
		91.300	10.000	0.676	6.763	1.000
		59.700	12.000	0.442	5.307	1.000
		35.900	14.000	0.266	3.723	1.000
		18.300	16.000	0.136	2.169	1.000
		7.250	18.000	0.054	0.967	1.000
		3.940	19.000	0.029	0.555	1.000
0.42	0.13	162.000	7.000	1.200	8.400	0.988
		132.000	8.000	0.978	7.822	0.979
		88.800	10.000	0.658	6.578	0.973
		57.500	12.000	0.426	5.111	0.963
		34.200	14.000	0.253	3.547	0.953
		16.800	16.000	0.124	1.991	0.918
		5.930	18.000	0.044	0.791	0.818
		2.950	19.000	0.022	0.415	0.749
0.57	0.28	152.800	7.000	1.132	7.923	0.932
		123.300	8.000	0.913	7.307	0.915
		81.300	10.000	0.602	6.022	0.890
		50.600	12.000	0.375	4.498	0.848
		27.500	14.000	0.204	2.852	0.766
		11.300	16.000	0.084	1.339	0.617
		2.850	18.000	0.021	0.380	0.393
		1.170	19.000	0.009	0.165	0.297
0.39	0.10	134.000	8.000	0.993	7.941	0.994

Table III (cont)

AIRCO 336-1-X

Non Cu area = 1.350E-007 Emax = 0.287 Ec = 2.00uV/cm

E (%)	Eo (%)	Ic (Amperes)	Field (Tesla)	Jc (GA/m^2)	JcB (GN/m^3)	Ic/Icm
0.71	0.42	140.500	7.000	1.041	7.285	0.857
		112.000	8.000	0.830	6.637	0.831
		71.000	10.000	0.526	5.259	0.778
		41.800	12.000	0.310	3.716	0.700
		19.700	14.000	0.146	2.043	0.549
		6.360	16.000	0.047	0.754	0.348
		1.180	18.000	0.009	0.157	0.163
		0.330	19.000	0.002	0.046	0.084
0.48	0.19	124.000	8.000	0.919	7.348	0.920
0.83	0.54	127.500	7.000	0.944	6.611	0.778
		100.300	8.000	0.743	5.944	0.744
		61.400	10.000	0.455	4.548	0.673
		33.400	12.000	0.247	2.969	0.559
		13.400	14.000	0.099	1.390	0.373
		3.370	16.000	0.025	0.399	0.184
		0.425	18.000	0.003	0.057	0.059
0.55	0.27	115.800	8.000	0.858	6.862	0.859

CONSTRUCTION AND INITIAL TESTING OF A TRANSVERSE-STRESS-EFFECT APPARATUS

J. W. Ekin and J. C. Brauch

An apparatus was designed and built to simultaneously apply transverse pressure, current, and a perpendicular magnetic field to superconductor strands at 4 K. The construction was started under a small grant (1/3 staff year) from the MIT Plasma Fusion Center. The apparatus was modified, construction completed, and the apparatus used to conduct initial tests on a single-strand Nb_3Sn superconductor in the first year of the present DOE/OFE contract.

In its present configuration the apparatus is capable of applying up to 600 A to a single strand superconductor in a transverse field of 10 T in pool-boiling liquid helium. The magnetic field is produced by a 10 T split-pair multifilamentary-Nb_3Sn magnet with 1-inch-square radial-access ports. Field accuracy is ±0.2% and homogeneity over the sample test section is on the order of ±0.2%.

An illustration of the apparatus is shown in Fig. 1 and photographs are shown in Figs. 2 and 3. Materials in the load frame were selected for low magnetic susceptibility. The sample is compressed between two stainless steel anvils. The edges of the anvils are rounded where the sample enters between the two anvil heads so as to reduce stress concentration at that point.

The ends of the sample are soldered to two copper blocks which introduce current into the superconductor. A thin sheet of fiberglass-epoxy composite is used to insulate the copper blocks and also to support the Lorentz force experienced by the conductor during testing. Compressive pressure is applied to the sample by a 13.3 kN (3000 lb) servohydraulic actuator capable of either load, stroke, or strain control.

An initial test was conducted on the Nb_3Sn conductor used as strand material in the Westinghouse LCP coil. The apparatus performed well for the first test. A preliminary threshold value for reversible transverse-stress degradation was measured. Additional samples, however, should be measured with several apparatus modifications before a threshold value can be reported which we could certify for engineering design purposes. Such tests are in progress.

The apparatus is extremely versatile and present plans under the DOE contract call for testing a variety of individual candidate strands for fusion magnets, as well as smaller ICCS conductors and larger monolithic superconductors.

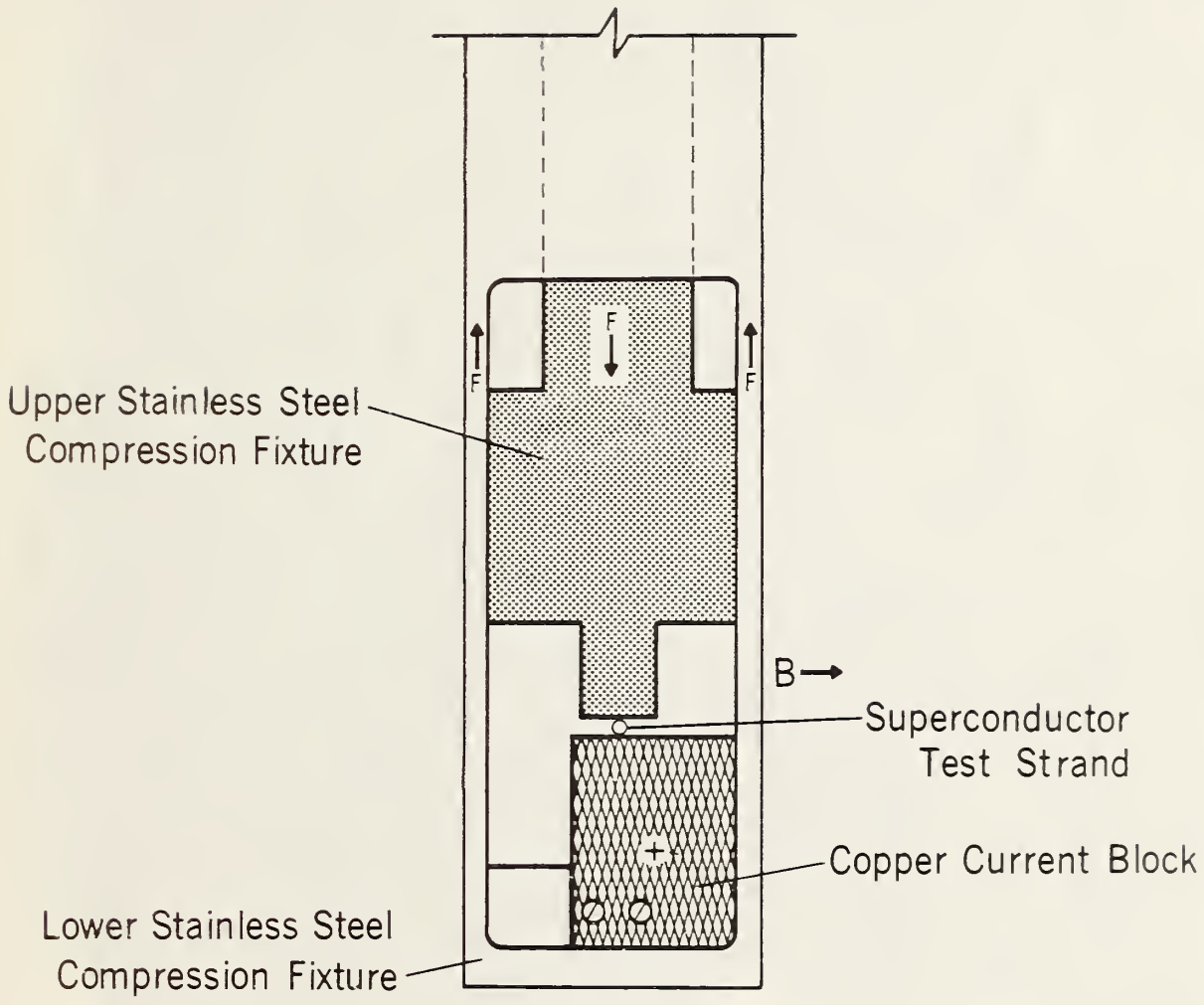

Figure 1. Apparatus for measuring the effect of transverse pressure on the critical current of superconductor strands.

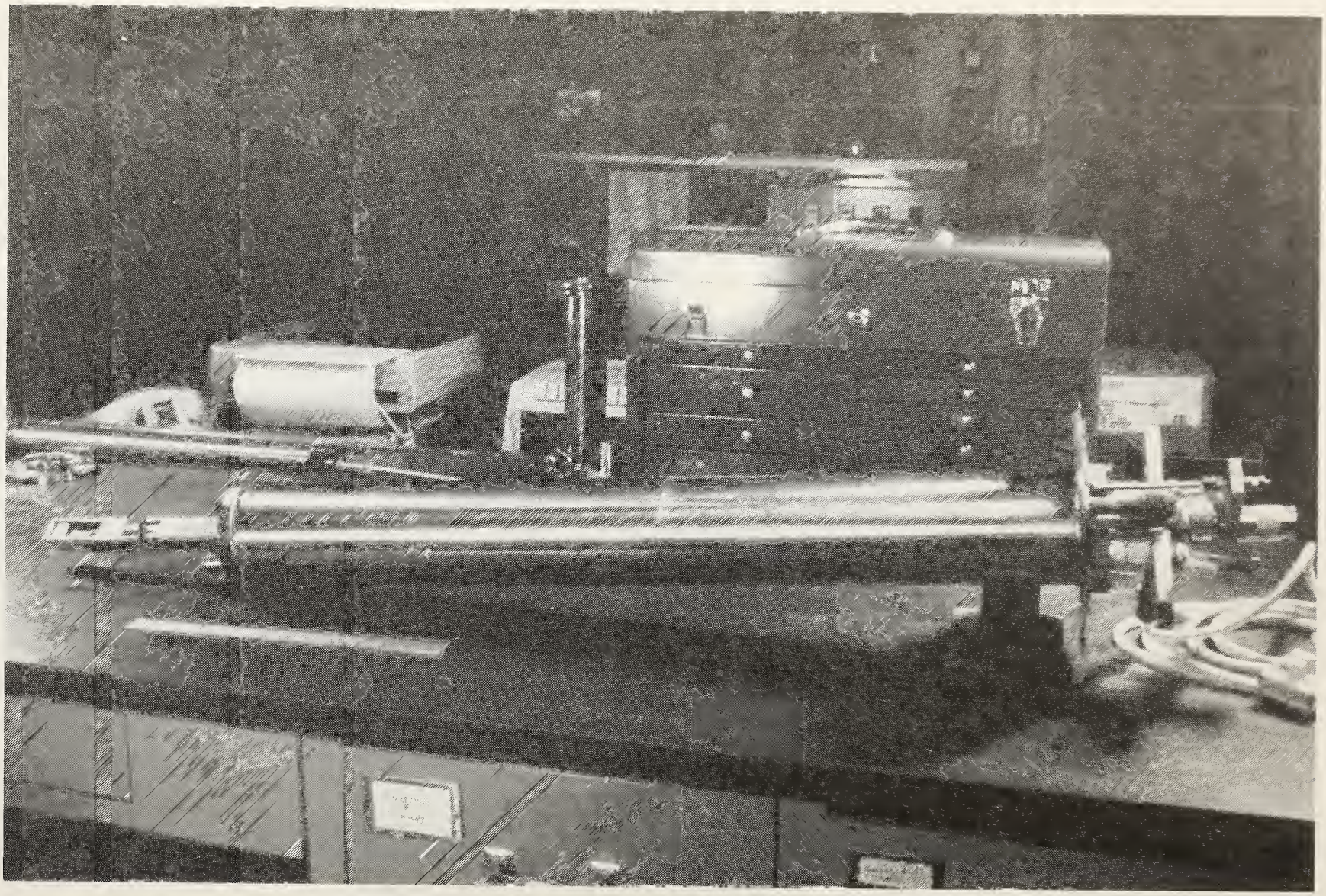

Figure 2. Overview of transverse compression apparatus, showing magnet-insert portion at left, main force-reaction cylinder in center, and head plate at right.

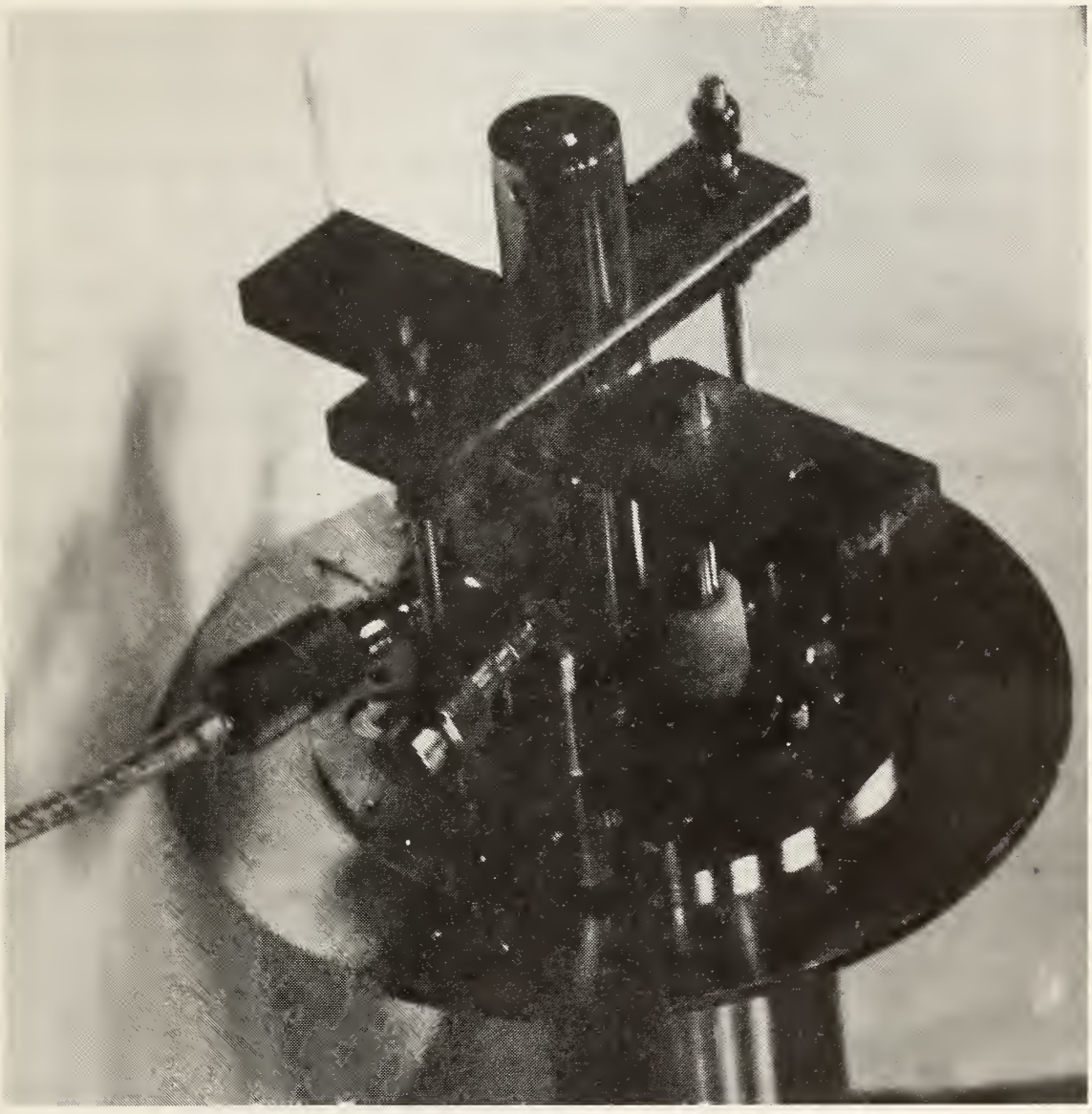

Figure 3. Head plate showing mechanical linkage to servo-hydraulic actuator and vapor-cooled sample current leads.

THERMAL CONTRACTION OF SEVERAL CANDIDATE SHEATHING AND STRENGTHENING MATERIALS FOR SUPERCONDUCTORS

J. W. Ekin

Most structural materials being considered for reinforcing or sheathing Nb_3Sn conductors significantly degrade the critical current of the superconductor.[1-4] In the case of austenitic stainless steel sheathing materials, such as JBK-75 for example, the critical current is degraded between 25% and 70% at 12 T for typical superconductor packing fractions; see Fig. 1.[4] (The degradation is greater at higher magnetic fields.[1]) This occurs because of a large mismatch in thermal contraction between Nb_3Sn and the sheathing material. If other candidate structural materials could be identified with a thermal contraction coefficient closely matching that of Nb_3Sn, the improvement in overall current density would be considerable. Consequently, thermal expansion measurements were made on several structural materials to quantitatively evaluate their suitability for superconductor sheathing and reinforcement applications.

Incoloy 903 and Incoloy 905* (4 to 400 K)

The first tests were made on Incoloy 903 and Incoloy 905 over a low temperature range from 4 K to 400 K. Samples of Incoloy 903 and Incoloy 905 were cut from bulk pieces of each alloy. The samples were in the shape of cylinders measuring approximately 1 cm in diameter and 3 cm in length.

* Certain commercial materials are identified to specify the experimental study adequately. In no case does such identification imply recommendation or endorsement by the National Bureau of Standards, nor does it imply that the material is necessarily the best available for the purpose.

Temperature was measured using a type E thermocouple. Tables 1 and 2 show the thermal expansion data as a function of temperature. A 6-data point smoothing routine was used to obtain thermal-expansion values at even-temperature values every 10 K. Figures 2 and 3 show the smoothed data.

From these data, the total thermal contraction was determined from 4 K to 700°C (the approximate reaction temperature for Nb_3Sn), assuming an extrapolation from 400°C to 700°C based on Reference 5. This extrapolation shows a significant change in slope at approximately 672 K. This is ascribed to a magnetic transformation since the alloy exhibits Curie temperature behavior.[5] The same extrapolation was used for both Incoloy 903 and 905, although the data of Ref. 5 were obtained for Incoloy 903 only. The results are tabulated in Table 3 and plotted in Fig. 4. Similar data for Nb_3Sn on cooling from 700°C are also tabulated in Table 3 and Fig. 4. Based on the comparison between these two materials shown in Fig. 4, the strain that would be introduced into Nb_3Sn from differential thermal contraction with Incoloy alloy sheathing material has a maximum value of 0.2%. (It may be less than that, depending on the tightness of the mechanical bond between the sheathing material and the superconductor, and the relative amount of each.[2,3])

Thus, the prestrain arising from using Incoloy sheathing material in ICCS should be significantly smaller than that from the stainless-steel sheath material used in the LCP ICCS. This is shown in Table 3 and Fig. 4 where the thermal contraction of stainless steel in cooling from 700°C is given for comparison.

In Fig. 4 the thermal contraction of a free-standing Nb_3Sn/Cu-bronze LCP strand is also presented, determined from a measurement of J_c versus uniaxial strain for this conductor (described in section 2 of this report).

A sheathing material such as Incoloy with a thermal contraction coefficient closely matching that of Nb_3Sn could also reduce the compressive prestrain introduced into the Nb_3Sn from the bronze and copper matrix in a free-standing strand. Some reduction in prestrain would be an advantage since the effect of 0.3% compressive prestrain on the critical current is still relatively significant (11% at 10 T, for example); see Fig. 1 of Sec. 2C. However a small compressive prestrain of about 0.2% is recommended since this provides a buffer for additional tensile strain introduced by the Lorentz force on energizing the magnet. An exact strain balance between differential thermal contraction, winding strain, and Lorentz force strain can be calculated in the critical regions of the magnet on a case-by-case basis.

High-Mn Steel Alloys (77 K to 1073 K)

Two high-Mn steel alloys were also tested. Because of some thermal contraction data reported for 25Mn-5Cr-1Ni steel by Yoshimura et al.,[6] it had been hoped that high-Mn steel alloys would have a low thermal contraction more closely matching Nb_3Sn. Yoshimura et al. obtained data at low temperatures from 77 K to 293 K. In this regime they reported a thermal contraction coefficient about 50% of that of 300-series austenitic stainless steels.

To test the potential of high-Mn steel alloys as a superconductor sheathing material, thermal contraction measurements were obtained on two compositions at both low and high temperatures from 77 K to 800° C. The first sample was 25Mn+5Cr+1Ni steel and was the same alloy tested by Yoshimura et al.[6] The second was 25Mn-14Cr-5Ni stainless steel and was chosen because it also had a high-Mn content, but in addition, it had sufficient Cr to make it rust resistant. The composition of each alloy is given in Table 4.

The measurements were carried out at Energy Materials Testing Laboratory (EMTL) under contract to NBS using a fused silica dilatometer in general accord with ASTM-E-228. Both heating and cooling data were obtained and no significant differences were observed between the two types of measurements. Overall accuracy based on measurements against NBS SRM-739 was estimated by EMTL to be ± 0.002% absolute. The coefficient of thermal contraction coefficients for each alloy are compared with those typical of JBK-75 and 300-series stainless steels in Table 5. The results for each alloy are shown in Figs. 5 and 6. The data are tabulated in Table 6.

The following conclusions can be drawn from these data:

1. Below room temperature, the coefficient of thermal contraction of the high-Mn steels is about 60% of that of the 300-series austenitic stainless steels.

2. Above room temperature, however, the thermal contraction coefficient of the high-Mn steels is significantly greater than for the 300-series austenitic stainless steels.

3. The combination yields a total thermal contraction from 700° C to 4 K that is just about the same for both the high-Mn and 300-series austenitic stainless steels.

These data indicate that the high-Mn steels will be no better than JBK-75 and 300-series austenitic stainless steels as sheath materials, with respect to degradation of the critical current of Nb_3Sn arising from differential thermal contraction. This is shown in Fig. 4 and Table 3 where the thermal contraction on cooling from 700° C is given for free-standing Nb_3Sn and compared with several other materials.

Conclusion

In summary, the data indicate the mismatch in thermal expansion between Nb_3Sn and Incoloy 903 or Incoloy 905 (amounting to 0.2%) is significantly less than that (0.9%) for conventional stainless-steel sheathing materials [Fe + (16-19)Cr + (6-14)Ni + X] or high-Mn steel alloys [Fe + (23-25)Mn + (5- 14)Cr + (1-5)Ni + X]. The use of Incoloy should result in significant increases in the critical current of sheathed and reinforced superconductors. The increase in the critical current of ICCS conductors, for example, can be greater than 50% at 12 T, depending on the conductor packing fraction (see Fig. 1). The increase will be more at higher fields.

It is suggested that further screening and testing of alternative Incoloy alloys be done. The high-temperature extrapolation of the data for Incoloy 905 were based on measurements of Incoloy 903 and should be measured directly. High-temperature thermal contraction and mechanical properties of Incoloy 905 and other modifications should be measured.

ACKNOWLEDGMENT

The skill and care of M. Austin in making the low-temperature thermal expansion measurements of Incoloy 903 and 905 are gratefully acknowledged.

REFERENCES

1. "Strain scaling law for flux pinning in practical superconductors. Part 1: Basic relationship and application to Nb_3Sn conductors," J. W. Ekin, Cryogenics 20, 611 (1980).

2. "Mechanical properties of high-current multifilamentary Nb_3Sn conductors," R. M. Scanlan, R. W. Hoard, D. N. Cornish, and J. P. Zbasnik, p. 221, Filamentary A15 Superconductors, ed. by M. Suenaga and A. F. Clark, Plenum Press, New York (1980).

3. "Effect of stainless steel reinforcement on the critical current versus strain characteristic of multifilamentary Nb_3Sn superconductors," J. W. Ekin, R. Flukiger, and W. Specking, J. Appl. Phys. 54, 2869 (1983).

4. "Effects of Incoloy 903 and tantalum conduits on critical current in Nb_3Sn cable-in-conduit conductors," M. M. Steeves, M. O. Hoenig, and C. J. Cyders, Adv. Cy. Eng. 27 (1982).

5. "Determination of structural engineering properties of Incoloy 903 and CTX-1 alloys," p. 121, George C. Marshall Space Flight Center, Alabama 35812, National Aeronautics and Space Administration, Contract NAS8-30929, Paul E. Ruff, Battelle, Columbus Laboratories, 505 King Ave., Columbus, Ohio 43201.

6. "Microstructures, low temperature toughness and thermal expansion coefficients of high manganese-chromium austenitic steels," H. Yoshimura, N. Yamada, H. Yada, H. Honma, and T. Ito, Trans. ISIJ 16, 98 (1976).

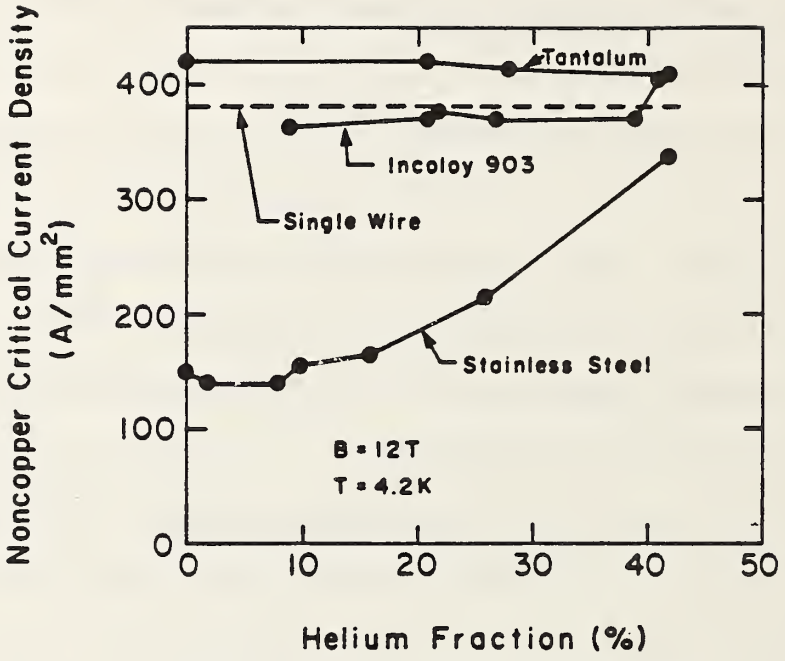

Fig. 1. Noncopper critical current density at 12 T and 4.2 K as a function of helium fraction for Incoloy 903, tantalum and stainless steel conduits. Single wire data (no conduit) are shown for reference. Volume fractions of I-903, Ta and steel were 0.68, 0.48 and 0.32 respectively. (From Ref. 4)

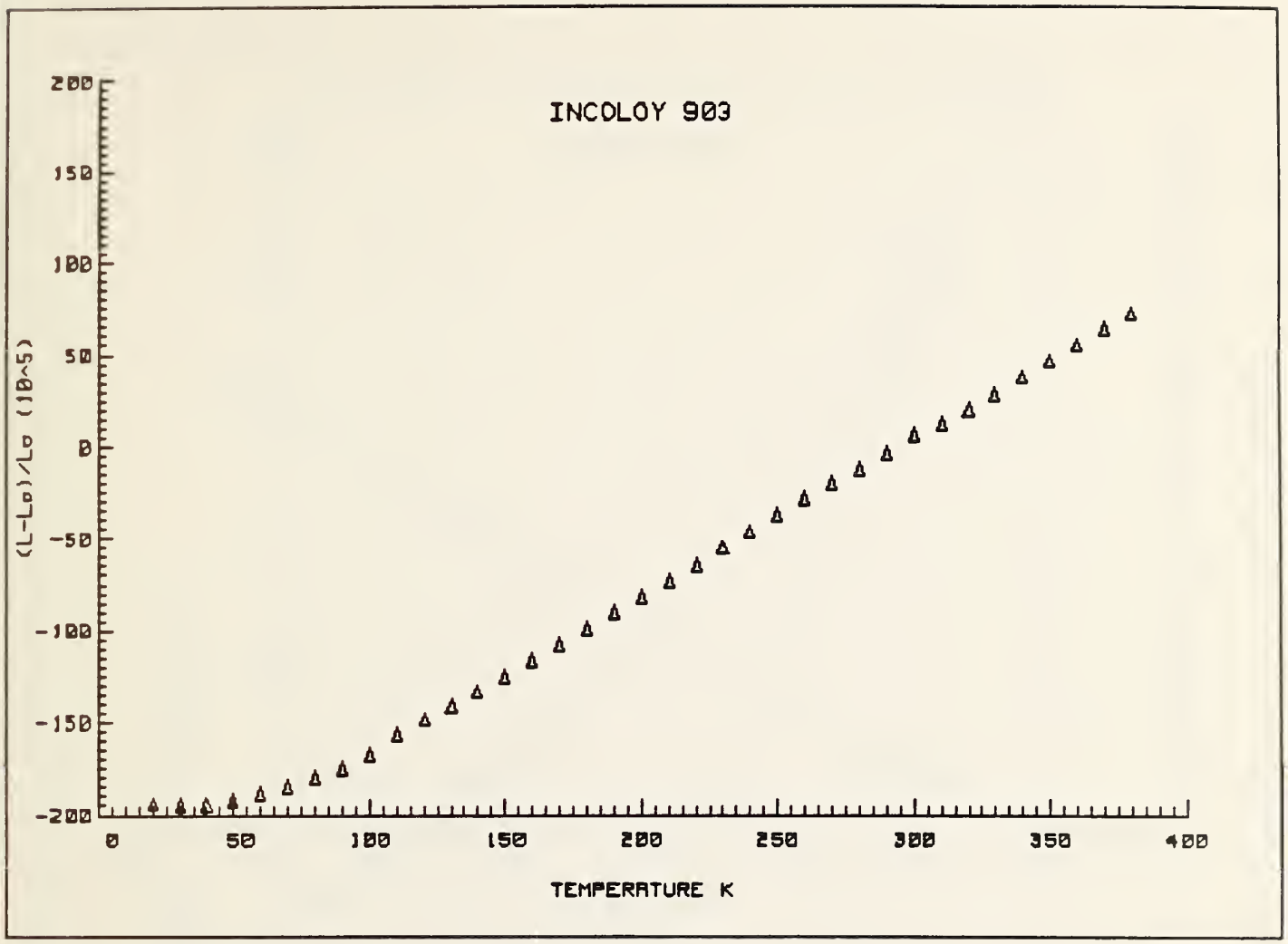

Figure 2. Thermal expansion versus temperature for Incoloy 903 interpolated to even temperature values.

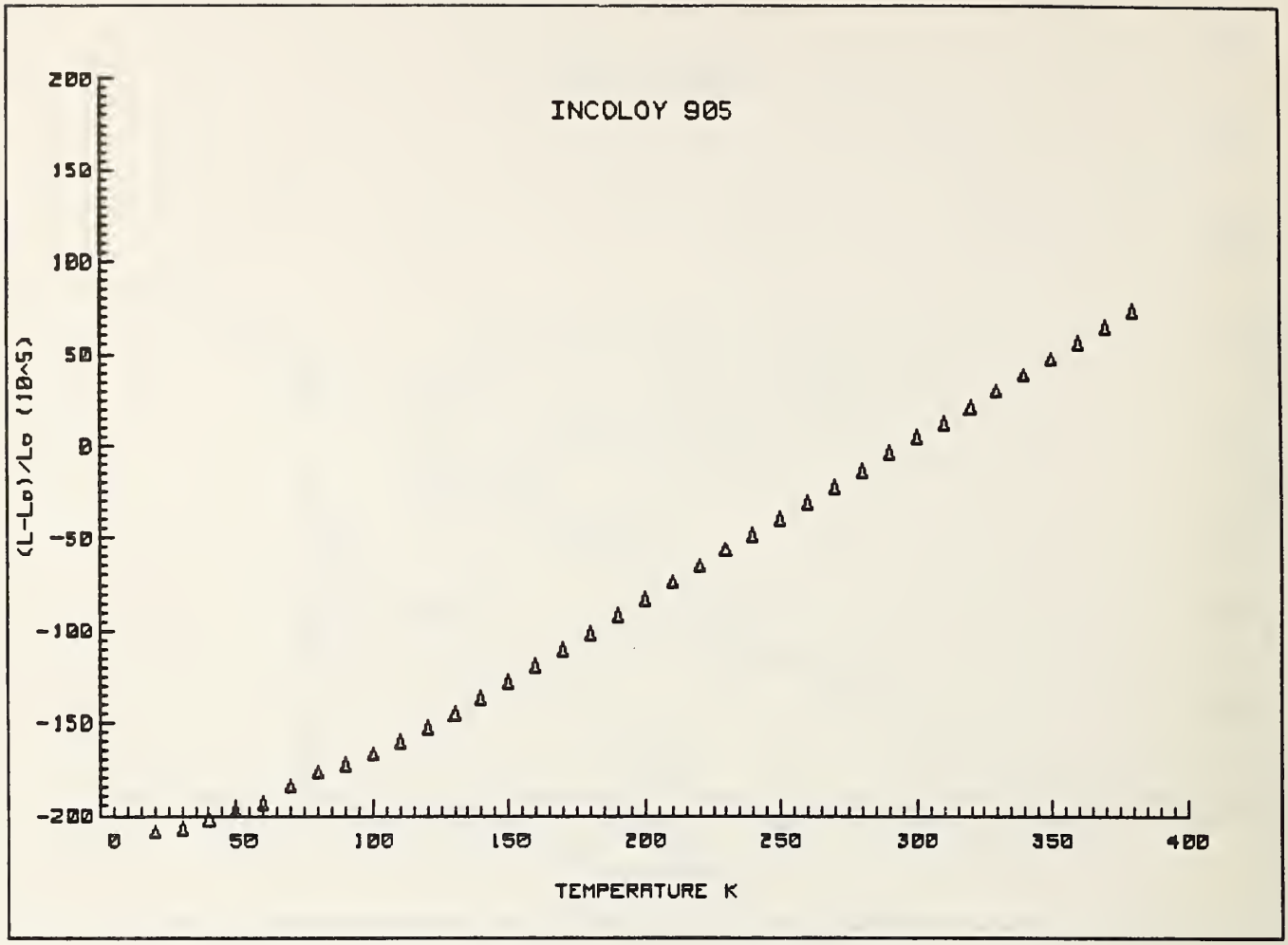

Figure 3. Thermal expansion versus temperature for Incoloy 905 interpolated to even temperature values.

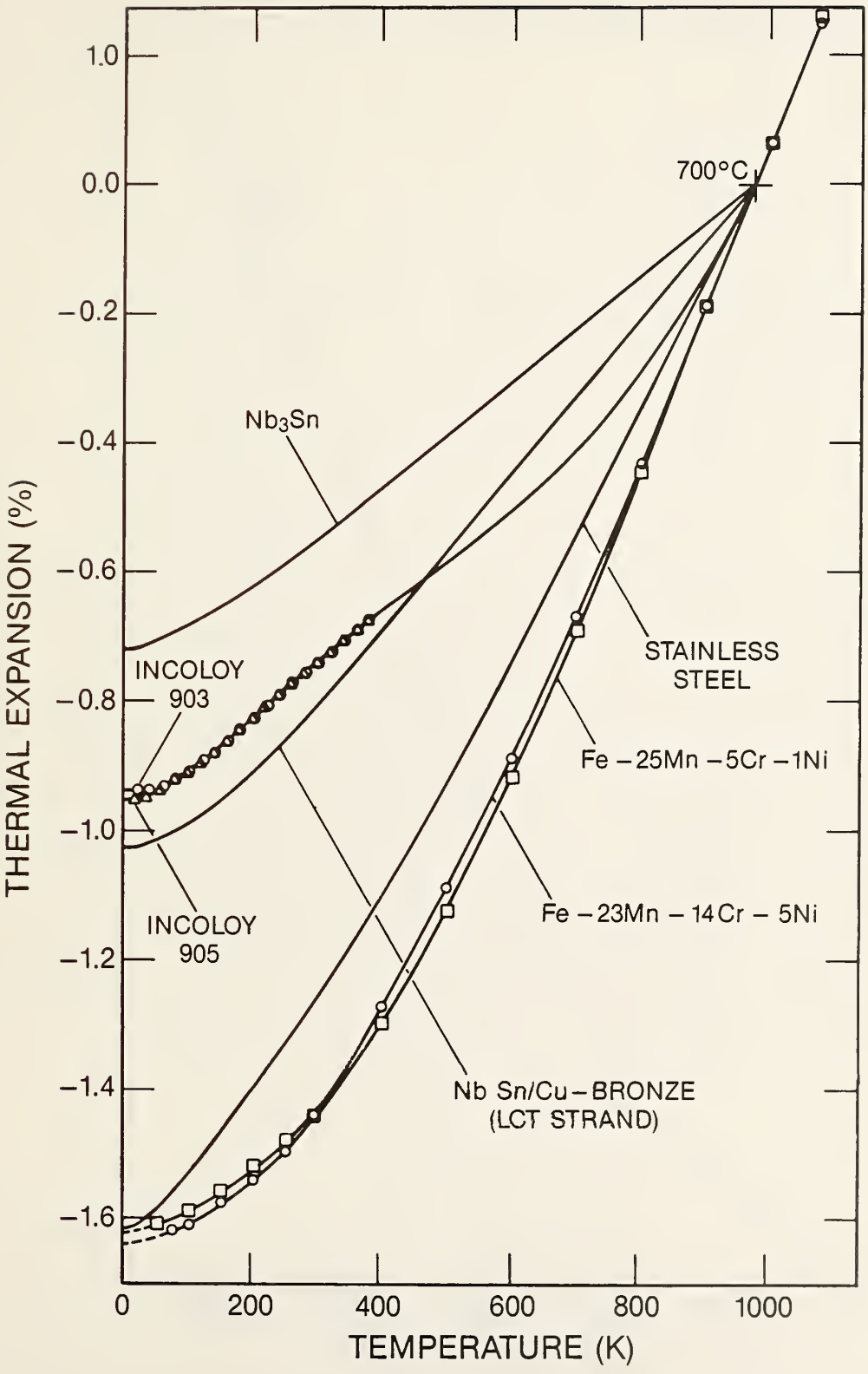

Fig. 4. Comparison of the thermal expansion of various materials with Nb_3Sn over the temperature range from 700 C to 4 K.

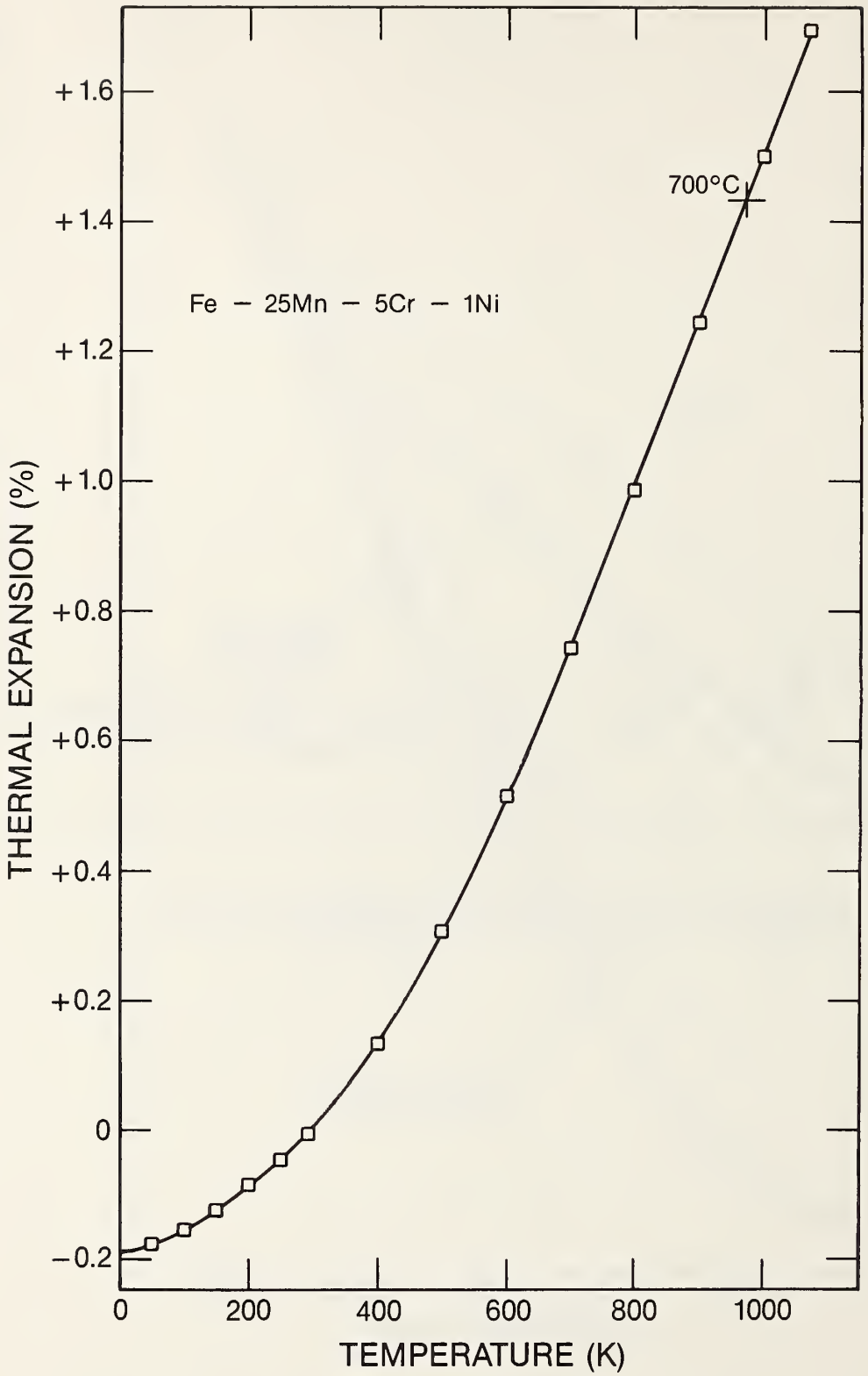

Fig. 5 Thermal expansion versus temperature for Fe-25Mn-5Cr-1Ni steel.

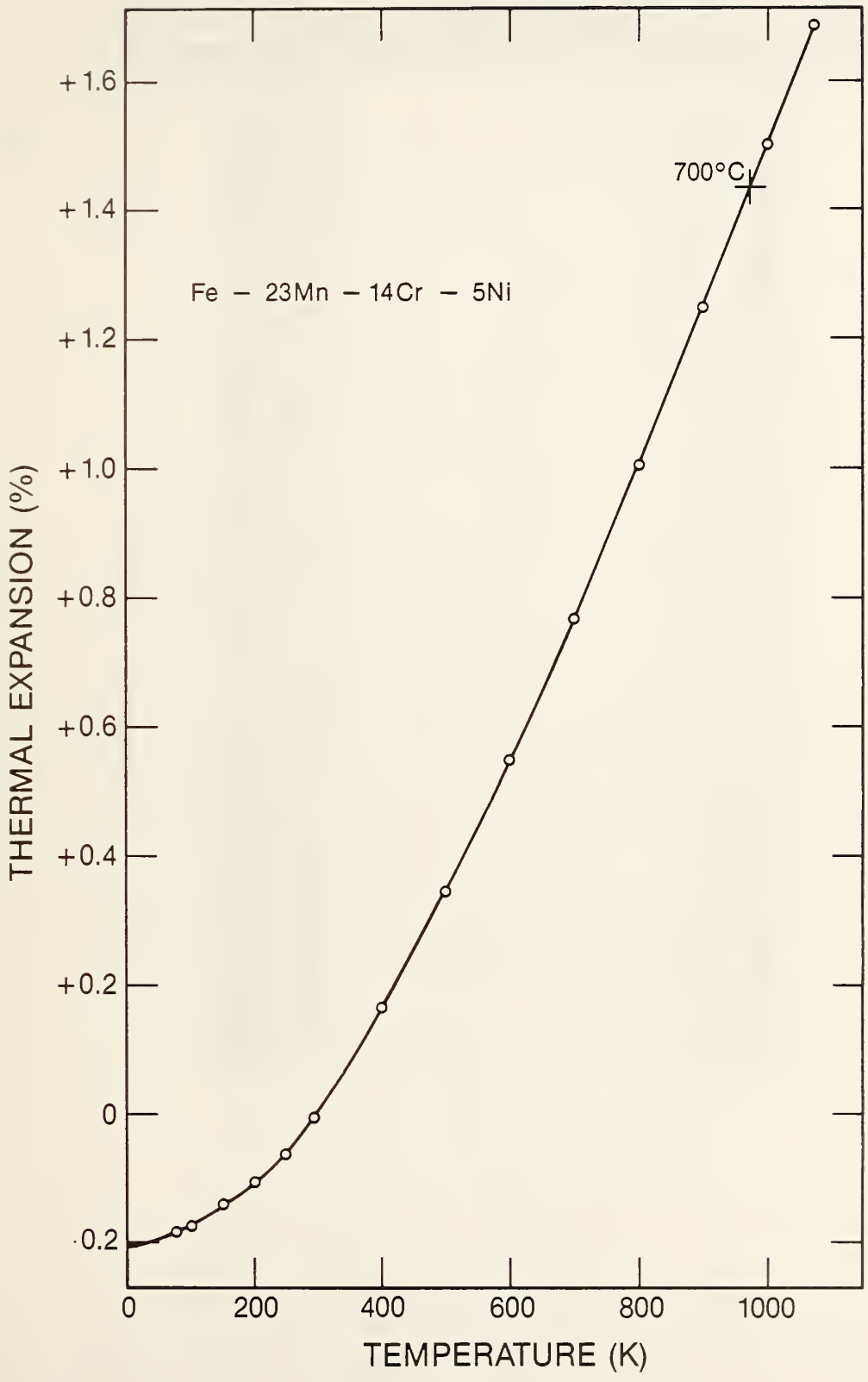

Fig. 6 Thermal expansion versus temperature for Fe-25Mn-14Cr-5Ni stainless steel.

Table 1. Thermal expansion data for Incoloy 903 from 20 K to 400 K interpolated to even temperature values.

	TEMPERATURE K	(L-Lo)/Lo (10^5)
903PLT	20	-193.157
	30	-193.583
	40	-194.107
	50	-191.537
	60	-187.417
	70	-183.991
	80	-178.91
	90	-174.401
	100	-166.774
	110	-155.792
	120	-147.507
	130	-140.506
	140	-132.556
	150	-124.37
	160	-115.997
	170	-107.513
	180	-99.0081
	190	-90.2096
	200	-81.307
	210	-72.5205
	220	-63.665
	230	-54.8301
	240	-45.9367
	250	-36.964
	260	-27.6313
	270	-19.7223
	280	-11.9646
	290	-2.96064
	300	6.30729
	310	12.8238
	320	20.2381
	330	29.2727
	340	38.1345
	350	46.9058
	360	55.6306
	370	64.3733
	380	72.8874

Table 2. Thermal expansion data for Incoloy 905 from 20 K to 400 K interpolated to even temperature values.

TEMPERATURE K	(L-Lo)/Lo (10^5)
20	-207.982
30	-206.09
40	-201.066
50	-196.351
60	-192.246
70	-183.461
80	-176.033
90	-171.393
100	-165.949
110	-159.503
120	-152.149
130	-144.191
140	-135.944
150	-127.472
160	-118.744
170	-109.846
180	-100.804
190	-91.5626
200	-82.3797
210	-73.3016
220	-64.4067
230	-56.047
240	-47.7631
250	-39.1919
260	-30.5982
270	-22.0411
280	-13.4566
290	-3.10587
300	5.69815
310	13.2291
320	21.8436
330	30.5793
340	39.3465
350	48.0927
360	56.9727
370	65.8374
380	74.662

Table 3. Total thermal contraction of various materials on cooling from 700°C to 4.2 K.

Material	ΔL/L (973 K - 4.2 K)
Nb_3Sn	0.74% †
Incoloy 903	0.94% *†
Incoloy 905	0.95% *†
Stainless Steel [Fe+(16-19)Cr+(6-14)Ni+ΣX_i]	1.62% †
High Mn Steel [25Mn-5Cr-1Ni]	1.62% *
High Mn Stainless steel [23Mn-14Cr-5Ni]	1.64% *
Nb_3Sn/Cu-bronze (LCT strand)	1.03% ††
Nb	0.68% †
Cu	1.63% †

* Measured

†† Calculated from $J_c(\varepsilon)$ data

† From following references:

1) Handbook on Materials for Superconducting Magnets (Battelle, Columbus, OH 1975).

2) Paul E. Ruff; Battelle, Columbus, OH; Determination of Structural Engineering Properties of Incoloy 903 and CTX-1 Alloys, p121; George C. Marshall Space Flight Center, Alabama 35812, National Aeronautics and Space Administration, Contract NA58-30929.

3) Y. S. Touloukian, R. K. Kirby, R. E. Taylor, and P. D. Desai, Thermophysical Properties of Matter (IFI/Plenum, New York, 1975), Vol. 12.

Table 4. Composition of the high-Mn steels.

Element	25Mn-5Cr-1Ni	23Mn-14Cr-5Ni
Mn	25.6	23.3
Cr	4.67	13.7
Ni	0.97	5.3
Si	0.86	0.302
N	0.040	0.15
Al	0.009	0.035
C	0.22	0.034
Nb	0.043	--
P	0.024	0.0025
S	0.001	0.0007

Table 5. Comparison of thermal contraction coefficients for 300-series and high-Mn steel alloys.

Material	α(77-293 K) (10^{-6}/K)	α(293-973 K) (10^{-6}/K)	$\Delta L/L$(4-973 K) (%)
Fe+(16-19)Cr+(6-14)Ni+ΣXi (304L,316,321,etc.)	12.9	18.6	1.626
Fe-25Mn-5Cr-1Ni (Nippon Steel)	7.3	21.2	1.622
Fe-23Mn-14Cr-5Ni (Nippon Kokan)	8.2	21.2	1.645

Table 6. Thermal Expansion Values for High-Mn and 300-Series Steel Alloys

T (K)	T (C)	(Composition A)* ΔL/Lo (%)	(Composition B)* ΔL/Lo (%)	(Composition C)† ΔL/Lo (%)
4	-269	(-0.18)	(-0.20)	(-0.36)
77	-196	-0.158	-0.178	-0.279
100	-173	-0.146	-0.167	-0.254
150	-123	-0.115	-0.135	-0.195
200	- 73	-0.079	-0.100	-0.130
250	- 23	-0.041	-0.056	-0.061
293	20	0.000	0.000	0.000
400	127	0.140	0.170	0.166
500	227	0.315	0.353	0.336
600	327	0.522	0.553	0.517
700	427	0.749	0.773	0.708
800	527	0.994	1.009	0.907
900	627	1.249	1.254	1.114
973	700	1.439	1.440	1.266
1000	727	1.507	1.505	1.322
1073	800	1.702	1.692	1.558

Composition A (Fe + 25Mn + 5Cr + 1Ni + ΣXi) High-Mn steel

Composition B (Fe + 23.3Mn + 13.7Cr + 5Ni + ΣXi) High-Mn stainless steel

Composition C (Fe + (16-19)Cr + (6-14)Ni + ΣXi): 300-series stainless steel alloys

* Measured

† From Y. S. Touloukian, R. K. Kirby, R. E. Taylor, and P. D. Desai, "Thermophysical Properties of Matter (IFI/Plenum, New York, 1975), Vol. 12.

Appl. Phys. Letters 47, 1-3 (1985)

ELECTRON TUNNELING INTO SUPERCONDUCTING FILAMENTS USING MECHANICALLY ADJUSTABLE BARRIERS

John Moreland and J. W. Ekin
Electromagnetic Technology Division
National Bureau of Standards
Boulder, Colorado 80303

Abstract

A new type of squeezable electron tunneling (SET) junction has been developed for tunneling into superconducting filaments. Stable, mechanically adjustable tunneling barriers between the native surfaces of sputtered Nb films and 30 μm diameter Nb filaments were established in liquid helium at 4 K. The current versus voltage characteristics of these SET junctions were used to determine the superconducting energy gap at the surface of the filaments. Since the filaments were etched from commercial superconducting magnet wire, this type of tunnel junction shows promise as a diagnostic probe of superconducting materials for high-field magnets.

PACS numbers: 74.50+r, 74.70.Ps, 73.40Gk, 73.40.Rw

Electron tunneling spectroscopy is an excellent probe of the superconducting state. It is the preferred method for determining the superconducting energy gap and the nature of the electron-phonon interaction since the conductance of a superconducting tunnel junction as a function of applied bias is directly related to the density of states of thermal excitations in a superconductor as a function of energy.[1,2]

Tunnel junctions stable enough for electron tunneling spectroscopy have traditionally relied on the formation of an insulating oxide barrier between conducting surfaces.[3,4] Native oxides grown under controlled conditions have been the foundation for tunneling experiments on superconductors[5,6] until recent developments that utilized artificial barriers including silicon oxide[7] and aluminum oxide[8,9] insulators, and squeezable electron tunneling (SET) junctions.[10,11]

The latter technique has also been adapted to bulk materials including Si (ref.12), $(TMTSF)_2 C\ell O_4$ (ref.13) and HgCdTe (ref.14) crystals. Though tunneling contacts to bulk materials have been made using some of the other methods mentioned above, mechanically adjustable junctions have additional versatility because a nondestructive tunneling contact can be translated relative to the surface of a sample. The electron tunneling microscope developed by Binnig and Rohrer[15], for example, works on this principle, substantially increasing the flexibility of tunneling measurements. Very recently Elrod, de Lozanne and Quate have shown that vacuum tunneling microscopes can be adapted to cryogenic experiments on superconductors.[16]

We present here a SET junction that takes advantage of the filamentary nature of superconductors drawn to small diameters in a reaction or stabilization matrix. Experimental current versus voltage (I-V) curves for SET junctions consisting of Nb filaments with Nb thin-film counter electrodes are discussed

along with data obtained for thin-film Nb-Nb junctions at 4 K. To our knowledge these are the first successful mechanically adjustable tunneling barriers between native Nb surfaces and the first SET junctions with a filament electrode.

Figure 1 shows the top view of a miniaturized SET junction used to determine the superconducting energy gap of the thin-film Nb counter electrodes. It consisted of electrode strips supported by flexible substrates that were separated by thin-film spacer strips. Alternating electrode and spacer strips were deposited on polished 50.8 mm (2 inch) diameter, 0.4 mm-thick Si wafers that were then scribed and broken into 6.4 x 12.7 mm (0.25 x 0.50 inch) chips. To obtain the geometry shown in Fig. 1, two of the chips were assembled at right angles with opposing electrodes to form the junction. A strip pattern was used to simplify the alignment of the opaque substrates. A layer of photoresist that protected the films from shards and dust that accumulated during scribing was removed with an acetone spin-wash just prior to junction assembly.

Superconducting counter electrodes were used because they gave rise to distinct structure in the I-V curves that provided a quality check for the tunneling barrier even if the sample electrodes were normal. A material with $T_c > 4$ K was experimentally convenient. Preliminary measurements of Nb filament-Pb film junctions revealed I-V characteristics identical to those obtained for Pb film-Pb film junctions. This indicated that the soft Pb had transferred to the Nb filaments. Sonnenfeld has observed the same phenomenon for Pb film-HgCdTe crystal SET junctions.[14] Sputtered Nb films were our next choice. Despite being more difficult to deposit, they showed no signs of rubbing off, and had larger T_c's and larger energy gaps than those obtained for Pb films.

All films were prepared using standard microelectronic photolithographic processing (based on Shipley 1350 photoresist[17]) in a clean room supplemented by laminar flow work stations. Evaporated SiO spacers were delineated using a lift off process. Evaporations took place at a pressure of 2×10^{-4} Pa and a rate of 1 nm/s. The target voltage was about 475 V. The Nb films were then etched in a reactive $O_2 - CF_4$ plasma.

Previously, dust contamination was minimized by acetone vapor degreasing precleaned substrates prior to evaporations.[11] We found that using Si wafers polished and precleaned by the manufacturer in conjunction with clean room processing without vapor degreasing also yielded reliable SET junctions. At first we were apprehensive about using contact masks to expose the photoresist; apparently the photoresist was tough enough to protect both the substrate and films deposited in preceding layers.

An iron electromagnetic squeezer scaled down from the original version[11] was used to compress the junctions to tunneling distances. The squeezer was mounted on the end of a dip stick for rapid experiments in a liquid helium storage Dewar. A copper chamber on top of the Dewar allowed the squeezer and junction assembly to warm in a dry helium atmosphere. This kept water from condensing on the apparatus and facilitated rapid ($\approx$ 10 min.) thermal cycling. The electrodes and spacers were 0.2 μm and 1.0 μm thick, respectively, so that the electrode surfaces were nominally 1.6 μm apart before squeezing. The squeezing force was applied along concentric circles 1 mm and 6 mm in diameter on either side of the junction. Under these conditions squeezing forces of about 0.25 N were necessary to make junction contact. This was in agreement with the force calculated for the given loading geometry of the Si substrates according to thin plate deflection formulas.[11]

Differential dI/dV (conductance) versus voltage curves were measured with a tunneling spectrometer that utilized a feedback circuit to keep a constant modulating voltage (250 μV, 100 Hz) across the junction.[18] Voltage was swept at a constant rate of 100 μV/s. All measurements were done at 4 K.

Figure 2 shows an experimental I-V curve typical of those obtained for Nb film-film SET junctions immersed in liquid helium at 4.0 K. Notice the distinct current inflections that, theoretically, should be separated by a voltage $\Delta V = 4\Delta_{film}/e$ for a tunnel junction with identical superconducting electrodes having an energy gap of Δ_{film} (e is the electron charge).[5] The junctions could be reversibly adjusted in that the I-V curves could be continuously changed from an open contact, to tunneling behavior, and finally to a short. Once a short was established, tunneling behavior could be obtained again by decreasing the squeezing force.

The superconducting energy gap was estimated from the position of the peaks in the dI/dV spectrum and found to be $\Delta_{film} = 1.4$ meV independent of the junction resistance measured at 10 mV bias for R(10 mV) > 10 kΩ. This value for the energy gap was close to the previous measurements by Broom et al[19] using native oxide and by Wolf, Zasadsinski, Osmun and Arnold[8] using aluminum oxide barriers. Both of these previous measurements gave about 1.5 meV at a lower temperature of 1.4 K. Assuming Tc ≈ 9 K, $\Delta_0 \approx 1.5$ meV, and a BCS energy gap temperature dependence (see, for example, ref. 5), this implies $\Delta = 1.43$ meV at 4 K. Thus the SET-junction results agreed with the earlier measurements using oxide barriers to within our experimental precision (≈ 0.1 meV).

The section of a SET junction that consisted of a superconducting filament held against the substrate of a thin-film counter electrode is shown in figure 3. The filament was held by a friction fit between tapered brass mandrels that press fit into tapered brass sleeves. A Be-Cu spring compressed

between the fiberglass-epoxy holder and one of the brass sleeves kept the filament in tension. This configuration provided rugged cryogenic electrical contacts to the filament. A pointed thumb screw reacted against the squeezing force of the electromagnet and allowed the holder to pivot so that the counter electrode substrate was flush against the plunger. Since the filament rested on the evaporated spacers, the counter electrode-filament spacing was determined by the amount of bow in the substrate supporting the electrode and the spacers. The amount of substrate bow was adjusted by applying forces as shown in the figure. Using the Nb film counter electrodes described above with different filaments from the same wire led to a variable series of junctions ranging from those that were shorted without any squeezing to those that required an unusually large squeezing force. This may have been due to inherent surface bowing of the Si chips in the fiberglass-epoxy holder, dust particles (all experiments occurred outside the clean room), or variations in the average filament diameter. Fortunately, the high compliance electromagnetic squeezer system allowed for large variations in the initial filament-film separation.

The Nb filaments ($\approx$ 30 μm in diameter) are obtained by etching away the Cu-Sn bronze matrix of an unreacted Nb_3Sn magnet wire using a 50/50 solution of nitric acid and water. Their surface topology is illustrated in figure 4 with electron micrographs of the filament-film SET junction and various magnifications of a single filament. Tunneling current(s) most likely flow through the small bump(s) ($\leq$1 μm in size) apparent along the surface of the filament (Fig. 4d).

Included in figure 2 is an experimental I-V curve measured for a Nb filament-Nb film junction immersed in liquid helium at 4.0 K. Like the film-film junctions, the filament-film junctions were reversibly adjustable. Since the counter electrodes used for filament measurements were calibrated in

the previous film-film SET junction experiment, the energy gap of the filament could be determined from the relation[5]

$$\Delta V = (2\Delta_{filament} + 2\Delta_{film})/e$$

where ΔV was the voltage separating the gap edges determined from the peaks of the dI/dV data.

Again ΔV was independent of the junction resistance for R(10 mV) > 10 kΩ. Given $\Delta_{film} = 1.4$ meV, we infer that $\Delta_{filament} = 1.0$ meV. A lower superconducting energy gap obtained for the filaments may not be surprising since they were fabricated in a Cu-Sn bronze matrix. X-ray microanalysis showed a minimum surface contamination of 10 wt.% Sn and 3 wt.% Cu.

Tunneling data could be repeated after establishing a short in the barrier. This implied that these SET junction contacts were nondestructive in the sense that the energy gap of the materials remained the same before and after contact.

In conclusion, SET junctions provide a viable method for tunneling to bulk superconducting materials. The following comments summarize some of our results for superconducting filaments.

1) We obtained small area ($\leq 1\ \mu m^2$) low leakage tunneling barriers between native Nb surfaces. They had continuously adjustable resistances. The adjustability was probably due to a combination of changes in the barrier area and thickness, possibly facilitated by the elasticity of the substrate and the Nb near contact points, or the presence of He between the Nb surfaces.
2) Tunneling gaps (ΔV) determined from differential dI/dV data were independent of junction resistance for R(10 mV) > 10 kΩ. Together,

tunneling gaps measured for Nb film-film and filament-film junctions gave Δ_{film} = 1.4 meV and $\Delta_{filament}$ = 1.0 meV. The difference was not surprising since the surfaces of the filaments contained Cu and Sn from the bronze matrix of the magnet wire (tunneling electrons probe only the surface of a superconductor to a depth of about one coherence length).

3) The junctions were stable against moderate room vibrations. They could be rapidly cycled ($\approx$ 10 min.) to cryogenic temperatures in a dry helium atmosphere so that counter electrodes could be calibrated and reused in later experiments.

We look forward to extending this technique to NbTi and Nb_3Sn filaments. Some particularly intriguing prospects include studying the effects of various chemical treatments on the properties of a superconducting surface and then depth profiling the energy gap by successively etching and probing the surface with a SET junction.

Acknowledgments

The authors wish to thank T. Capobianco, A. Clark, F. Fickett, R. Goldfarb, L. Goodrich, P. Hansma, R. Harris, K. Kilhstrom, F. Lloyd, D. Moreland, D. Moses,D. Rudman, and A. West, for their advice and helpful expedition of this project. This work was partially sponsored by the Department of Energy, Office of Fusion Energy, under interagency agreement #DE-AI01-84ER52113. Additional support was provided to one of us (J.M.) as a National Research Council Postdoctoral Associate.

References

1. D. J. Scalapino, J. R. Schrieffer, and J. W. Wilkins, Phys, Rev. 148, 263 (1966).
2. W. L. McMillan and J. M. Rowell, Superconductivity, Vol. 1, edited by R. D. Parks, 561 (Dekker, New York, 1969).
3. Tunneling Spectroscopy, edited by P. K. Hansma, (Plenum, New York, 1982).
4. R. V. Coleman, R. C. Morris, and J. E. Christopher, Methods of Experimental Physics v. 11 Solid State Physics, edited by R. V. Coleman, 123 (Academic, New York, 1974).
5. I. Giaever, Tunneling Phenomena in Solids, edited by E. Burstein and S. Lundqvist, 255 (Plenum, New York, 1969).
6. E. L. Wolf, Rep. Prog. Phys. 41, 1439 (1978).
7. D. A. Rudman and M. R. Beasely, Appl. Phys. Lett. 36, 1010 (1980).
8. E. L. Wolf, J. Zasadzinski, J. W. Osmun, and G. B. Arnold, J. Low Temp. Phys. 40, 1980).
9. J. S. Moodera, R. Meservey, and P. M. Tedrow, Appl. Phys. Lett. 41, 488 (1982).
10. J. Moreland, S. Alexander, M. Cox, R. Sonnenfeld, and P. K. Hansma, Appl. Phys. Lett. 43, 387 (1983).
11. J. Moreland and P. K. Hansma, Rev. Sci. Instrum. 55, 399 (1984).
12. J. Moreland, J. Drucker, J. P. Kotthaus, A. Adams, R. Kvass, and P. K. Hansma, Appl. Phys. Lett. 45, 104 (1984).
13. J. Moreland, Ph.D. Thesis, University of California, Santa Barbara (1984).
14. R. Sonnenfeld, J. Moreland, A. Adams, R. Kvass, and P. K. Hansma, to be published in J. Appl. Phys.

15. G. Binnig and H. Rohrer, Surf. Sci. 126, 236 (1983).

16. S. A. Elrod, A. L. de Lozanne, and C. F. Quate, Appl. Phys. Lett. 45, 1240 (1984).

17. Certain commercial materials are identified in this paper to specify the experimental study adequately. In no case does such identification imply recommendation or endorsement by the National Bureau of Standards, nor does it imply that the material identified is necessarily the best available for the purpose.

18. A. F. Hebard and P. W. Shumate, Rev. Sci. Instrum. 45, 529 (1974).

19. R. F. Broom, S. I. Raider, A. Oosenbrug, R. E. Drake, and W. Walter, IEEE Electron Dev. ED-27, 1998 (1980).

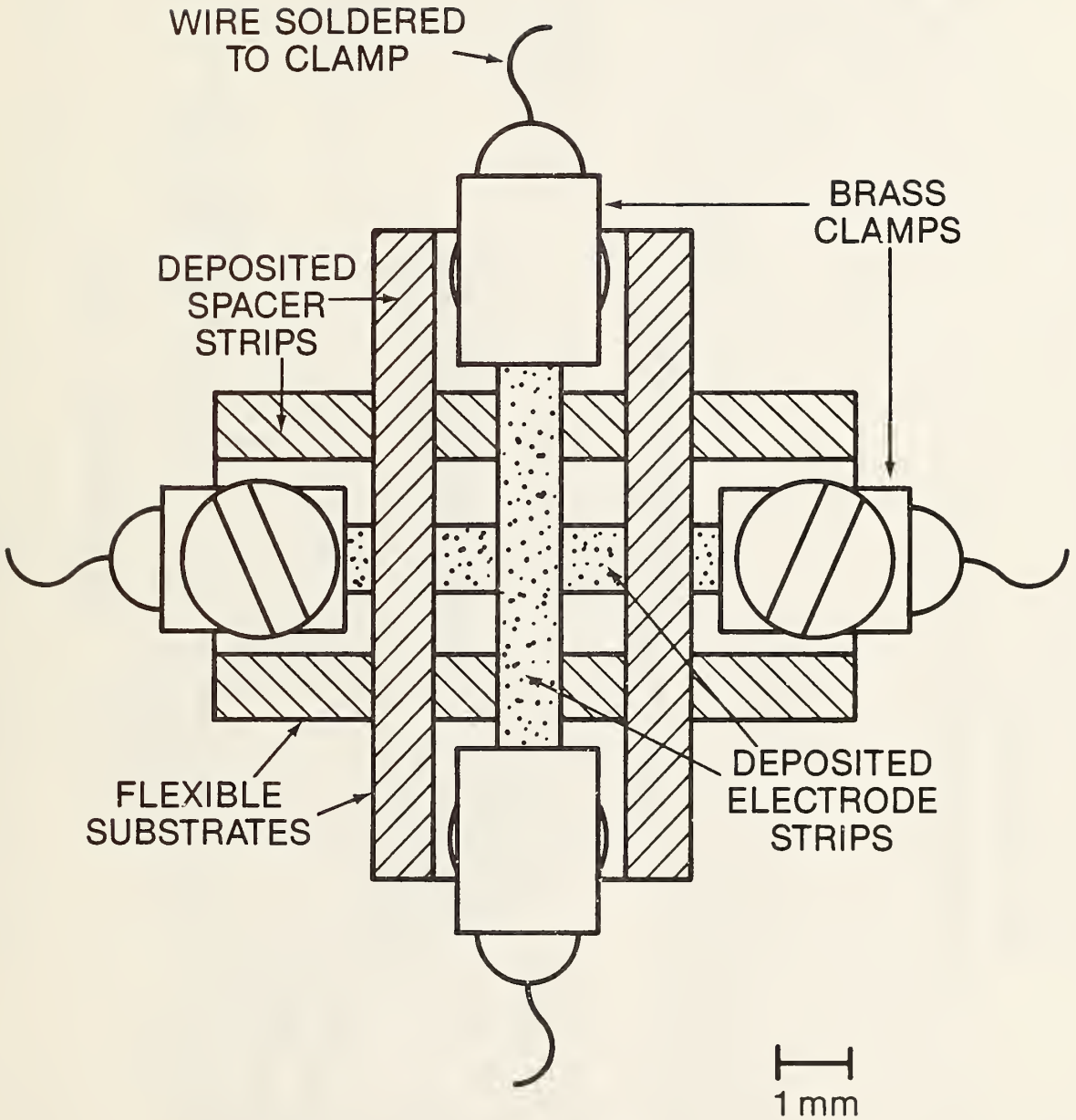

Figure 1. Top view of a miniaturized SET junction showing intersecting deposited spacer and electrode strips. Though opaque Si chips were used, transparent substrates are shown for clarity. Brass screw clamps are used to make electrical contact to the electrodes.

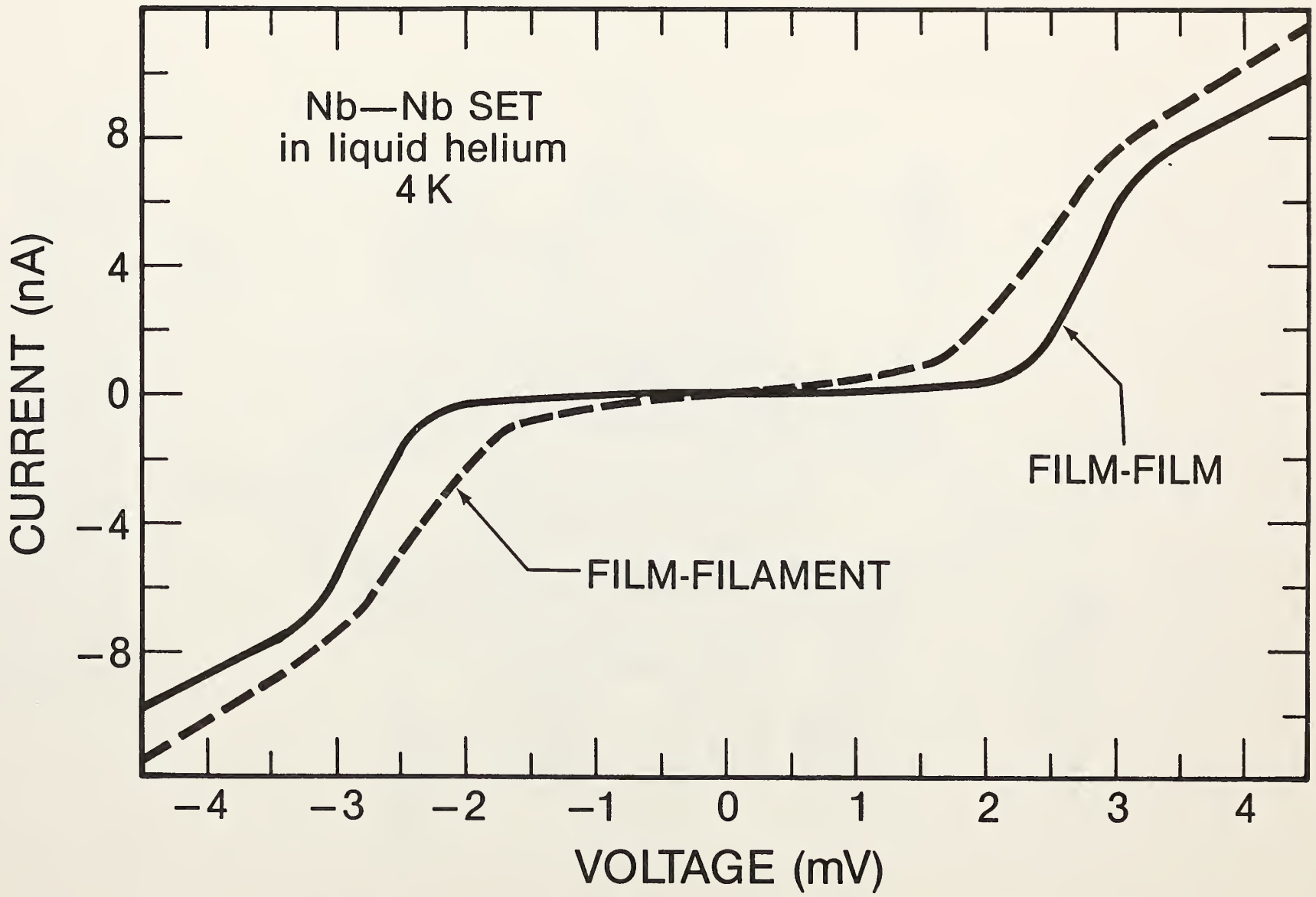

Figure 2. Typical I-V curves of Nb film-Nb film, and Nb film-Nb filament SET junctions. The squeezer apparatus was immersed in liquid helium at 4 K.

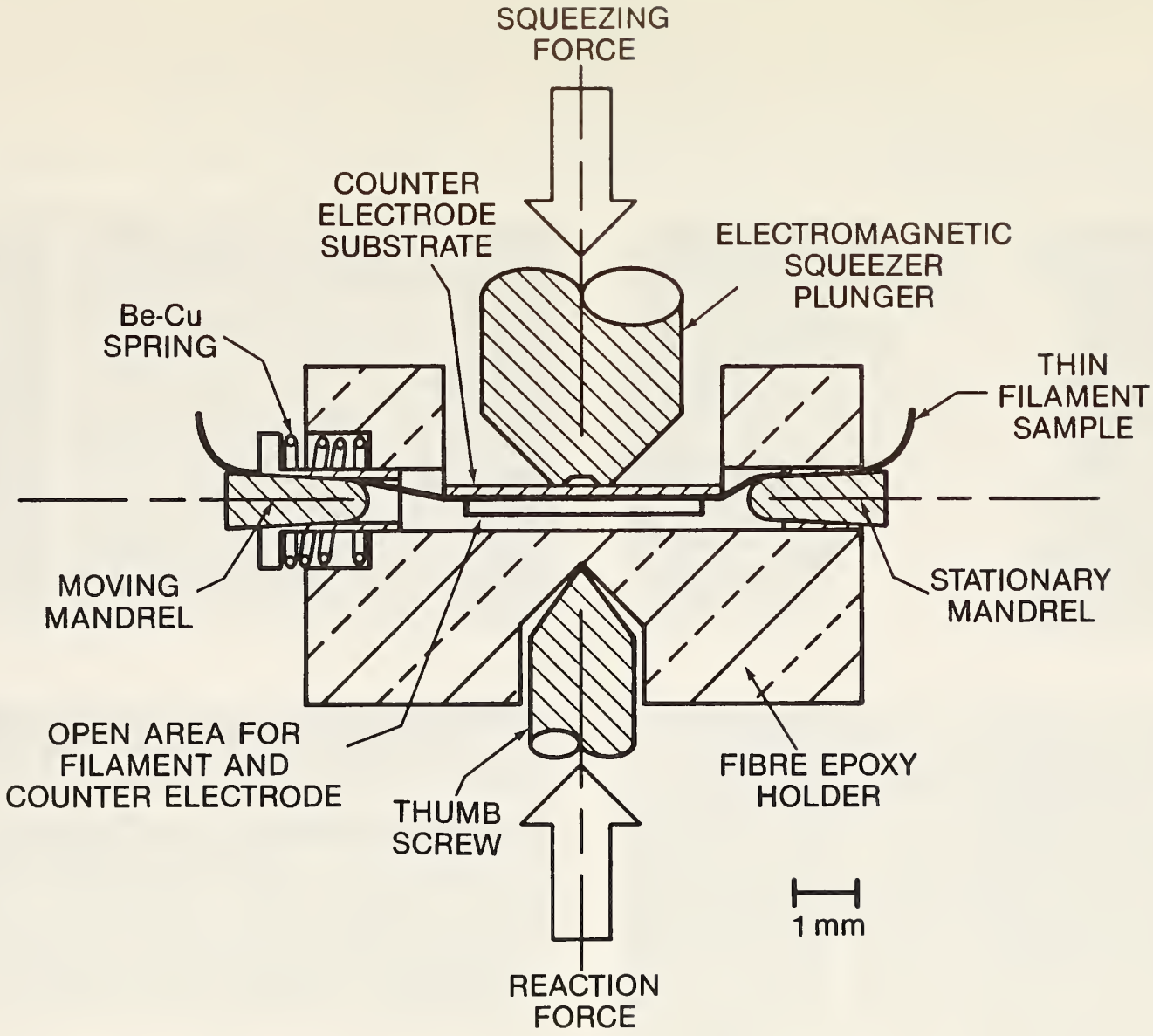

Figure 3. Section of the filament holder for film-filament tunneling experiments. The squeezing force from an electromagnet bows the counter electrode substrate against a filament. The filament is tensioned against the substrate by the spring loaded mandrel holder.

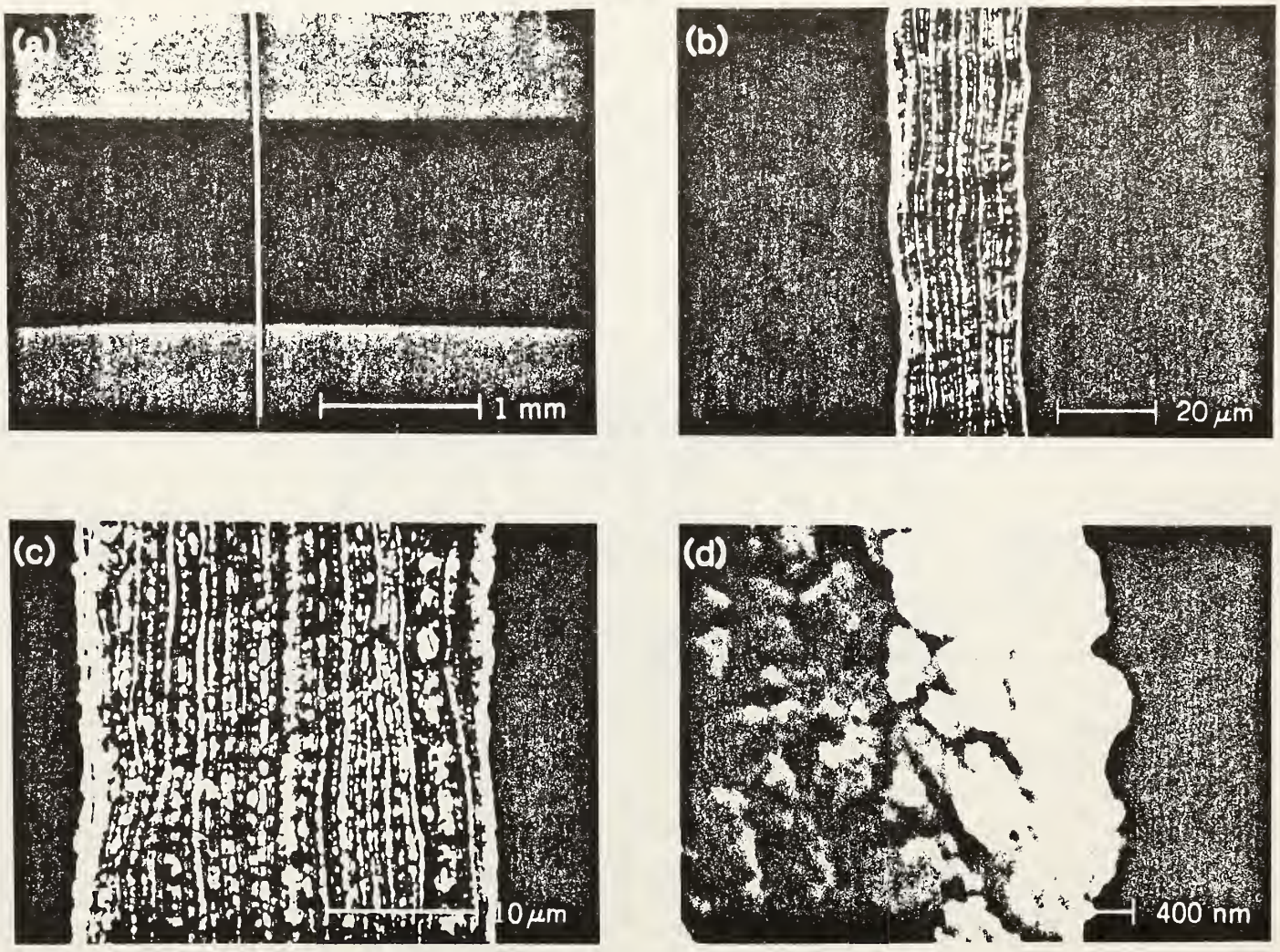

Figure 4. Electron micrographs of a Nb filament etched from an unreacted Nb_3Sn magnet wire showing the types of roughness that affect film-filament SET junctions. a) Nb filament crossing a counter electrode. b) undulations of filament diameter. c) striations. d) small bumps $\leq$ 1 μm in size.

APPENDICES

A. "Effect of Stainless Steel Reinforcement on the Critical Current Versus Strain Characteristic of Multifilamentary Nb_3Sn Superconductors" J. W. Ekin, R. Flukiger, and W. Specking, published in J. Appl. Phys. 54, 2869 (1983).

B. "Further Investigations of the Solid-liquid Reaction and High-field Critical Current Density in Liquid-infiltrated Nb-Sn Superconductors" M. Hong, D. M. Maher, M. B. Ellington, F. Hellman, T. H. Geballe, J. W. Ekin, and J. T. Holthuis, IEEE Trans. Magn. MAG-21, 771 (1985).

C. Trip report covering visits made December 5-14, 1984 to superconductor research laboratories at Kyushu University, (Fukuoka, Japan); Japanese National Railway "MAGLEV" Test Site, (Miyazaki, Japan); Japanese Atomic Energy Research Institute (Tokai, Japan); Tohoku University (Sendai, Japan); and the DOE Japan-US Workshop on High-Field Superconducting Materials for Fusion (Tsukuba, Japan).

Effect of stainless steel reinforcement on the critical current versus strain characteristic of multifilamentary Nb_3Sn superconductors

J. W. Ekin
Electromagnetic Technology Division, National Bureau of Standards, Boulder, Colorado 80303

R. Flükiger and W. Specking
Kernforschungszentrum Karlsruhe, Institut für Technische Physik, 7500 Karlsruhe, Postfach 3640, Federal Republic of Germany

(Received 25 August 1982; accepted for publication 11 January 1983)

A series of multifilamentary Nb_3Sn superconductors were fabricated containing from 0% to 52 vol % stainless steel reinforcement strands as an integral part of the conductor. Critical current versus strain measurements are reported which show that the stainless steel introduces a relatively large compressive prestrain, ϵ_m, into the superconductor, ranging from $\epsilon_m \simeq 0.3\%$ for no stainless steel reinforcement to $\epsilon_m = 0.84\%$ for 52 vol % stainless steel. Accompanying this high compressive prestrain in the reinforced conductors is a large degradation of the conductor's critical current, I_c. The I_c degradation relative to the strain-free value has been measured, for example, to be more than 50% at 13 T for $\epsilon_m = 0.64\%$. Several methods are discussed for reducing the large I_c degradation in A15 superconductors containing internal reinforcement.

PACS numbers: 74.70.Ps, 74.70.Lp

In the design of large superconducting magnet systems, a great amount of structural reinforcement is necessary to contain the magnetic forces generated when the magnet is energized. For example, it has been calculated that a fully stabilized Nb_3Sn conductor in a 12 T fusion magnet would consist of nearly 50% stainless steel, while the Nb_3Sn itself would occupy only about 10% of the volume.[1] To be effective in providing adequate support for the superconductor, it is essential to have this large amount of reinforcing material distributed throughout the winding. A superconductor fabricated with stainless steel as an integral part of the wire would provide direct and uniform support of the superconductor as well as simplify magnet construction, particularly if the reinforcement were prefabricated with compound superconductors in their unreacted (ductile) state. In such a composite, however, the reinforcing material will have an effect on the mechanical prestrain state of the superconducting material after reaction heat treatment. This is of particular interest in the A15 superconductors where the critical current is affected strongly by the presence of strain.[2,3]

In an earlier experiment, a large compressive prestrain was reported in a loosely cabled Nb_3Sn conductor slipped inside a stainless steel tube.[4] In the test, the ends of a short length of the conductor were compacted in order to "pin" the superconducting strands to the stainless steel jacket. Presumably because of this end compaction, it was found that significant prestrain was introduced into the Nb_3Sn by thermal contraction of the outer stainless steel tube. The effect should be even greater in conductors where the superconductor and stainless steel are continuously bonded along their entire length.

This paper reports the first results on the prestrain effect of stainless steel reinforcement *internally bonded* to multifilamentary Nb_3Sn strands. The test conductor was fabricated as a monolith with stainless steel reinforcement bonded to the Nb_3Sn along its entire length through a solid copper interface. The results indicate that at 13 T the critical current of the conductor is severely degraded relative to the same conductor without internal steel reinforcement.

Several reinforced Nb_3Sn superconductors were fabricated by combining small (0.2 mm diam) unreacted strands (Nb + bronze) with fine stainless steel strands (0.1 mm diam) into a copper matrix, see Fig. 1. The superconducting strands were multifilamentary bronze-process Nb_3Sn consisting of 9072 niobium filaments embedded in a Cu-13 wt. % Sn bronze matrix. The stainless steel strands were German Mat. No. 1.4455 which is similar to AISI 316LN. A compositional breakdown of both types of strands is given in Table I.

Several methods were tried for combining the stainless steel with unreacted superconducting composite strands. The most successful consisted of the following procedure. The stainless steel and superconducting strands were first annealled in an inert atmosphere for 30 min at 1000 and 550 °C, respectively, to remove work hardening. They were then loosely cabled together, lightly etched with nitric acid and electroplated with a ~ 0.1-mm layer of copper. The soft copper sheath served to protect the superconducting strands as the cable was swaged (12% reduction by area) into a solid unit. The conductor was then lightly etched again with nitric

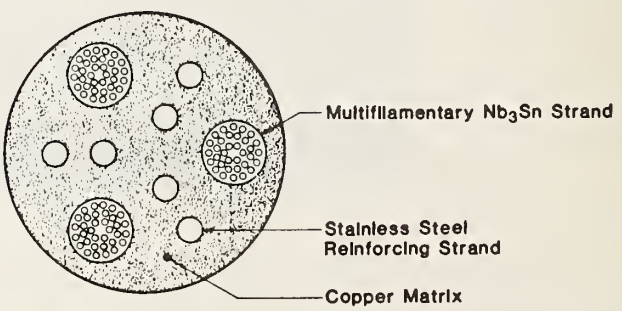

FIG. 1. Schematic cross-sectional view of multifilamentary Nb_3Sn conductor with internal stainless steel strand reinforcement.

 0021-8979/83/052869-03$02.40

TABLE I. Compostion of strands.

Superconductor strands	Stainless steel strands	
Strand diam 0.2 mm	C	0.03%
No. filaments 9072	Cr	20.5%
Filament diameter 1.1 μm	Fe	55.3%
Bronze (Cu-13 wt. %Sn)/Nb = 2.5:1	Mn	5.0%
Reaction temp. 700 °C	Mo	3.0%
Reaction time 20 h	N	0.17%
	Ni	16.0%

acid and finally electroplated with an additional layer of copper for stability. Nb_3Sn was then formed by reacting the entire composite (superconductor + stainless steel) at 700 °C for 20 h in an inert atmosphere of argon. Samples were fabricated with stainless steel fractions as high as 52% (where the copper stabilizer volume has been omitted from the stainless-steel volume fraction determination).

The critical current of several of the samples was measured as a function of uniaxial strain applied at 4.2 K using an apparatus described in Ref. 2. The measurements were carried out in a magnetic field perpendicular to the wire axis, produced by a 13 T solenoidal magnet. A critical-current criterion of 2 μV/cm was used.

Figure 2 shows the strain dependence of the critical current measured for a single (uncombined) strand of superconductor. The critical current has been normalized by its maximum (strain-free) value I_{cm} in order to show the relative degradation. Also, the results have been plotted as a function of *intrinsic* strain defined as $\epsilon_0 \equiv \epsilon - \epsilon_m$. Here ϵ_m is the strain at which the critical current is maximum and corresponds to the magnitude of compressive prestrain introduced into the superconducting material by thermal contraction of the surrounding matrix material.[5] This normalization has been made to remove the effect of the compressive prestrain in comparing the data. ϵ is the strain applied to the conductor as a whole, where ϵ_0 is the intrinsic strain actually experienced by the superconducting filaments within the conductor. Negative values of the intrinsic strain ϵ_0 indicate the

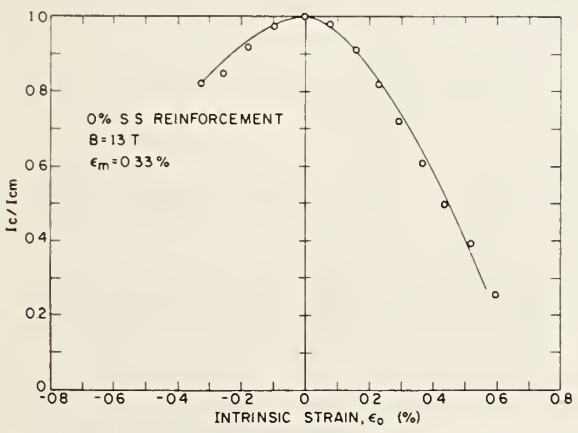

FIG. 2. Relative critical current degradation I_c/I_{cm} as a function of intrinsic strain ϵ_0 in a multifilamentary Nb_3Sn conductor containing no stainless steel reinforcement. ϵ_m is the compressive prestrain introduced into the superconductor by thermal contraction of the matrix material, $\epsilon_0 \equiv \epsilon - \epsilon_m$.

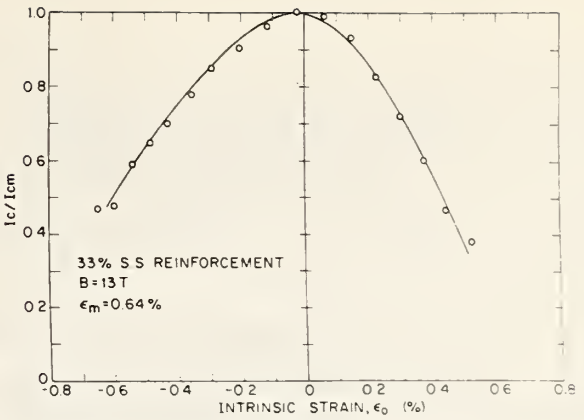

FIG. 3. Relative critical current degradation I_c/I_{cm} as a function of intrinsic strain ϵ_0, in a multifilamentary Nb_3Sn conductor containing 33 vol % stainless steel reinforcement. Note the large increase in ϵ_m compared with Fig. 2 and the accompanying degradation of the initial critical current value.

superconducting material is under compression, while positive values indicate tension.

Figure 3 shows similar data obtained on a conductor containing 33 vol % stainless steel reinforcement. Note that the I_c/I_{cm} vs ϵ_0 curve is exactly the same as in Fig. 2, except the magnitude of the compressive prestrain ϵ_m present in the reinforced conductor (0.64%) is more than double that for the unreinforced superconducting strand. The curve in Fig. 3 is simply an extension of the curve in Fig. 2 to larger compressive strain values. The shapes of these curves also agree within 5% with those previously measured on other unreinforced commercial Nb_3Sn conductors[2] and is characteristic for all Nb_3Sn.

Results obtained on another stainless-steel reinforced superconductor containing 52 vol % stainless steel were similar to those shown in Fig. 3, except the amount of compressive prestrain present in the superconductor was significantly greater (0.83%). Thus the magnitude of ϵ_m is a strong function of the volume fraction of reinforcing stainless steel present.

The irreversible strain, ϵ_{irrev},[6] where the conductor was permanently damaged was also measured to be quite high for these materials. Values of ϵ_{irrev} of up to 1.87% were measured in the samples with the highest amount of stainless steel reinforcement. However, this high value of ϵ_{irrev} is due to the exceptionally large values of ϵ_m in these samples. In terms of the *intrinsic* tensile strain experienced by the superconductor, permanent fracture consistently occurred at $\epsilon_0 \simeq 1\%$.

These results can be explained in terms of the differential thermal contraction between the Nb_3Sn superconductor and the stainless steel reinforcing strands. When cooled from the reaction heat treatment temperature of 700 °C to 4.2 K, stainless steel contracts about 1.64%,[7,8] whereas Nb_3Sn contracts only 0.75%,[8] see Table II. The difference in thermal contraction for the two materials, ~ 0.9%, is the maximum amount of precompression that could be introduced into the Nb_3Sn by thermal contraction of the stainless steel. The actual compressive prestrain, ϵ_m, depends on the relative

TABLE II. Relative thermal contraction for the indicated temperature ranges.

	700 °C to 4.2 K	20 °C to 4.2 K
Stainless steel	1.64%	0.30%
Nb_3Sn	0.75%	0.15%

strengths and volume fractions of the two materials.

In a typical nonreinforced multifilamentary Nb_3Sn conductor, the thermal contraction of bronze (1.68%)[8] is similar to that of stainless steel, but bronze alone yields at high temperatures during cooldown from ~700 °C, resulting in an ϵ_m of typically only 0.2%–0.4% (the copper stabilizer has an even lower yield strength than bronze and, to first order, its thermal contraction effect has been neglected here).

In stainless steel reinforced conductors, however, the stainless steel strands have a much higher yield strength than bronze. Because the steel yields very little during cooldown, the superconductor is subjected to a much greater compressive prestrain. In the example shown in Fig. 3, 33% stainless steel reinforcement resulted in $\epsilon_m = 0.64\%$. As described in the previous section, 52% stainless steel reinforcement resulted in $\epsilon_m = 0.83\%$. The latter conductor has an ϵ_m near the maximum (0.9%) that would be expected, based on the difference in thermal contraction rates for stainless steel versus Nb_3Sn in Table II. So, to summarize, the stainless steel reinforcement results in a significantly larger compressive prestrain than in conventional bronze-matrix superconductors, not because its thermal contraction is any greater than bronze (or copper), but because of its higher yield strength, particularly at high temperatures.

The very high compressive prestrain introduced by the stainless steel presents a significant mechanical design problem. The conductor cannot be left in this state of high precompression or more than 50% of the current carrying capibility of the conductor is lost, as shown in Fig. 3. On the hand it is very hard to apply the uniaxial strain design criterion[9] in this case and simply design the magnet so the combination of fabrication strain and magnetic forces compensate the thermal contraction effect. A tensile applied strain of 0.6%–0.9% is too much compensation to safely introduce without the possibility of a major mechanical failure in the conductor or magnet structure.

At least four possibilities exist for handling the problem of large compressive prestrain in reinforced conductors.

(1) Partially compensate the compression by prestraining the conductor a moderate amount during magnet fabrication. Only about 0.2%–0.3% strain can be compensated by this technique, however, because of the practical tensile limits of the structural materials in the conductor. The remaining compressive strain in the superconducting material will still result in a reduced current-carrying capacity.

(2) Join the reinforcing material to the superconductor at room temperature after reaction. In this manner, only an additional 0.15% compressive prestrain is introduced by the stainless steel in cooling to 4.2 K (see Table II). The potential for damage to the superconductor during joining and handling can be extreme in this case, however.

(3) Use structural reinforcement with a smaller thermal contraction coefficient more nearly matching that of the superconductor.

(4) Use a superconducting material with a lower strain sensitivity such as Nb–Ta/Sn (Ref. 10) or Nb–Hf/Sn–Ga.[11] For example, Nb-Hf/Cu-Sn-Ga conductors have been fabricated and tested in which the strain degradation of the critical current has been measured to be about half that for commercial Nb_3Sn at 13 T.[11] In this case the large compressive prestrain introduced by the structural reinforcement does not result in such a large critical current degradation, and the added precompression acts as an extra safety margin in conductor handling during magnet fabrication. These materials are only in the development stage, but their decreased strain sensitivity would be particularly advantageous in this situation.

This work was performed while J. W. Ekin was a visiting scientist at the Kernforschungszentrum Karlsruhe (KfK) from June to August 1981. Support was provided by KfK and partially by the Naval Ship Research and Development Center, Maryland. Helpful discussions with C. Schmidt, W. Maurer, F. Arendt, P. Komarek, W. Heinz, P. Turowski, A. Nyilas, W. Schauer, N. Tonk, and A. F. Clark during the course of this work are gratefully acknowledged.

[1]W. Maurer and F. Arendt (private communication).
[2]J. W. Ekin, Cryogenics **20**, 611 (1980).
[3]J. W. Ekin, IEEE Trans. Magn. **MAG-17**, 658 (1981).
[4]R. M. Scanlan, R. W. Hoard, D. N. Cornish, and J. P. Zbasnik, in *Filamentary A 15 Superconductors*, edited by M. Suenaga and A. F. Clark (Plenum, New York, 1980), p. 221.
[5]G. Rupp, IEEE Trans. Magn. **MAG-13**, 792 (1977).
[6]J. W. Ekin, IEEE Trans. Magn. **MAG-15**, 197 (1979).
[7]R. J. Corruccini and J. Gniewek, *Thermal Expansion of Technical Solids at Low Temperatures*, NBS Monograph 29 (National Bureau of Standards, Boulder, Colorado, 1961).
[8]Y. S. Touloukian, R. K. Kirby, R. E. Taylor, and P. D. Desai, *Thermophysical Properties of Matter* (IFI/Plenum, New York, 1975), Vol. 12, p. 1138, 601, 790.
[9]J. W. Ekin, Adv. Cryog. Eng. **24**, 306 (1978).
[10]R. Flükiger, in *Filamentary A 15 Superconductors*, edited by M. Suenaga and A. F. Clark (Plenum, New York, 1980), p. 299.
[11]J. W. Ekin, H. Sekine, and K. Tachikawa, J. Appl. Phys. **52**, 6252 (1981).

IEEE TRANSACTIONS ON MAGNETICS, VOL. MAG-21, NO. 2, MARCH 1985

FURTHER INVESTIGATIONS OF THE SOLID-LIQUID REACTION AND HIGH-FIELD CRITICAL CURRENT DENSITY IN LIQUID-INFILTRATED Nb-Sn SUPERCONDUCTORS

M. Hong, D. M. Maher, and M. B. Ellington
AT&T Bell Laboratories, Murray Hill, NJ 07074

F. Hellman and T. H. Geballe*
Department of Applied Physics, Stanford University, CA 94305

J. W. Ekin
National Bureau of Standards, Boulder, CO 80303

J. T. Holthuis
Lawrence Berkeley Laboratory, Berkeley, CA 94720

ABSTRACT

Superior superconducting properties, such as high J_c's and T_c's, have been obtained from reacted liquid-infiltrated Nb-Sn composite wires. These excellent properties are attributed to the chemistry and structure of the material, which is prepared by a unique solid (Nb) - liquid (Sn) reaction. From heat capacity measurements, sharp bulk superconducting transitions of the A15 phase occur at 17.2-18 K and the weight fraction of A15 in the composite wire is ~23%. Analytical electron microscopy techniques have shown that: the microstructure of these conductors consists of alternating large-grain and small-grain filaments; these two types of filaments correspond to BCC Nb(Sn) and cubic A15 $Nb_{75\pm x}Sn_{25\mp x}$ phases, respectively; the A15 filaments ($\leq$0.5 μm) are chemically homogeneous in terms of measured X-ray intensity ratios to within ±7%, which implies that $x \sim 1.5$; and the A15 grains are essentially free of extended lattice disorder down to a resolution of ~0.34 nm. Recent work in which Nb is alloyed with Ta has shown that these superconducting properties can be improved upon; e.g. high overall J_c's of $\sim 1.8\times10^4$ A/cm^2 at 20 T and 4.2 K have been measured. Also, the liquid-infiltrated Nb(Ta)-Sn composites have a damage strain tolerance nearly double that of commercial bronze-processed Nb-Sn conductors.

I. INTRODUCTION

High critical current densities (J_c) in superconducting wires operating at fields of 12 T and above are always needed, especially for applications in magnetic fusion reactors. Considerable effort has been made to achieve this objective. Reacted liquid-infiltrated Nb-Sn multifilamentary composite wires carry the highest J_c measured thus far among Nb-Sn based superconductors at fields above 12 T.[1,2] Unlike the "in-situ" method, the bronze-process technique, and their variants in which A15 is formed through a solid-state diffusion mechanism, the A15 phase formation in the liquid-infiltrated wire results from a rapid solid Nb-liquid Sn reaction.

The difference between these two reaction mechanisms was discussed previously.[3] The present work was undertaken in order to extend our understanding of this solid-liquid reaction by using both heat capacity measurements and analytical electron microscopy (AEM). AEM techniques [4-6] included selected-area diffraction, high-resolution imaging, scanning transmission electron microscopy (STEM), and energy-dispersive x-ray spectroscopy (EDXS). The heat capacity measurements showed that sharp bulk superconducting transitions of the A15 phase occur at 17.2-18 K. The AEM studies showed that the A15 filaments are chemically homogeneous to within ±1.5at%Sn.

Finally, when a small amount of Ta (~1at%) is alloyed with the Nb, we found an enhanced B^*_{c2}, high overall J_c's at high fields, and excellent mechanical properties.

Manuscript received September 10, 1984.

II. EXPERIMENT

1. MATERIAL PREPARATION

The liquid-infiltration technique is a well established technique in powder metallurgy. The experimental procedure used to fabricate the laboratory-scale wire was described earlier.[1] The wire was in the form of a multifilamentary composite containing Nb [or Nb(Ta)] (~5.0 μm) and Sn (<0.5 μm). The Nb [or Nb(Ta)] and Sn filaments are intimately tangled with each other. The diameter of the tested composite wire was 0.22 mm or smaller. The overall chemical composition was approximately Nb-8at%Sn (or Nb-1at%Ta-8at%Sn). The chemical composition can be controlled by the starting Nb [or Nb(Ta)] powder size, the compacting pressure, and the sintering condition. The A15 phase was then formed by a reaction at 750°C or above.

For the Nb(Ta)-Sn wire, first a Nb-1at%Ta alloyed ingot was made by arc-melting pure components under a high-purity argon atmosphere. The starting materials were Nb and Ta of 99.9% purity and very low oxygen content. The arc furnace was equipped with a water-cooled nonconsumable tungsten electrode and a copper hearth. The arc-cast ingot was homogenized at 1250°C for 24 hours. The Nb(Ta) powder was then obtained from the homogenized ingot using a hydride-dehydride technique.

2. SUPERCONDUCTING TRANSITION MEASUREMENTS

Normal-superconducting transition temperatures were measured using resistive (electrical), inductive (magnetic), and calorimetric methods. Inductive critical temperatures were measured at a frequency of 100 Hz and an applied field of 4×10^{-5}T. The samples used in the inductive T_c measurements were in a wire form. They were either cut into small pieces or wrapped helically so that several turns were contained within a 3 mm diameter.

The sample chosen for heat capacity measurements was cut from the same wire that was used for the inductive T_c and the critical current J_c measurement, as well as the AEM studies. Heat capacity was measured from 1.8 to 30 K using a method developed for small sample calorimetry and described elsewhere.[7]

3. ANALYTICAL ELECTRON MICROSCOPY

For AEM studies, longitudinal sections (~3 mm in length) were obtained by mechanical polishing and ion milling. The results reported here are for a reaction treatment of 96 hours at 750°C.

EDXS was carried out in the scanning transition mode using a 5 nm probe, and area selection was done from annular dark-field images (only reacted zones which extended into the vacua were analyzed) and considerable care was taken to ensure that individual grains were oriented into a weakly diffracting condition. Net peak intensities (FWHM) for the Nb and Sn K-alpha lines (K_α) at 16.6 keV and 25.3 keV, respectively, were ratioed. This ratio $(I_{Nb}/I_{Sn})_{K_\alpha}$ was taken as a figure of merit in assessing homogeneity of reacted A15 filaments.

0018-9464/85/0300-0771$01.00

4. CRITICAL CURRENT MEASUREMENTS

Critical currents were obtained using an apparatus designed to simultaneously apply tensile strain, current, and a perpendicular magnetic field to short wire samples at 4.2 K.[8] A critical-current criterion of 2 μV/cm was used. The overall non-copper critical current density described below was determined using the combined area of A15 and BCC phases, excluding only the copper-stabilizer area.

III. RESULTS AND DISCUSSION

1. NORMAL-SUPERCONDUCTING TRANSITIONS

For the Nb-Sn wires, inductive T_c onsets of 17.9 K with a very sharp transition width of 0.2 K were obtained at the very initial stage of a 950°C reaction. This indicates that the solid-liquid reaction is rapid. Prolonged heat treatments up to 200 hours at 950°C did not change either the T_c onsets or the transition width. The reaction rate is slower with heat treatments at 750°C. A slightly lower T_c onset of 17.6 K was observed and a somewhat wider transition width of 3.1 K occurred at the initial stage of this heat treatment. Nevertheless, aging for 24 hours increased the T_c to 17.9 K and narrowed the transition width. This may be due to an improvement of the ordering parameter within the A15 phase.

For the Nb(Ta)-Sn wires, inductive T_c onsets of 18.1-18.2 K along with a very sharp transition width of <0.3 K were observed with reaction at 800-950°C. The measured T_c onsets are slightly higher than those of the reacted binary Nb-Sn composite wires.

Heat capacity data for a sample which was heat treated at 950°C for 3 hours and weighed 7.6 mg are shown in Fig. 1. The y-axis units are mJ/g-atom-K^2 where 1 g-atom of Nb-8at% Sn weighs 94.96 grams. The superconducting transitions of the BCC and A15 phases occur at 6.7-7.0 K and 17.7-18 K, respectively. The detailed analysis of the data has been given elsewhere.[9] The amount of A15 in the sample was estimated to be 1.76 mg or 23 wt%. For the area of high transitions, the discontinuity between 17.7 K and 18 K represents 1.2 mg which is approximately 70% of the presumed A15 phase in the sample. Extrapolating the data to an ideally sharp transition, as shown by the solid line in Fig. 1, gives 1.7 mg of A15, the same value as found above, but with a T_c from 17.2 to 18.0 K. This transition is still quite sharp and, using T_c versus at %Sn data,[10] indicates less than a 0.5at% variation in the Sn concentration within the A15 phase.

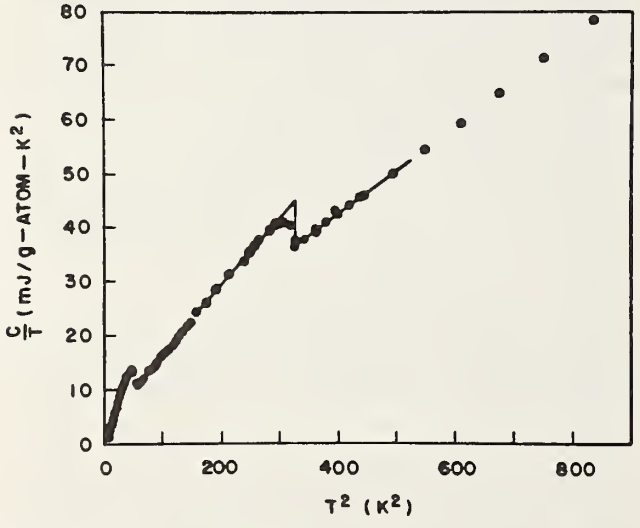

Fig. 1. Heat capacity data for a liquid-infiltrated Nb-at%Sn wire reacted at 950°C for 3 hours.

By contrast, the discontinuity at 7 K only represents 1.7 mg or 30% of the presumed BCC phase. The transition temperature of the remaining BCC phase is smeared out below 6.7 K. This wide transition width indicates a variation in the amount of Sn dissolved in the Nb. This variation of Sn concentration in the Nb was also found earlier using STEM/EDXS.[11]

This sharp superconducting transition of the A15 phase, which forms by reacting liquid-infiltrated Nb-Sn composite wire and is observed by heat capacity measurements, is in strong contrast to the transitions which are observed for in-situ and bronze-processed Nb-Sn conductors. Heat capacity measurements exhibited small and very broad superconducting transitions for these two conductors.[12,13] It should be borne in mind that the A15 phase in the latter conductors forms through a solid-state diffusion reaction while the A15 formation in the liquid-infiltrated conductors is due to a rapid solid-liquid reaction. It is clear that the solid-liquid reaction gives a uniform composition across the A15 while significant compositional variations result from the solid-state diffusion reaction.

Data in Fig. 1 indicate that the heat capacity technique is, indeed, a proper method to measure the exact amount of A15 in the wire. This is the first time that a 23 wt% of A15 phase has been detected in a reacted liquid-infiltrated Nb-Sn wire. Since an overall J_c of nearly 2×10^4 A/cm^2 at 20 T and 4.2 K has been achieved in this wire,[2] the true critical current density carried by the A15 region may be near 10^5 A/cm^2 at 20T and 4.2 K. It is also suggested that this heat capacity measurement may be used to study other multifilamentary A15 superconducting wires when the information on the amount of A15 is needed.

2. ANALYTICAL ELECTRON MICROSCOPY

The microstructure of a liquid-infiltrated Nb-Sn composite which was reacted for 96 hours at 750°C has been characterized by conventional transmission electron microscopy[4] and high-resolution electron microscopy.[5] The basic microstructure of the composite consists of alternating large-grain and small-grain filaments (see Fig. 2). The small-grain filaments are typically 0.3 to 0.5 μm in width and several tens of micrometers in length. Selected-area diffraction patterns (spatial resolution ~1 μm diameter) which were obtained from areas similar to that shown in Fig. 2 could be indexed self-consistently in terms of a BCC Nb phase and a cubic A15 phase (i.e. $Nb_{75\pm x}Sn_{25\mp x}$). If the Nb lines were taken as the reference for obtaining the camera constant of the microscope, then each pattern up to 14 d-spacings was consistent with those expected from the A15 phase $Nb_{75}Sn_{25}$.

From the point of view of extended lattice defects the two filaments were quite different. The BCC Nb filaments contained a very high density of dislocation arrays, mostly comprised of small dislocation loops (see right-hand filament in Fig. 2), whereas the A15 filaments consisted of a heterogeneous population of nearly perfect grains ranging in size from ~10 nm to ~0.2 μm. A significantly high percentage of the grain boundaries exhibited image contrast behavior typical of low-angle boundaries, and no evidence for inclusions was observed either within grains or at grain boundaries. Moreover no dislocation contrast was observed within the grains. The degree of perfection was further confirmed from high-resolution images, which were obtained,, from individual grains and across adjacent grains. An example is shown in Fig. 3, where the (110) lattice spacings are resolved and no contrast features that are above the point-to-point resolution limit of the microscope (0.34 nm) can be attributed to lattice disorder.

Energy-dispersive X-ray spectroscopy was used to assess the chemical homogeneity of these reacted A15 filaments. The measured intensity ratio $(I_{Nb}/I_{Sn})_{K_\alpha}$, where I is the net integrated intensity from the K_α lines of Nb and Sn, was taken as a figure of merit and is denoted here as χ. Spectra were obtained only from thin, isolated filaments (<100 nm thick) which protruded into the vacuum. Typically three spectra were recorded "across" a filament and the number of sets recorded "along" the filament varied

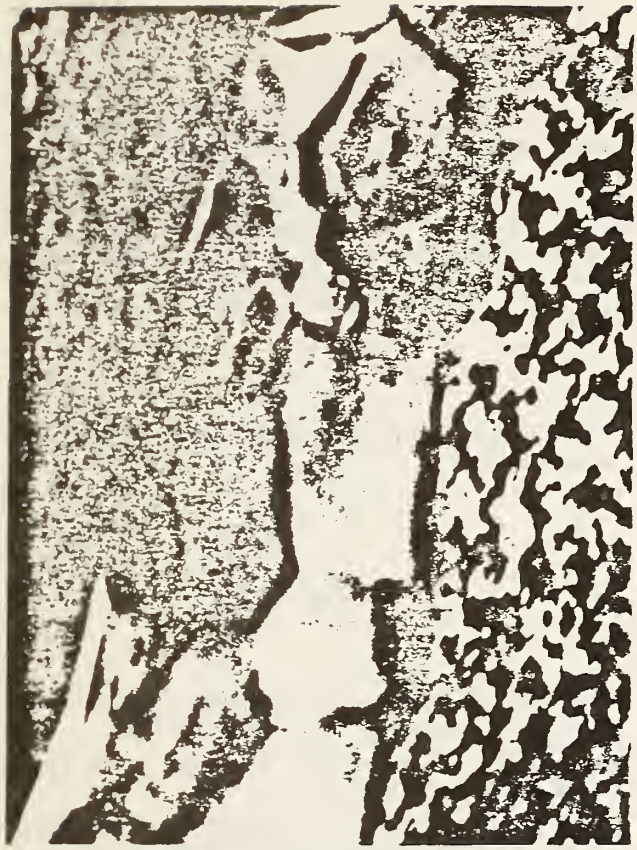

Fig. 2. Bright-field image illustrating the filamentary nature of reacted liquid-infiltrated Nb-Sn. The A15 phase (~0.35 μm wide) is bounded on both sides by the BCC phase.

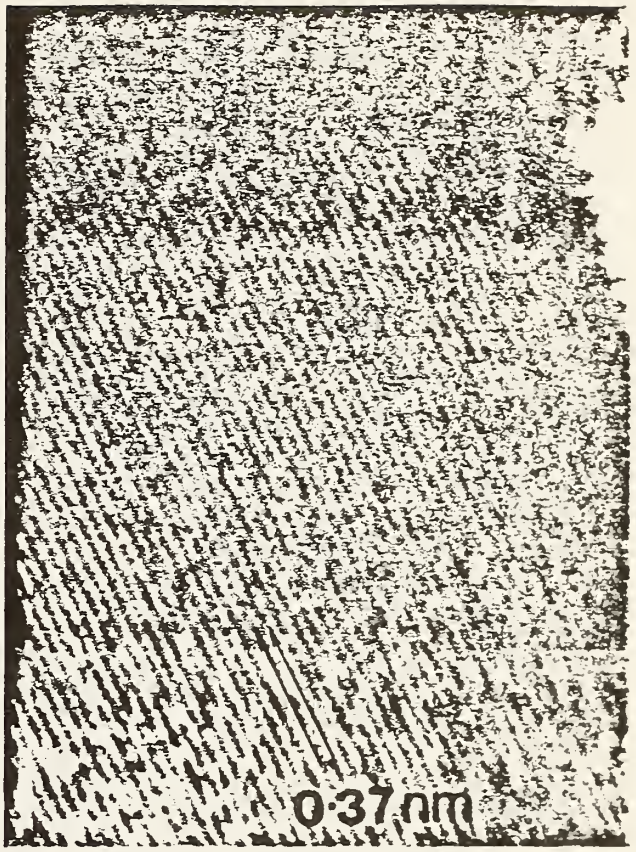

Fig. 3. A high-resolution image from an individual grain within an A15 filament where only the <110> Bragg beams (d_{110} = 0.374 nm) and zero-order beam were included in the aperture and the image was taken near the Scherzer defocus.

depending on the extent to which the filament protruded into the vacuum. Results from 60 spectra (i.e. 5 filaments) gave $\chi = 5.5 \pm 0.4$ which is a variation of ±7%. If the following assumptions are made: i) $C_{Nb} + C_{Sn} = 100$, where C is in at %; and ii) $C_{Nb}/C_{Sn} = K_{NbSn} \cdot \chi$, where K is the k ratio;[5] then the observed variation in χ can be expressed as a variation in composition for any value of C_{Nb}. For C_{Nb} in the range 72 to 76at% the result is ±1.5at%. Clearly this degree of homogeneity is consistent with the sharp superconducting transitions which are observed in the heat capacity data at 17.2 to 18 K.

3. $J_c(\epsilon, H)$ OF Nb(Ta)-Sn WIRES

Figure 4 shows the strain dependence of the critical current of the Nb(Ta)-Sn wires at fields from 10 to 23 T. J_c passes through a maximum at a strain ϵ_m of 0.13%. The parameter ϵ_m indicates the strain at which the critical current is a maximum. This is quite low compared with conventional bronze-processed conductors where ϵ_m is typically between 0.2 and 0.4%. The low value of ϵ_m is the result of the absence of a bronze matrix in liquid-infiltrated conductors; thermal contraction of the bronze-matrix material is primarily responsible for the compressive prestrain introduced in the reacted A15 regions of conventional bronze-processed conductors.

From Fig. 4, the irreversible strain limit ϵ_{irrev} for this conductor is more than 1.1%. Note that the ϵ_{irrev} indicates where the superconducting composite wire is permanently damaged. This corresponds to an intrinsic irreversible strain limit $\epsilon_{o,irrev} = \epsilon_{irrev} - \epsilon_m$ of about 0.9%, which is nearly double that for bronze-processed conductors where $\epsilon_{o,irrev}$ is consistently about 0.5% regardless of the value of ϵ_m. Correspondingly, the bending strain limits on the mechanical design of high-field magnets are also about double those of bronze process conductors.

A comparison of peak J_c values eliminates the effect of varying compressive prestrain among different conductors. Figure 4 shows that the critical current density of the liquid-infiltrated conductor is more than three times higher than that of bronze-processed conductors at low fields and more than an order of magnitude higher at high fields. The overall critical current density is about 1.8×10^4 A/cm^2 at 20 T, which is high enough to consider the feasibility of Nb-Sn superconducting magnets which will be used at or above 20 T. The extremely high overall J_c at high fields is the result of the combination of a unique A15 microstructure and a uniform stoichiometric Sn concentration across the A15 region, as shown in the AEM analyses and the heat capacity measurement of the present work. Detailed discussion on the mechanical properties of this wire was given elsewhere.[14]

In this work the Ta concentration of 1at% may not be optimal. From recent work of Schwall et al.,[15] a higher concentration of Ta, e.g. 3-5at%, should produce better properties. Research along this line is in progress.

IV. SUMMARY

We have used heat capacity measurement and AEM techniques to study the solid (Nb) - liquid (Sn) reaction in multifilamentary liquid-infiltrated Nb-Sn superconducting wires. A uniform stoichiometric chemical composition of Nb-25at%Sn was found at the reacted A15 regions from both the heat capacity and the AEM studies. Furthermore, the heat capacity data indicate that the weight fraction of the A15 in the reacted wire is ~23%. Correspondingly the volume fraction is ~21%. This value is slightly lower than the A15 volume fraction in bronze-processed Nb-Sn wire, which is usually around 30%.

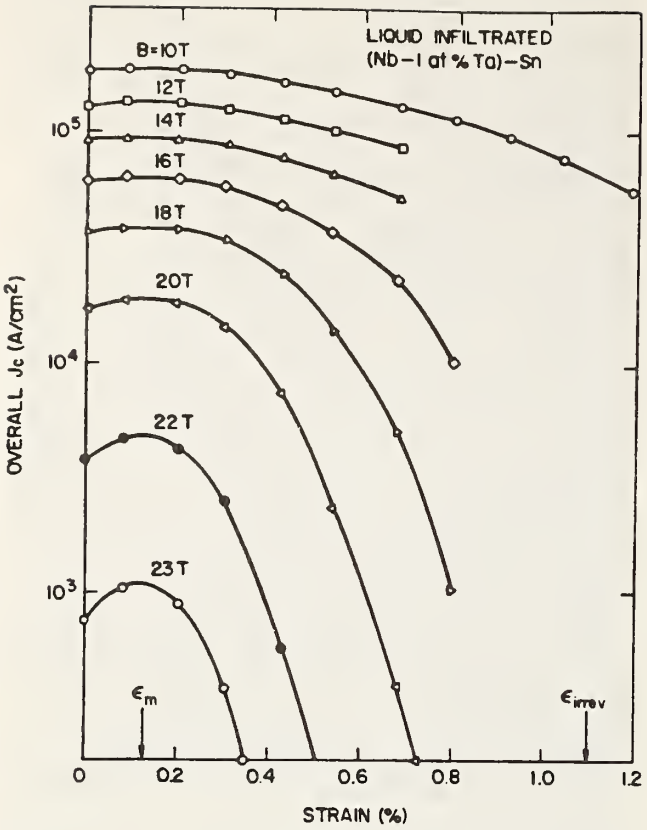

Fig. 4. Overall critical current density (J_c) of liquid-infiltrated (Nb-1at%Ta)-8at%Sn wire as functions of magnetic fields and uniaxial strain at 4.2 K.

The rapid solid-liquid reaction, in which the Nb predominantly diffuses into the liquid Sn, produces A15 grains with an equiaxial shape. Moreover, from the lattice-imaging studies, these A15 grains are essentially defect-free down to a resolution of 0.34 nm.

We have also found that 1at%Ta alloyed with Nb has further enhanced the superconducting properties such as J_c's and the mechanical strain tolerance. These improvements are believed due to the increase of the bulk upper critical fields. Further optimization in terms of the Ta concentration is now in progress.

Another important aspect of the research on the liquid-infiltrated Nb-Sn wire is the feasibility for an industrial scale-up. We have discussed this point in the Appendix.

V. APPENDIX

SCALE UP

Previously, we were able to fabricate the Nb-Sn liquid-infiltrated wire of 0.13 mm diameter from a starting composite rod of 5 mm diameter. In order to test the feasibility of the industrial scale up of this process, in this work, a starting billet 13 mm in diameter was drawn down to a wire of 0.13 mm in diameter. An area reduction of 10^4 has been achieved. No intermediate annealing was applied during the wire-drawing process. The overall J_c's carried by the wire with the heavy area reduction is similar to what we have previously reported. Currently, research along the line is two-fold: a larger starting billet of 25 mm in diameter and a rebundling technique. The results will be reported in the near future.

ACKNOWLEDGEMENTS

We thank S. Nakahara of AT&T Bell Laboratories for valuable discussions. The $J_c(\epsilon,H)$ data were obtained at the Francis Bitter National Magnet Laboratory which is supported by the National Science Foundation. The work performed at Stanford University was supported by Air Force Office of Scientific Research under contract F 49620-83-C-0014. The work performed at the National Bureau of Standards was supported by the Naval Ship Research and Development Center and the Department of Energy, Office of Fusion Energy under interagency agreement #DE-AI01-84ER52113.

• Also with Bell Communication Research, Inc., Murray Hill, New Jersey 07974

REFERENCES

[1] M. Hong, G. W. Hull, Jr., J. T. Holthuis, W. V. Hassenzahl, and J. M. Hong, Appl. Phys. Lett. **42**, 621 (1983).

[2] M. Hong, G. W. Hull, Jr., E. O. Fuchs, and J. T. Holthuis, Mater. Lett. **2**, 165 (1983).

[3] M. Hong, G. W. Hull, Jr., J. T. Holthuis, W. V. Hassenzahl, and J. W. Ekin, IEEE Trans. Magn. **MAG-19**, 912 (1983).

[4] M. H. Lovetto and R. E. Smallman, "Defect Analysis in Electron Microscopy," Science Paperbacks, Chapman and Hall, London (1975).

[5] J. C. H. Spence, "Experimental High Resolution Electron Microscopy," Clarendon Press, Oxford (1981).

[6] N. J. Zaluzec, "Introduction to Analytical Electron Microscopy," Eds., J. J. Hren, J. I. Goldstein, and D. C. Joy, Plenum Press, New York, pp. 121-167 (1979).

[7] S. R. Early, F. Hellman, J. Marshall, and T. H. Geballe, Physica **107B**, 327 (1981).

[8] J. W. Ekin, Cryogenics **20**, 611 (1980).

[9] M. Hong, F. Hellman, T. H. Geballe, and G. W. Hull, Jr., to be published in Appl. Phys. Lett.

[10] H. Devantay, J. L. Jorda, M. Decroux, J. Muller, and R. Flukiger, J. Mater. Sci. **16**, 2145 (1981).

[11] D. M. Maher, M. Hong, M. B. Ellington, D. L. Stubbs, T. H. Geballe, and G. W. Hull, Jr., Bull. Am. Phys. Soc. **28**, 261 (1983).

[12] H. L. Gegel, D. C. Yeh, J. T. Pajor, and J. C. Ho, IEEE Trans. Magn. **MAG-13**, 788 (1977).

[13] S. S. Eucker, J. D. Verhoeven, and D. K. Finnemore, J. Appl. Phys. **54**, 1471 (1983).

[14] J. W. Ekin and M. Hong, Appl. Phys. Lett. **45**, 297 (1984).

[15] R. E. Schwall, G. M. Ozeryansky, S. Foner, and E. J. McNiff, Jr., J. Appl. Phys. **56**, 814 (1984).

APPENDIX C

Summary Foreign Trip Report

December 4-14, 1984

Fukuoka, Japan
Miyazaki, Japan
Tsukuba, Japan
Tokai, Japan
Sendai, Japan

by

John W. Ekin
Electromagnetic Technology Division
Center for Electronics and Electrical Engineering
National Bureau of Standards
Boulder, Colorado 80303

Submitted to the Office of Energy Research
Department of Energy
Washington, D.C. 20545

January 15, 1985

Report No. 500

January 15, 1984

SUMMARY FOREIGN TRIP REPORT

From: John W. Ekin
Physicist
Superconductors and Magnetic Materials Group, 724.05

Locations Visited:

Fukuoka, Japan	5-6 December 1984
Miyazaki, Japan	7-8 December 1984
Tsukuba, Japan	9-11 December 1984
Tokai, Japan	12 December 1984
Sendai, Japan	13-14 December 1984

Purpose of Trip:

1) To obtain information on new superconductor materials being developed in Japan needed for several NBS, NBS/DoE, research programs on superconductors.

2) To reach agreement on an exchange of superconductor samples for electromechanical testing and an exchange of reference materials for development of international standards for critical-current testing.

3) To present an invited talk on electromechanical properties of high-field superconductors at the Third U.S./Japan Workshop on High-Field Superconducting Materials for Fusion.

Trip Summary:

KYUSHU UNIVERSITY (Fukuoka, Japan)

1) The Faculty of Engineering is a very active group with a strong emphasis on theory of superconductors. I obtained much information pertinent to our own electromechanical research effort here.

2) Research areas include: Flux pinning and basic electromagnetic properties (Profs. Matsushita and Yamafuji), electromagnetic properties of wires and conductors (Profs. Sumiyoshi and Yamafuji), stability and safety of wires and conductors (Profs. Funaki and Irie), stability and safety of magnets (Profs. Takeo and Irie), and Josephson junctions (Profs. Yoshida and Irie).

3) Recent topics include: Flux pinning in Chevrel superconductors (Profs. Matsushita and Yamafuji), longitudinal field effects on different pin types (Profs. Matsushita and Yamafuji), powder metallurgy wire (Prof. Sumiyoshi), powder metallurgy wire for ac use (Prof. Sumiyoshi), ac loss of wires and cables (Prof. Sumiyoshi), transmission of normal parts (Prof. Funaki), Josephson ac oscillator (Prof. Irie), and magnet fabrication research (Prof. Irie).

4) Prof. Irie, who is quite famous for his theories on pinning, will be retiring at the end of next year. Kyushu University intends to hold a world conference on superconductor pinning in his honor. We discussed some details of the conference which will probably be held in November of 1985.

5) Prof. Matsushita predicts that there will be a different power dependence of the pinning term in the strain-scaling law for irradiated superconductors. We discussed a collaborative experiment to test this and are now pursuing the preliminary phases.

6) Prof. Matsushita thinks that powder processed wire will ultimately be the best conductor for pulsed magnets because of the very fine filament size (and hence low hysteretic losses) that can be achieved. Twenty percent Nb can be introduced into the conductor before filament-to-filament contact is achieved, compared to only ten percent Nb for in-situ superconductors.

JAPANESE NATIONAL RAILWAY "MAGLEV" TEST SITE (Miyazaki, Japan)

1) They have achieved speeds of 500 km/hr in an unmanned test vehicle and 300 km/hr in a manned test vehicle.

2) Currently, tests are being conducted in three different areas: stress and vibration, damping, and aerodynamic shapes.

3) They are also developing on-board liquid-helium refrigerators.

4) One of the major problems for the utilization of this technology in Japan is the mountainous terrain. The cost of tunneling would make it prohibitively expensive. Consequently there are no near-term plans to build commercial MAGLEV tracks in Japan. A superconducting MAGLEV link from Tokyo to Narita airport had been planned but recently has been ruled out. They think there are possibilities for commercialization in the U.S. and Germany.

JAPAN-U.S. WORKSHOP ON HIGH-FIELD SUPERCONDUCTING MATERIALS FOR FUSION (Tsukuba, Japan)

Eight scientists were invited from the U.S. and about 40 research scientists attended from Japanese universities, government laboratories, and industry.

During the last four years there has been a rapid growth in both basic and applied superconductor research programs in Japan. Basic superconductor research is now conducted at many research laboratories in Japan, and Japanese industry has built up the engineering know-how and manufacturing processing for a large variety of NbTi, Nb_3Sn and other materials. The Japanese have demonstrated that large Nb_3Sn coils can be fabricated commercially. In short, superconductor research for fusion has been targeted for

major support by the Japanese government, and their programs now appear to have reached, and in some area, passed ours in both scope and depth.

Agreement was reached at the workshop to broaden the exchange in superconductor research. Emphasis at first will be given to exchanging laboratory reference sample materials for testing by both countries and for joint development of standard testing procedures and standard reference materials. Arrangements were made for collaborative studies of the electromechanical properties of a number of new experimental conductors being developed in Japan.

Specific highlights include:

1) In the area of critical current measurements, I emphasized that the current practice of intercomparing commercial superconductors in terms of their prestrain critical current density can be very misleading. Comparisons should be made in terms of the strain-free critical current, especially at high fields (10 tesla and above). Other problems emphasized at the conference included exactly those problems we are working on: critical-current characterizations in terms of the power law dependence of the voltage-current curve, field-angle dependences, current-transfer effects, and sausaging effects.

2) Radiation -- two radiation limits were discussed which will affect the choice of materials for fusion applications:

   a) The waiting time after reactor shut down before maintenance can begin. Prof. T. Okada presented some data on superconductor performance in this regard. The elements Sn, Ta, Hf, Mo, Ga, Cr have the longest waiting time and should be avoided! Ti and V were the best performers. Conclusion -- Nb_3Sn and V_3Ga present serious design problems in fusion applications! On the other hand, Nb_3Al and NbTi are good choices. NbN should also be good, but no data were available. Another conclusion is that Ta, Hf, and Ga should be avoided as additives to Nb_3Sn in favor of Ti.

   b) The operating time before significant radiation damage occurs to the superconductor. Prof. T. Okada and Dr. E. Dalder presented some preliminary data from the literature on radiation degradation of critical current density. Nb_3Sn was among the worst conductors. No data on the B1 or C15 superconductors were presented. This appears to me to be an area where we have insufficient information on which to base any decisions.

   The first problem is fundamental and may well dictate which superconductors are ultimately selected for fusion magnets. The second of these two problems is more amenable to solving by providing enough radiation shielding for the superconductor. The problem is to know how much is enough.

3) The irreversible strain damage limit can be increased sixty percent by adding Ti to the bronze matrix of Nb_3Sn conductors. It can be doubled in commercial Nb_3Sn conductors by a hot-isostatic-pressure (HIP) treatment.

4) In-situ V_3Ga and V_3Ga-tape conductors are being developed commercially in Japan because they offer the possibility to achieve significantly higher magnetic fields than Nb_3Sn conductors, even Nb_3Sn with additives.

5) Arrangements were made for collaboration on a study of electromechanical properties at high fields of a number of new experimental conductors being developed in Japan. The following organizations agreed to send superconductor specimens for strain effect testing by NBS:

Tohoku University	T. Anayama	Standard Nb_3Sn
NRIM*	Y. Tanaka, K. Tachikawa	Nb_3Ge
NRIM*	K. Togano, K. Tachikawa	$Nb_3(Al,Ge)$
Kobe Steel	T. Horiuchi	HIP of Ti added Nb_3Sn
Hitachi-NRIM	K. Kamata, K. Tachikawa	Ti-in-bronze conductor
Univ. of Nagaoka	K. Hamasaki, T. Yamashita	$PbMo_6S_8$ with minimum Mo
Furukawa	Y. Tanaka	In-situ V_3Ga
Toshiba	S. Murase	Internal Sn Nb_3Sn
Vacuum Metallurgical Co.	T. Noguchi	In-situ V_3Ga

*NRIM is the Japanese National Research Institute for Metals

JAPANESE ATOMIC ENERGY RESEARCH INSTITUTE (Tokai, Japan)

Privately, S. Shimamoto commented to me that Japan has considerable concern about the possibility of insulation failure in wind-and-react magnet construction, which would result in coil melt-down in the shorted region. This is the reason for their strong preference for react-and-wind construction of magnets for fusion. It permits much more reliable coil insulation since the insulation does not have to be subjected to a high-temperature heat treatment.

Shimamoto also commented that for superconductor coils larger than Large Coil Task (LCT) magnets, he likes the Internal Cable in Conduit Superconductor (react and wind), not because of stability reasons, but for the distributed reinforcement feature to handle the very large forces.

TOHOKU UNIVERSITY (Sendai, Japan)

Since my visit last March they now have their 23-tesla hybrid magnet operating. A 15-tesla copper poly-helix magnet has also been in regular operation. The 30-tesla hybrid magnet is still under construction.

A. Nagata is very much interested in setting up to measure uniaxial strain effects on the critical current of superconductors using their high-field magnet facilities.

Benefits

Information obtained from these visits and the workshop will provide direction to our work on electromechanical properties of superconductors for fusion-magnet development.

The agreement reached to exchange superconductor standard reference materials is necessary to the establishment of international standards in this new field.

The collaborative agreements for electromechanical property testing were made on experimental Japanese conductors which are not being fabricated in the U.S., or represent a modification of U.S. made superconductors. An evaluation of their performance will help U.S. programs by guiding our own efforts toward those superconductors having the best performance or promise of performance, eliminating wasted U.S. effort on development of lower performance conductor types and providing the needed data base to develop advanced high-field superconductors in the U.S.

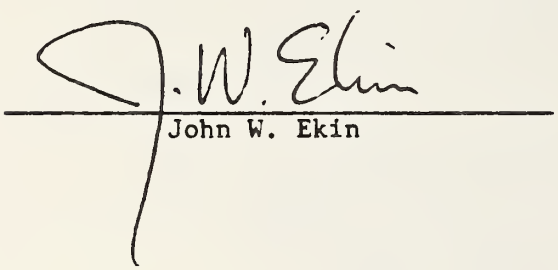

John W. Ekin

NBS-114A (REV. 2-8C)

U.S. DEPT. OF COMM. BIBLIOGRAPHIC DATA SHEET (See instructions)	1. PUBLICATION OR REPORT NO. NBSIR-86/3044	2. Performing Organ. Report No.	3. Publication Date March 1986

4. TITLE AND SUBTITLE

ELECTROMECHANICAL PROPERTIES OF SUPERCONDUCTORS FOR DOE FUSION APPLICATIONS

5. AUTHOR(S)

J. W. Ekin, J. Moreland, and J. C. Brauch

6. PERFORMING ORGANIZATION (If joint or other than NBS, see instructions)

NATIONAL BUREAU OF STANDARDS
DEPARTMENT OF COMMERCE
WASHINGTON, D.C. 20234

7. Contract/Grant No.

8. Type of Report & Period Covered

9. SPONSORING ORGANIZATION NAME AND COMPLETE ADDRESS (Street, City, State, ZIP)

Department of Energy
Office of Fusion Energy
Washington, DC 20545

10. SUPPLEMENTARY NOTES

☐ Document describes a computer program; SF-185, FIPS Software Summary, is attached.

11. ABSTRACT (A 200-word or less factual summary of most significant information. If document includes a significant bibliography or literature survey, mention it here)

This is an interim report presenting data on superconductor performance under mechanical load, which are needed for the selection of superconductors and the mechanical design of superconducting magnets for DOE fusion energy systems. A further aim of the reported research is to measure and understand the electromechanical properties of promising new superconductor materials with strong application potential at high magnetic fields. Results include the following. The first strain vs. critical-current studies were made on a Chevrel-phase superconductor, $PbMo_6S_8$. Chevrel-phase superconductors were found to have a large strain effect, comparable in magnitude to A-15 superconductors like Nb_3Sn. Electromechanical-property measurements of an experimental liquid-tin-infiltrated Nb_3Sn conductor showed it to have an irreversible strain limit twice as large as bronze-process superconductors and a significantly higher overall critical-current density; the liquid-infiltration process thus has the potential for development of a practical Nb_3Sn conductors with both superior critical-current density and extremely good mechanical properties. Electromechanical parameters were obtained on several Nb_3Sn conductors that are candidate materials for superconducting fusion magnets, including conductors fabricted by the bronze, internal-tin, and jelly-roll processes. Thermal contraction data are reported on several new structural materials for superconductor sheathing and reinforcement, and a new diagnostic tool for probing the energy gap of practical superconductors has been developed using electron tunneling.

12. KEY WORDS (Six to twelve entries; alphabetical order; capitalize only proper names; and separate key words by semicolons)

electromechanical; electron tunneling; energy gap, fusion; ICCS superconductor; liquid-infiltration superconductor; Nb_3Sn; $PbMo_6S_8$; stress effect; transverse stress effect; uniaxial stress effect

13. AVAILABILITY

☒ Unlimited

☐ For Official Distribution. Do Not Release to NTIS

☐ Order From Superintendent of Documents, U.S. Government Printing Office, Washington, D.C. 20402.

☒ Order From National Technical Information Service (NTIS), Springfield, VA. 22161

14. NO. OF PRINTED PAGES 118

15. Price

USCOMM-DC 6043-P80

☆U.S. GOVERNMENT PRINTING OFFICE:1986—671-642/45190